

Alma Mater Studiorum - Università di Bologna

**DOTTORATO DI RICERCA IN
SCIENZE E TECNOLOGIE AGRARIE, AMBIENTALI E
ALIMENTARI**

Ciclo XXXII

Settore Concorsuale: 07/E1

Settore Scientifico Disciplinare: AGR/07

**GENETIC DISSECTION OF RESISTANCE
TO ABIOTIC AND BIOTIC STRESSES IN DURUM WHEAT**

Presentata da: Giuseppe Emanuele Condorelli

Coordinatore Dottorato

Prof. Massimiliano Petracchi

Supervisore

Prof.ssa Elisabetta Frascaroli

Esame finale anno 2020

CONTENTS

ABSTRACT	6
GENERAL INTRODUCTION	8
Objectives and outline of present thesis	8
CHAPTER 1	10
INTRODUCTION	10
MATERIALS AND METHODS.....	11
Plant material and field management	11
Chlorophyll fluorescence imaging (CFI) by the “Lemnatec” field scanalyzer	13
NDVI and IRT values by UAV and ground-based platforms	15
Chlorophyll fluorescence (ChlF) by the manually pushed cart.....	19
Physiological drought adaptive traits	19
Additional drought adaptive traits	22
Dry biomass.....	23
Statistical analysis	23
Genetic analysis: SNP genotyping, population structure and GWAS model.....	23
RESULTS.....	26
Population Structure	26
Chlorophyll fluorescence imaging (CFI) by the “Lemnatec” field scanalyzer	27
NDVI and IRT values by UAV and ground-based platforms	29
Chlorophyll fluorescence (ChlF) by the manually pushed cart.....	32
Physiological drought adaptive traits	34

Additional drought adaptive traits	35
Dry biomass.....	36
Genetic analysis	36
Chlorophyll fluorescence imaging (CFI) by the “Lemnatec” field scanalyzer	39
NDVI and IRT values by UAV and ground-based platforms	40
Chlorophyll fluorescence (ChlF) by the manually pushed cart.....	42
Physiological drought adaptive traits	44
Additional drought adaptive traits	47
Dry biomass.....	48
QTL clusters	49
DISCUSSION.....	55
Chlorophyll fluorescence imaging (CFI) by the “Lemnatec” field scanalyzer	55
NDVI and IRT values by UAV and ground-based platforms	55
Chlorophyll fluorescence (ChlF) by the manually pushed cart.....	57
Physiological drought adaptive traits	58
Additional drought adaptive traits	60
Dry biomass.....	61
QTL clusters	61
CONCLUSIONS.....	62
CHAPTER 2	64
INTRODUCTION	64
MATERIALS AND METHODS.....	66

1. GWAS on Fusarium Panel	66
1.1. Plant materials and field management.....	66
1.2. Phenotypic analysis	67
1.3. Statistical analysis	68
1.4. Genetic analysis.....	68
2. Linkage mapping on RIL population Simeto × Levante	70
2.1. Plant material and field management	70
2.2. Phenotypic analysis	71
2.3. Statistical analysis	71
2.4. Genetic analysis.....	71
3. Selection of QTL hotspots and haplotype analysis.....	72
3.1. Haplotype analysis.....	72
3.2. KASP assays.....	72
4. KASP validation on Fusarium Panel.....	73
RESULTS.....	73
Phenotypic analyses.....	73
Genetic analyses	77
DISCUSSION.....	88
Phenotypic analyses.....	88
Genetic analyses	89
Haplotype analysis and KASP assays	90
CONCLUSIONS.....	92
APPENDIX	93
GENERAL CONCLUSIONS	113
REFERNCES	115

ABSTRACT

This thesis was aimed to investigate the genetic response to abiotic and biotic stresses in durum wheat (*Triticum turgidum* L. var. *durum*), a cultivated tetraploid subspecies (AABB; $2n = 28$) used for the production of pasta, couscous and various types of bread. Two research areas were focused: i) the high-throughput phenotyping (HTP) to detect novel drought tolerance quantitative trait loci (QTL) clusters and ii) the Kompetitive Allele Specific Polymerase chain reaction (KASP) marker development for the genetic dissection of Fusarium head blight (FHB) resistance.

Concerning the first area, I investigated drought adaptive traits on durum wheat elite accessions (Durum Panel) in three consecutive years (2017-2019) at Maricopa Agricultural Center (University of Arizona, USA) which provided the experimental field and the high-throughput phenotyping platforms (HTPP). The genome-wide association study (GWAS) results indicated the presence of thirty-one QTL clusters for two or more drought adaptive traits unrelated to the major loci responsible for phenology and plant height. Twelve of them overlapped with the major QTL for grain yield and related traits previously reported in studies carried out across a broad range of soil moisture availability and field drought conditions in wheat.

Concerning the second area, I investigated two plant materials: i) 130 durum wheat accessions artificially inoculated with *Fusarium culmorum* (FC) and *F. graminearum* (FG) species and evaluated for incidence (INC), severity (SEV), FHB index, Fusarium-damaged kernels (FDK) and deoxynivalenol (DON) content; ii) 165 F₆ recombinant inbred lines (RILs) from the cross between the cultivars Simeto (susceptible) and Levante (moderately resistant) evaluated for SEV using FG as inoculum. The genetic dissection led to sixteen QTL clusters, in part unrelated to the phenology and unknown in bread wheat, from which specific loci

(*QFHB.ubo-1A.1*, *QFHB.ubo-1B.1* and *QFHB.ubo-6A.1*) significantly influenced DON content. The haplotype analysis allowed me to validate KASP Single Nucleotide Polymorphisms (SNPs) suitable for marker-assisted selection (MAS) programs, i.e., for the high-throughput screening of large populations as well as for the selection of cultivars by pyramiding loci for resistance/tolerance to DON content and other FHB traits.

GENERAL INTRODUCTION

Durum wheat, *Triticum turgidum* L. ssp. *durum*, is a tetraploid species evolved from domesticated emmer wheat, *T. turgidum* ssp. *dicoccum*. It is mainly used for pasta production, couscous and various types of bread and planted annually on an estimated area of 18 million hectares, which represents approximately 8–10% of all the wheat-cultivated area in the world (De Vita and Taranto, 2019).

Biotic and abiotic stresses are major limiting factors for durum wheat productivity worldwide (Mohammadi et al. 2015) and the discovery of their genetic bases represents an essential priority (Wang et al. 2019) to perform marker-assisted selection (MAS), a highly efficient method to select resistance loci in breeding programs and particularly to pyramid multiple resistance genes in new varieties (Pei, 2019). Recently, an international consortium has generated a high quality reference sequence of the modern durum wheat cultivar Svevo (Maccaferri et al. 2019) in order to lead to the selection of new cultivars with higher quality, higher yield and more resistance to diseases.

Objectives and outline of present thesis

This thesis dissects the genetic bases of durum wheat responses to drought and Fusarium head blight (FHB) disease through the common approach of genome-wide association study (GWAS) (Zhu et al. 2008) using a high-density 90K wheat single nucleotide polymorphism (SNP) array (Wang et al. 2014). GWAS is optimal for examining multiple traits (Atwell et al. 2010) as well as suitable for phenotyping materials under multiple environments, thereby reducing environment-induced errors and enhancing accuracy (Hall et al. 2010).

Even though recurrent drought associated with climate change is among the principal constraints to global productivity of wheat (Mwadzingeni et al. 2016), yet, how it affects the vulnerability of wheat production in combination with several co-varying factors, i.e., agro-climatic regions,

phenological phases and soil texture, it remains unclear (Daryanto et al. 2016). For clarifying the role of drought, *Chapter 1* focuses on emergent high-throughput phenotyping (HTP) approaches to genetically investigate difficult, time-sensitive drought adaptive traits in durum wheat, providing innovative opportunities to detect novel proxy traits governing the drought adaptive responses (Concorelli et al. 2018).

FHB is a devastating fungal disease in wheat worldwide, and it results in yield losses and mycotoxin accumulation, such as deoxynivalenol (DON), in infected grains (He et al. 2018). Durum wheat is notorious for its higher susceptibility to FHB (Miedaner et al. 2017) in comparison to the hexaploid bread wheat, *Triticum aestivum*, due to a narrow genetic diversity (Giancaspro et al. 2018; Rudd et al. 2001) and numerous small-effect resistance quantitative trait loci (QTL) which are difficult to be combined in selective breeding (Steiner et al. 2019). *Chapter 2* reports the validation of Kompetitive Allele Specific Polymerase chain reaction (KASP) markers suitable for haplotype-based MAS programs, i.e., for the high-throughput screening of large populations as well as for the selection of durum wheat cultivars by pyramiding loci for resistance/tolerance to DON content and other FHB traits.

High-throughput phenotyping to detect novel drought tolerance QTL clusters in durum wheat

INTRODUCTION

Projected future effects of global climate change on agriculture indicate an increased frequency and severity of drought events (Luo et al. 2019) resulting in yield losses for many crops and threatening regional/global food security (Wang et al. 2018). Additionally, an estimated doubling in crop production is required for 2,050 year in response to the rapid growth human population (Tilman et al. 2011) and an approximate 38% increase in annual crop production rate is necessary (Sadeghi-Tehran et al. 2017). In order to overcome these challenges, an important plant breeding approach is the better understanding of the genotype-phenotype relationship to unravel the genetic basis of complex traits (Sun et al. 2018; Knoch et al. 2019). In the last decade, the crop genetic improvement tools have benefited from rapid advances in the genomic sequencing but not from the throughput of the traditional plant phenotyping (Sadras and Lawson, 2011; Fahlgren et al. 2015; Araus et al. 2018) by inducing a shift of the research bottleneck in plant sciences from genotyping to phenotyping (Mir et al. 2019).

For this purpose, the field-based high-throughput phenotyping (HTP) represents an emerging approach to quantify difficult, time-sensitive plant traits in limiting growing conditions (Thompson et al. 2018) providing innovative opportunities to detect novel proxies governing drought adaptive crop responses (Condorelli et al. 2018). Robotic field scanners as well as ground-based and Unmanned Aerial Vehicle (UAV) platforms provide unprecedented opportunities to accurately measure proxy traits in hundreds of plots (Pauli et al. 2016; Trapp et al. 2016; Duan et al. 2017; Shakoor et al. 2017; Shi et al. 2017) with dense temporal and spectral resolution (Virlet et al. 2017).

The objective of this work was to identify genetic determinants of durum wheat adaptation to drought. For detecting loci controlling adaptive traits, a panel of durum wheat elite accessions suitable for GWAS was field-evaluated in three years at University of Arizona (USA) under conditions of progressive drought severity as well as well-watered and water-limited treatments. Drone and ground-based platforms were employed for the acquisition of multiple drought sensitive traits, while a semi-automated robotic field phenotyping platform was employed for the acquisition of multispectral and hyperspectral data referring to the physiological response of plants subjected to water limiting growing conditions. In addition, traditional phenotyping protocols for plant metabolism reaction and for photosynthetic activity as result of adaptation/damage in water-limited conditions and under the “Rehydration method” were performed. Finally, the total biomass was evaluated at harvest to quantify the photosynthate loss due to the stress.

A GWAS was performed including the Kinship and the genetic structure of the population, as well as the flowering time, as covariate. Twelve major QTL hotspots were identified for two or more Drought Resistance (DR) proxies, unrelated to the major loci responsible for phenology and overlapped with the major loci for grain yield and related traits previously reported in wheat.

MATERIALS AND METHODS

Plant material and field management

The field trial was conducted at Maricopa Agricultural Center (MAC, 33.070° N, 111.974° W, elevation 360 m) on a Casa Grande soil (fine-loamy, mixed, superactive, hyperthermic Typic Natrargids) for three consecutive years (2017-19). In the first two, the plant material included 248 durum wheat elite accessions in two replicates from the association mapping population UNIBO-Durum Panel (hereafter referred to as “Durum Panel”) assembled at the University of Bologna

(UNIBO), representing a large portion of the genetic diversity present in the most important improved durum wheat gene pools (Figure 1). The germplasm list is available through the following link: <https://www.frontiersin.org/articles/10.3389/fpls.2018.00893/full>. The Durum Panel was selected and released from breeding programs at the International Maize and Wheat Improvement Center (CIMMYT), the International Center for Agricultural Research in the Dry Areas (ICARDA), the National Institute for Agricultural Research (INRA, France) and the Institute of Agrifood Research and Technology (IRTA, Spain). Other accessions were released by public or private breeding programs in Australia, Italy, France, Northern Great Plains of the USA and Canada (North Dakota, Montana, Saskatchewan and Alberta) and Pacific Southwest of the US, commonly referred to as “Desert-Durum®”. According to a Randomized Complete Block Design (RCBD), the Durum Panel was planted on 20 December 2016 in the first year and on 28 November 2017 in the second year using Orita and Tiburon cultivars as border plots. Each accession was evaluated in two-row plots (3.5 m long, 0.76 m apart) with a final density of 22 plants/m². Before planting, nitrogen at 112 kg ha⁻¹ and phosphorus (P205) at 56 kg ha⁻¹ were incorporated into the soil and 28 days after sowing, irrigation was managed by a pressurized drip system using lines buried ~10 cm deep. The drip irrigation was stopped on 16 March (days after planting, DAP: 86) in the first year and 11 March (DAP: 103) in the second year. A progressive drought stress was induced on plant material until the harvest on 3 April 2017 (DAP: 104) in the first year and 2 April 2018 (DAP: 125) in the second year. The harvest was carried out before the growth stage (GS) of ripening to allow for planting the next phenotyping experiment. Therefore, the dry biomass mentioned below indicates the status at a point in time rather than direct estimates of final yields. Disease and insect pest pressure were negligible throughout the crop.

A subset of 215 elite accessions from Durum Panel was planted on 20 December 2018 in three replicates and using Orita and Tiburon cultivars as border plots. Each accession plot consisted in two-rows (3.5 m long, 0.76 m apart) of which the east one was well-watered (WW) and the west

one was water-limited from 6 March (75 DAP) to 8 April (107 DAP) when harvest was carried out to measure the dry biomass. Soil moisture data were collected for monitoring the water stress conditions using time domain reflectometry (TDR) probes spatially distributed across the experimental field and measure moisture time series at different depths throughout the durum wheat growth seasons.

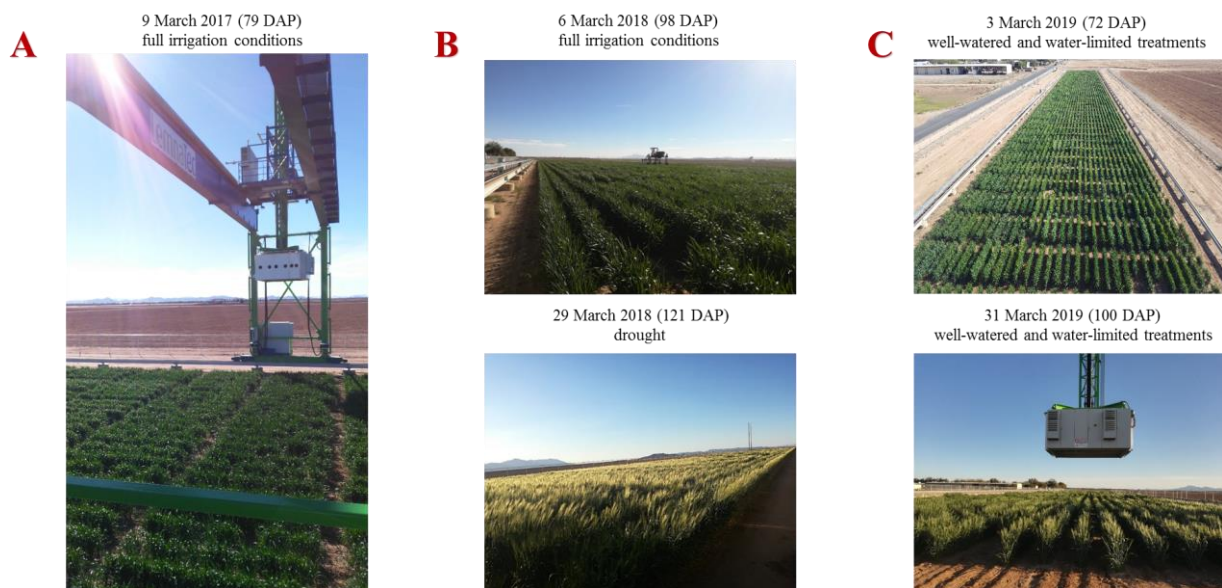


Figure 1 | The UNIBO-Durum Panel at Maricopa Agricultural Center. The pictures refer to three different days after planting (DAP) in 2017 (A), 2018 (B) and 2019 (C).

Chlorophyll fluorescence imaging (CFI) by the “Lemnatec” field scanner

The Danforth Plant Science Center (St. Louis, Missouri, US) announced in 2015 a multi-institutional \$8 million grant from the U.S. Department of Energy ARPA-E TERRA division to support the building of a scanning robot “Lemnatec” field scanner (LFS) assembled in 2016 at MAC-USDA Arid Land Research Station. The LFS is the largest field crop analytics robot in the world with 30-ton steel gantry that autonomously moves along two 200-meter steel rails. It includes

a diverse array of cameras which facilitates specific crop measurements with dense temporal and spectral resolution: chlorophyll fluorescence imaging (CFI) system, visible and near-infrared (VNIR), short-wave infrared (SWIR), forward-looking infrared (FLIR) and light detection and ranging (LiDAR). In three consecutive years, the LFS produced a big dataset of multispectral and hyperspectral imagery, even if the gigabytes of information are still processing by researchers of Danforth Plant Science Center with a view to producing plot means per genotype as essential step for GWAS. However, CFI data means were generated in the third year on four progressive days (DAP: 71, 97, 102 and 106) in darkness, since the plants were not subject to non-photochemical quenching (NPQ) mechanisms and quenched the light harvesting limits (Loriaux et al. 2013) (Figure 2). In detail, light-emitting diode (LED) bulbs generated flashes of red light (620 nm) for 1400 ms to saturate the electron transfer in the plant photosystem II (PSII). The camera recorded the emitted fluorescence in 101 images over two seconds during and after the flash with an optimal distance between the camera and the canopy of 70 cm and a final view of 1.10 m. The *R-project* scripts were produced to generate Fq/Fm data means and estimate the efficiency at which light absorbed by PSII was used for primary electron acceptor (QA) reduction, according to the emitting local fluorescence (Fq) referring only to the reduction of QA and the maximum fluorescence (Fm).



Figure 2 | Light-emitting diode (LED) bulbs generated flashes of red light (620 nm) for 1400 ms to saturate the electron transfer in the plant photosystem II (PSII) and produced chlorophyll fluorescence imaging (CFI) data in darkness.

NDVI and IRT values by UAV and ground-based platforms

Two UAVs and a ground-based platform were used during the first year (2017) to measure the normalized difference vegetation index (NDVI) and infrared thermography (IRT) at midday on progressive DAP under well-watered and water-limited conditions (Figure 3). NDVI is an effective indicator of vegetation response to drought (Ji and Peters, 2003), based on the difference between the maximum absorption of radiation in the Red spectral region (from 620 to 690 nm) and the maximum reflectance in near infrared light (NIR, from 760 to 900 nm) as result of the leaf cellular structure (Tucker, 1979). Healthy and living canopies absorb most of the Red light by the photosynthetic pigments, while the NIR light is mostly reflected due to light scattering in leaf internal structure and canopy architecture (Tattaris et al. 2016; Yousfi et al. 2016). IRT is an effective indicator of the canopy temperature, a surrogate for stomatal conductance, used to investigate the plant water status and potential tool for phenotyping and irrigation scheduling (Prashar and Jones, 2016). NDVI and IRT were extracted from georeferenced orthomosaic GeoTIFFs generated from imagery captured using autopiloted flights of either a MicaSense

RedEdge multi-spectral camera (MicaSense, Seattle, WA) carried on a hexacopter, or a Parrot Sequoia (Parrot, Paris, France) multi-spectral camera carried on an eBee (SenseFly, Lausanne) fixed wing aircraft. The multispectral cameras showed dissimilar features in terms of band centers and bandwidths (Table 1).

The flights were conducted at 40 - 42 m above ground level, resulting in ground sampling distances of ~3 cm/pixel for the RedEdge, and 4.4 cm/pixel for the Sequoia. Mission planning was done with UgCS (UgCS, Riga) for the RedEdge camera, and either eMotion 3 (senseFly, Lausanne) or Atlas Flight (MicaSense, Seattle, WA) for the Sequoia camera. All flights were planned for 80% image overlap along flight corridors. Both the Sequoia and RedEdge cameras use global shutters.

Pix4DMapperPro desktop software (Pix4D SA, Switzerland, <http://pix4d.com>) was used to generate orthomosaics for each camera band. Six to eight ground control points (GCP) geolocated with Real Time Kinematic (RTK) survey precision were used to georeference the orthomosaics. Camera images were calibrated using manufactured supplied reflectance panels that were imaged at the beginning of each flight. The Pix4D processing options were essentially the same as those of Pix4D's "Ag Multispectral" template version 4.1.10, except that GeoTIFF tiles were merged to create the NDVI/IRT orthomosaic. Plot-level means from UAV were created in QGIS software version 2.18.3 (QGIS, US, <http://www.qgis.org>). Shape files containing annotated single plot polygons were generated with an *R-project* script. Shape files with GCPs as features (points) were also employed based on RTK survey grade measuring devices. For all flights, the GeoTIFF with the NDVI/IRT orthomosaic from Pix4D was combined with the plot polygon and GCP shape files in a single QGIS project. Confirmation of proper geolocations of the Pix4D orthomosaics was achieved by visually confirming alignment of the visible GCPs with the corresponding points in the feature shape file. The plot means were generated using the Zonal Statistics function in QGIS. The tractor-based system was similar to that described by Andrade-Sanchez and Heun (2013) but carried five GreenSeeker spectral sensors (Table 1) and RT200 communication module (Trimble, Inc.,

Sunnyvale, CA) mounted in a frame at the front of the vehicle. These active sensors were equipped with their own source of modulated white light, which was directed toward the top of the crop canopy with the platform in motion at an average speed of 0.84 m s^{-1} . A portion of the sensor-generated light reflects off the crop and was measured by Red and Near Infrared (NIR) wide-band filters located in the sensor head. The height position of the sensors was set to 1.32 m above ground in every event. Since the approximate view angle of this sensor model is 28° , the field-of-view (FOV) of each sensor was $\sim 50\text{-cm}$ at the soil surface. The ground platform was retrofitted with an ultra-precise RTK Global Navigation Satellite System (GNSS) receiver, AgGPS332 (Trimble, Inc., Sunnyvale, CA) to generate positioning data via “GGA” National Marine Electronics Association (NMEA) messages. The data acquisition system used in the tractor platform was a CR3000 micro-logger (Campbell Scientific, Logan, UT) programmed to record the NDVI/IRT output of all five spectral sensors plus latitude and longitude coordinates at a rate of 5 Hz. The combination of data sampling frequency and platform speed of operation produced an average of 20 data for each plot.

Table 1 | Properties of Sequoia, RedEdge and GreenSeeker sensors including type of recorded spectral band, bandcenter and bandwidth.

^a <https://www.micasense.com/parrotsequoia/>

^b <https://agriculture.trimble.com/precision-ag/products/greenseeker/>

^c <https://www.micasense.com/>

Sensor	Spectral Band	Band center (nm)	Band width (nm)
UAV-Sequoia ^a	Green	550	40
	Red	660	40
	RedEdge	735	10
	NIR	790	40
	Blue	475	20
Tractor-GreenSeeker ^b	Red	660	25
	NIR	770	25
UAV-RedEdge ^c	Green	560	20
	Red	668	10
	RedEdge	717	10
	NIR	840	40



Figure 3 | High-throughput phenotyping at Maricopa Agricultural Center: A) “Lemnatec” field scanalyzer for multispectral and hyperspectral imagery at high spatial and temporal resolution, B) NDVI and IRT acquisition by UAV- and ground-based platforms and C) LIFT instrument on a manually pushed cart for ChlF investigation.

Chlorophyll fluorescence (ChlF) by the manually pushed cart

In the second year, chlorophyll fluorescence (ChlF) measurements were carried out in collaboration with the Institute of Bio- and Geosciences (IBG) in Jülich (Germany). Their researchers provided a light-induced fluorescence transient (LIFT) sensor mounted on a manually pushed cart at 60 cm distance from the canopy (Figure 3). A rapid and non-invasive characterization of the following photosynthetic traits was carried out after anthesis in sunny days (hours: 11-13 am) in well-watered (103 DAP) and water-limited (115 DAP) conditions: Fq'/Fm' refers to the operating efficiency of PSII, while $Fr1'/Fq'$ and $Fr2'/Fq'$ to the re-oxidation efficiency of QA at 0.65 ms and 120 ms, respectively (Keller et al. 2019). The datasets were processed using *R-project* scripts as well as Genstat 19 software tools to produce plot means per genotype for GWAS.

Physiological drought adaptive traits

The carbon isotopic composition is an indicator of water-use efficiency in crops (Farquhar et al. 1984; Dixon et al. 2019). During the photosynthetic CO₂ fixation, healthy plants discriminate against the minor, naturally occurring stable isotope ¹³C (ca. 1.1149% in CO₂ in air). In wheat, a C₃ species, the carbon isotope composition of plant material is primarily caused by the discrimination occurring during carboxylation by the rate-limiting enzyme ribulose-1,5-bisphosphate carboxylase/oxygenase (Rubisco), and during the diffusion of CO₂ from the atmosphere to the chloroplast (Caemmerer et al. 2014). In the first year, the Durum Panel was evaluated for stable carbon ($\delta^{13}\text{C} = ^{13}\text{C}/^{12}\text{C}$) isotope ratios using an elemental analyzer (Flash 1112 EA; Thermo Finnigan, Bremen, Germany) coupled with an isotope ratio mass spectrometer (Delta C IRMS, Thermo Finnigan), operating in a continuous flow mode. Flag leaf samples for each plot (about 1 mg) were collected after anthesis at midday under well-watered (85 DAP, GS59) and drought (93 DAP, GS71) conditions, then weighed into tin capsules, sealed and loaded into an automatic sampler (Thermo Finnigan) prior to EA-IRMS analyses, as described by Araus et al. (2013). The

measurements were carried out at the Scientific Facilities of the University of Barcelona. The $^{13}\text{C}/^{12}\text{C}$ ratios were expressed in δ notation (Coplen et al. 2006): $\delta^{13}\text{C} = (^{13}\text{C}/^{12}\text{C})_{\text{sample}} / (^{13}\text{C}/^{12}\text{C})_{\text{standard}} - 1$ (Farquhar et al. 1989), where “sample” refers to plant material and ‘standard’ to Pee Dee Belemnite (PDB) calcium carbonate.

The Durum Panel was evaluated for osmotic adjustment (OA) in flag leaves in two consecutive years (2018-19) as result of an active accumulation of low molecular weight organic solutes like soluble sugars (Munns and Weir, 1981; Blum, 2017) and proline (Johnson et al. 1984; Mattioni et al. 1997; Liang et al. 2013) in response to a leaf water potential reduction. In parallel, the relative water content (RWC) was evaluated in three consecutive years (2017-19) in flag leaves to measure the plant water status in terms of the physiological consequence of cellular water deficit. In 2018, the first sampling for OA and RWC was carried out in fully-irrigated conditions (104 DAP, awns visible on approximately 50% of the Durum Panel accessions) while the second sampling was carried out 15 days after under drought (119 DAP, most accessions were at early grain-filling). In 2019, a single date of sampling (95 DAP) was carried out for accessions of the east rows (well-watered) and west rows (water-limited) when awns were visible on approximately 50% of the Durum Panel.

In both years, fully expanded flag leaves of eight different plants were sampled for each plot (experimental unit) at dawn from 6.00 to 7.00 a.m. Leaves were immediately placed in sealed plastic bags, stored in portable coolers (4 °C) to minimize water loss due to evaporation and transported to the lab where leaves were removed from the bags. After cutting the leaf tips (5 cm), the remaining leaf portion (average length 15 cm) was cut in the middle to obtain two homogeneous pieces of similar weight, then mixed and stored in Falcon 50 ml Conical Centrifuge Tubes. One batch was used to measure OA following the “Rehydration method” (Babu et al. 1998). Leaves were re-hydrated in distilled water to full turgor (4 hours), then dried and stored in freezer (-20 °C).

After thawing, the cell sap was collected using a garlic press and 10 μl were micropipetted and placed onto a paper sample disc covering the sampling cuvette of a vapor pressure osmometer (Wescor 5520) previously calibrated using the 290, 1000 and 100 mmol kg^{-1} standards. After each measurement, the osmometer cuvette was cleaned using deionized water. Finally, the resulting osmolality (mosmol kg^{-1}) was converted to osmolarity (MPa) using the following formula: ψ_s (MPa) = - c (mosmol kg^{-1}) $\times 2.58 \times 10^{-3}$ (Bajji et al. 2001) and osmotic adjustment (OA) was evaluated as the difference between the ψ_s at full turgor in control and in stressed conditions: ψ_s (control) - ψ_s (stress). The other batch was used to measure RWC. Fresh leaves were weighed (FW) then submerged in distilled water in the Falcon tubes and stored at 4 °C for rehydration overnight (ten hours). Rehydrated leaves were wiped thoroughly with blotting paper and weighed (TW). Then leaves were oven-dried at 65 °C for three days prior to measuring the dry weight (DW). In the end, RWC values were computed as follows: $[(\text{FW}-\text{DW})/(\text{TW}-\text{DW})] \times 100$ (Barrs, 1968) (Figure 4).

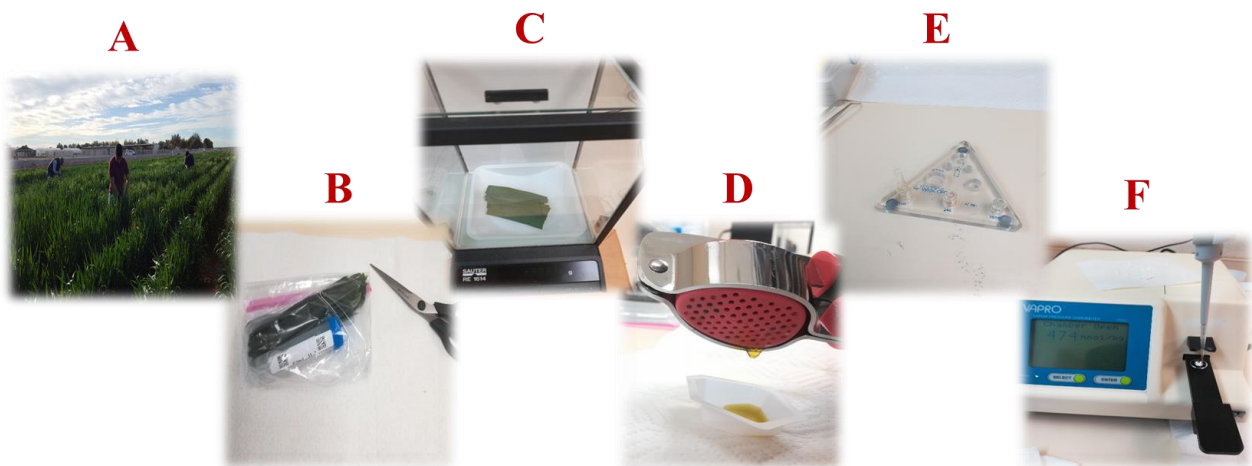


Figure 4 | Major “Rehydration method” steps for osmotic adjustment (OA) and relative water content (RWC) in Maricopa Agricultural Center (MAC). A) Sampling of eight fully expanded homogeneous flag leaves before dawn for each replicate of the durum panel for OA and RWC measurements. B) Package of the leaves one over the others and cutting of the tips. The remaining

leaf parts (15 cm long) were cut in the middle to obtain two homogeneous pieces of similar weight, then mixed and inserted in Falcon 50 ml Conical Centrifuge Tubes. C) One of the three weight measurements of the leaf samples for RWC using precision balances. D) Collection of leaf cell sap for OA analysis using a garlic press. E) Calibration with sodium chloride solution of increasing concentration. F) Extraction of leaf cell sap (10 μ l) using a pipette and insertion onto a paper disc placed on the sampling cuvette of the Wescor 5520 osmometer.

Additional drought adaptive traits

Leaf movements are common adaptive responses to drought stress in plants (Begg, 1980; Ehleringer and Forseth, 1980). Many species are able to reduce the quantity of radiation that they intercept when suffering from drought either by leaf folding (LF) or by leaf rolling (LR). In this study, LR was visually estimated under drought conditions in two years (2017-18). The evaluation was carried out at early milk (GS71) at midday with a score from 0 (no leaf rolling) to 9 (all leaves severely rolled) when the majority of the Durum Panel leaves showed a LR > 5.

The accessions were investigated for the chlorophyll content under drought at GS71 for two consecutive years (2017-18) based on Soil-Plant Analysis Development (SPAD) estimates obtained with a non-destructive chlorophyll meter SPAD-502Plus (Konica Minolta Sensing, Inc., Japan) as an indicator of leaf chlorophyll content status.

The cuticular wax phenotype on the flag leaves (WAXL) and spikes (WAXS) was estimated at GS71 under drought conditions in 2017 (100 DAP) and 2018 (120 DAP) in relation to the well-known association with drought tolerance in wheat (Guo et al. 2016). The visual evaluation was carried out at midday using a score from 0 (wax absence) to 9 (wax accumulation).

Significant differences in phenological growth stages were detected among cultivars during the trials. Phenology was evaluated for three consecutive years (2017-19) using the Zadoks scale (Zadoks et al. 1974), from which flowering time (FT) scores were obtained and used to adjust the genetic analyses. In parallel, the plant height (PH) of the accessions was monitored constantly on progressive growing stages.

Dry biomass

At the end of the first two seasonal field trials (2017-18), the plots were harvested with a mechanical machine (Carter mfg equipment). A number of plants were manually collected and placed directly in a drying oven at 60 °C for dry biomass (DB) estimation (kg/ha). At the end of the third seasonal field trial (2019), the harvest was carried out including two replicates; three plants per genotype were manually collected for the east (WW) and west (WL) rows and transferred to an oven at 60 °C for DB estimation (g/m²). As mentioned before, the plants were harvested in advance (GS71) to allow for planting the next phenotyping experiment and therefore the dry biomass represented the status at a point in time rather than direct estimates of final yields.

Statistical analysis

Each of the investigated raw phenotypic data, mentioned above, was optimized using *lme4* package (*R-project*) and custom *R* scripts to conduct a spatial adjustment analysis. A mixed procedure was carried out including row and column random effects and a moving mean of two. Heritability (h^2) values were also calculated in *R-project*, while the Pearson correlation r coefficients as well as the normal distributions were generated using Genstat 19 software (Payne, 2009).

Genetic analysis: SNP genotyping, population structure and GWAS model

The Durum panel genomic DNA was extracted using the NucleoSpin® 8/96 Plant II Core Kit from Macherey Nagel and sent for SNP genotyping to TraitGenetics (<http://www.traitgenetics.com/en/>).

The Illumina iSelect 90K wheat SNP assay (Wang et al. 2014) was used and genotype calls were acquired as reported in Maccaferri et al. (2015b). Markers were assigned on the basis of the tetraploid wheat consensus map reported in Maccaferri et al. (2015a). Haploview 4.2. software (Barrett et al. 2005) was used to calculate the Linkage Disequilibrium (LD) among markers for A and B genomes and only Single Nucleotide Polymorphisms (SNPs) with minor allele frequency (MAF) > 0.05 were considered. LD decay pattern as result of consensus genetic distances was inspected considering squared allele frequency correlation (r^2) estimates from all pairwise comparisons among intra-chromosomal SNPs in TASSEL (Trait Analysis by aSSociation, Evolution and Linkage) software v. 5.2.37. The Hill and Weir formula (Hill and Weir, 1988) was used in *R-project* to define the confidence interval (CI) for QTL in accordance with the curve fit and the distance at which LD decays below r^2 0.3 (Liu et al. 2017).

Haploview 4.2 tagger function set to $r^2 < 1.0$ was used to calculate a Kinship matrix (K) of genetic relationships among individual accessions of the durum panel with all non-redundant 7,723 SNP markers. Kinship based on Identity-by-State (IBS) among accessions was obtained in TASSEL. In addition, a subset of non-redundant 2,382 SNP markers ($r^2 < 0.5$) was used to evaluate the population structure (Q) in STRUCTURE software 2.3.4. (Pritchard et al. 2000) using the corresponding tagger function in Haploview 4.2 (Barrett et al. 2005). Numbers of hypothetical subpopulations ranging from $k = 2$ to 10 were assessed using 50,000 burn-in iterations followed by 100,000 recorded Markov-Chain iterations in five independent runs for each k in order to estimate the sampling variance (robustness) of population structure inference. Then the rate of change in the logarithm of the probability of likelihood [LnP(D)] value between successive k values was considered (Δk statistics, Evanno et al. 2005) together with the rate of variation (decline) in number of accessions clearly attributed to subpopulations (accessions with Q membership's coefficient ≥ 0.5). Finally, the level of differentiation among subpopulations was measured using the Fixation Index (F_{st}) among all possible population pairwise combinations (Condoirelli et al. 2018).

Subsequently, 17,721 SNP markers with $MAF > 0.05$, imputed with LinkImpute (LDkNNi) (Money et al. 2015), were used for GWAS-Mixed Linear Model (MLM) (Yu et al. 2006; Bradbury et al. 2007) in TASSEL. MLM was specified as follows: $y = X\beta + Zu + e$ (Zhang et al. 2010), where y is the phenotype value, β is the fixed effect due to marker and u is a vector of random effects not accounted for by the markers; X and Z are incidence matrices that related y to β and u while e is the unobserved vector of random residual. In this study, both Kinship matrix (K) and Structure Population (Q) were included as random effects in the model (MLM-Q+K) while flowering time was included as a covariate taking into account GWAS QQ-plot results. Then P values and R^2 effects were analyzed and QTL significance was determined as follows: “highly significant” for P value < 0.0001 and “significant” for P value < 0.001 .

RESULTS

Population Structure

The Durum Panel showed a clear population genetic structure as reported in previous analyses (Maccaferri et al. 2011; Letta et al. 2013; Liu et al. 2017). I investigated the number of optimal k subpopulations, from two to eight, on 248 elite Durum Panel accessions. The analysis indicated an optimal number of eight ($k = 8$) subpopulations on the basis of pairwise comparisons among and within subgroups with 155 accessions (62.5%) clearly grouped into one of the eight main gene pools at a Q membership coefficient ≥ 0.5 , while the remaining 93 were considered as admixed. Subgroup S1 corresponded to native Mediterranean and North African germplasm. Subgroup S2 included germplasm specifically bred for dryland areas at ICARDA (Syria) from the early 1970s. Subgroup S3 included Spanish and Moroccan cultivars from early 1970s, and CIMMYT and ICARDA selections for temperate areas. Subgroup S4 mostly included ICARDA high-yielding lines/cultivars for temperate areas and contemporary (1970s) Italian accessions obtained from cultivar Creso, an important Italian founder also related to CIMMYT materials. Subgroup S5 included accessions derived from widely adapted (photoperiod insensitive) CIMMYT germplasm released in the late 1970s to early 1980s. Subgroup S6 included accessions from the mid-1970s breeding program in Italy (Valnova group) while subgroup S7 included accessions from the high-yielding CIMMYT germplasm released in the late 1980s to early 1990s (founders Altar84 and Gallareta). Finally, subgroup S8 (founders Edmore and Neodur) showed the widest within-group variation (40 accessions), as expected based on the concomitant presence within the same genetically highly homogeneous group of conventional plant height accessions from the Northern Plains of the US and Canada and semidwarf (*RhtB1b*) accessions from France and Australia.

The division into eight subpopulations was supported by pairwise comparisons among and within subgroups based on the Fixation Index (F_{st}) which provides a measure of subpopulation diversity

and by Neighbor Joining tree (Saitou and Nei, 1987; Figure 5). High genetic diversity was detected between the old Italian cultivars (S1) and the modern French, North American, Canadian and Australian cultivars (S8), while a considerable admixture among subgroups characterized the ICARDA, CIMMYT, and Italian groups. As a further note, only a relatively small portion of the molecular variation was accounted for by the origin of the accessions, as expected based on the high exchange rate of germplasm among breeding programs.

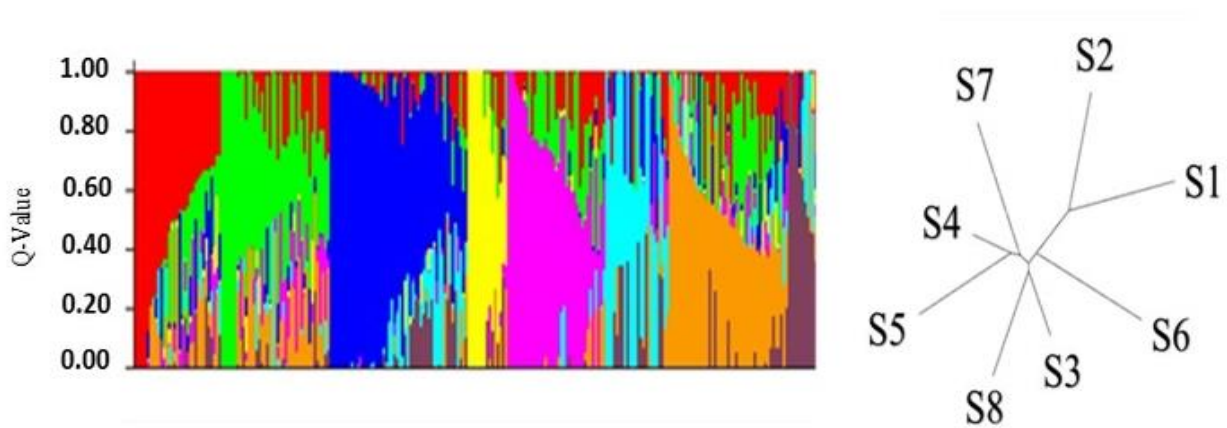


Figure 5 | Bar plot and Neighbor Joining tree show the eight ($k = 8$) subpopulations on the basis of pairwise comparisons among and within subgroups (S1-S8). A total of 155 accessions (62.5%) clearly grouped into one of the eight main gene pools at a Q membership coefficient ≥ 0.5 , while the remaining 93 were considered as admixed.

Chlorophyll fluorescence imaging (CFI) by the “Lemnatec” field scanalyzer

The PSII values captured by LFS under progressive drought (71, 97, 102 and 106 DAP) were normally distributed and showed a heterogeneous heritability (h^2) ranging from 0.00 (DAP: 97) to 64.0 (DAP: 106) (Table 2). Additionally, a decreased trend of PSII values from 71 DAP to 106 DAP was observed (Figure 6). Concerning the Pearson correlation coefficients (r) with other

drought adaptive traits, PSII (DAP: 106) significantly correlated with IRT (DAP: 91) ($r = -0.37$) and IRT (DAP: 98) ($r = -0.34$) acquired by UAV-RedEdge, contrary to IRT (DAP: 94) ($r = -0.02$) acquired by tractor. PSII (DAP: 102) and PSII (DAP: 106) were more positively correlated with NDVI (DAP: 91) by UAV-Sequoia ($r = 0.31$ and $r = 0.46$ respectively) than NDVI (DAP: 94) by tractor ($r = 0.27$ and $r = 0.40$ respectively). Moreover, PSII data showed a weak positive correlation with $Fr1'/Fm'$ (DAP: 115) ($r = 0.11$ and $r = 0.15$) and $Fr2'/Fm'$ (DAP: 115) ($r = 0.10$ and $r = 0.19$) acquired in light hours by the manually pushed cart.

Table 2 | Summary statistics for the drought adaptive traits in 2019: photosystem II (PSII) data (71-106), osmotic adjustment (OA), delta (Δ) for relative water content (RWC), dry biomass (DB) and plant height (PH) on different days after planting (DAP) in a panel of 215 durum wheat elite advanced lines and cultivars.

Trait (2019)	Min.	Max.	Average	St.dev.	h^2
PSII (DAP: 71)	0.00	0.04	0.03	0.00	17.0
PSII (DAP: 97)	0.01	0.04	0.03	0.00	0.00
PSII (DAP: 102)	0.01	0.04	0.02	0.00	36.0
PSII (DAP: 106)	0.00	0.04	0.02	0.00	64.0
OA (DAP: 95)	0.00	0.57	0.26	0.13	74.8
Δ RWC (DAP: 95)	0.01	8.24	1.91	1.76	30.0
Δ DB (g/m²) (DAP: 107)	-45.92	348.5	124.1	71.99	15.0
Δ PH (cm) (DAP: 102)	0.00	18.66	8.60	3.14	27.0

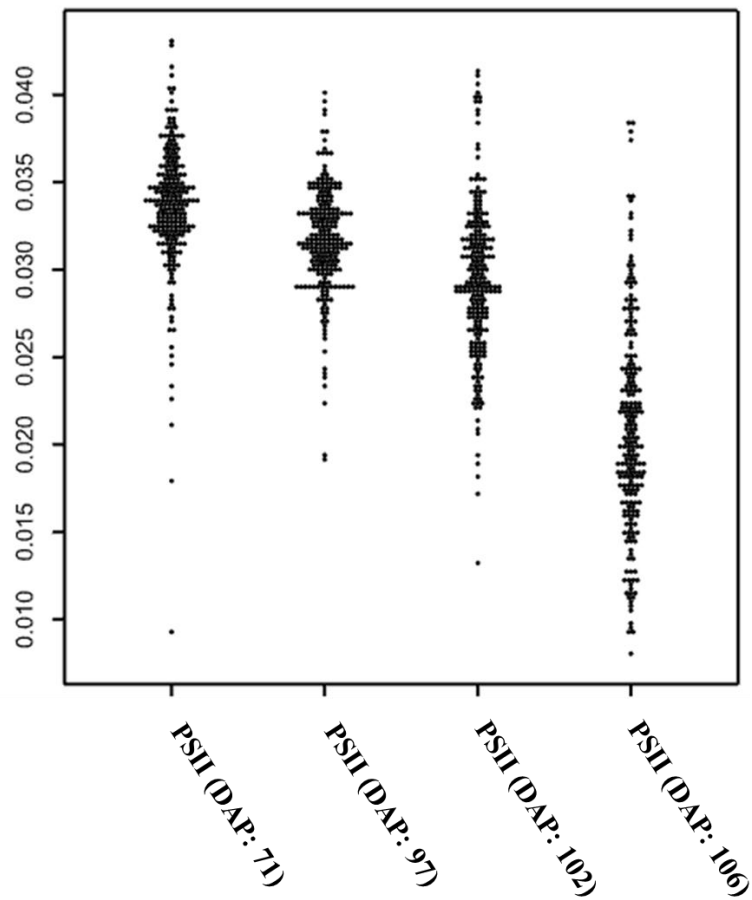


Figure 6 | The decreased trend of PSII values from 71 DAP to 106 DAP. The data were acquired in darkness under progressive drought by the “Lemnatec” field scanalyzer (LFS).

NDVI and IRT values by UAV and ground-based platforms

NDVI was captured in multiple dates: 55 and 77 DAP (pre-anthesis) as well as 83 and 91 DAP (post-anthesis) by UAV-Sequoia; 91 and 98 DAP (post-anthesis) by UAV-RedEdge; 58 and 76 DAP (pre-anthesis) as well as 84 and 94 DAP (post-anthesis) by tractor-GreenSeeker. NDVI values were normally distributed and h^2 ranged from 77.2 to 87.3 (UAV-Sequoia), 80.0 and 88.6 (UAV-RedEdge) and 61.1 and 67.5 (tractor-GreenSeeker) (Table 3 and Figure 7). In addition, a temporal

trend of increased NDVI values was observed in response to the field conditions of progressive drought severity and phenological development. Concerning the Pearson correlation coefficients (r), NDVI by UAVs (91 DAP) positively correlated with NDVI by tractor (94 DAP) with r from 0.49 to 0.60. In addition, OA and Δ RWC measured in 2018 more positively correlated with NDVI (DAP: 91) by UAV-Sequoia ($r = 0.37$ and $r = -0.40$) than NDVI (DAP: 94) by tractor-GreenSeeker ($r = 0.25$ and $r = -0.31$).

As with NDVI, IRT was captured in multiple times: 91 and 98 DAP by UAV-RedEdge as well as 58, 76, 84 and 94 DAP by tractor-GreenSeeker. IRT showed a progressive increased trend in response to the progressive drought severity. The IRT values were normally distributed while h^2 were higher using UAVs ($72.2 < h^2 < 77.3$) than the tractor ($25.8 < h^2 < 47.0$) (Table 3). Concerning the Pearson correlation coefficients (r), IRT by UAV (91 DAP) weakly correlated with IRT by tractor (94 DAP) with r of 0.19. In addition, IRT and NDVI by UAV-RedEdge (DAP: 91) were more negatively correlated ($r = -0.57$) than by tractor-GreenSeeker (DAP: 94) ($r = -0.26$).

Table 3 | Summary statistics for the drought adaptive traits in 2017: normalized difference vegetation index (NDVI), infrared thermography (IRT), carbon isotope discrimination in well-watered ($\delta^{13}C-c$) and water-limited ($\delta^{13}C-s$) conditions, leaf chlorophyll content (SPAD), leaf rolling (LR), wax leaf (WAXL), wax spike (WAXS) and dry biomass (DB) on different days after planting (DAP) in a panel of 248 durum wheat elite advanced lines and cultivars.

Trait (2017)	Min.	Max.	Average	St.dev.	h^2
NDVI-UAV/S (DAP: 55)	0.40	0.63	0.54	0.01	77.2
NDVI-UAV/S (DAP: 77)	0.66	0.81	0.74	0.03	83.9

NDVI-UAV/S (DAP: 83)	0.64	0.79	0.71	0.03	88.5
NDVI-UAV/S (DAP: 91)	0.84	0.91	0.87	0.03	87.3
NDVI-UAV/RE (DAP: 91)	0.78	0.87	0.82	0.02	80.0
NDVI-UAV/RE (DAP: 98)	0.64	0.84	0.77	0.03	88.6
IRT-UAV/RE (DAP: 91)	36.6	41.96	40.0	0.86	72.2
IRT-UAV/RE (DAP: 98)	28.5	32.27	30.6	0.69	77.3
NDVI-tractor (DAP: 58)	0.30	0.42	0.36	0.02	61.1
NDVI-tractor (DAP: 76)	0.54	0.70	0.64	0.02	66.3
NDVI-tractor (DAP: 84)	0.63	0.75	0.69	0.03	66.9
NDVI-tractor (DAP: 94)	0.58	0.73	0.66	0.02	67.5
IRT-tractor (DAP: 58)	19.46	22.91	20.90	0.49	35.6
IRT-tractor (DAP: 76)	20.36	22.39	21.22	0.35	28.0
IRT-tractor (DAP: 84)	29.59	32.24	30.68	0.47	25.8
IRT-tractor (DAP: 94)	25.42	28.92	26.99	0.54	47.0
$\delta^{13}\text{C-c}$ (DAP: 85)	-2.00	1.20	-0.28	0.57	86.7
$\delta^{13}\text{C-s}$ (DAP: 93)	-27.6	-24.7	-26.29	0.52	70.0
SPAD (DAP: 100)	35.3	53.6	45.90	3.04	87.5
LR (DAP: 100)	1.00	8.00	4.45	1.44	40.4
WAXL (DAP:100)	0.00	8.00	5.66	1.18	71.5
WAXS (DAP:100)	0.00	8.25	5.56	2.17	98.3
DB (kg/ha) (DAP: 104)	1,887	3,697	2,674	285.4	63.5

Stop irrigation (DAP: 86)

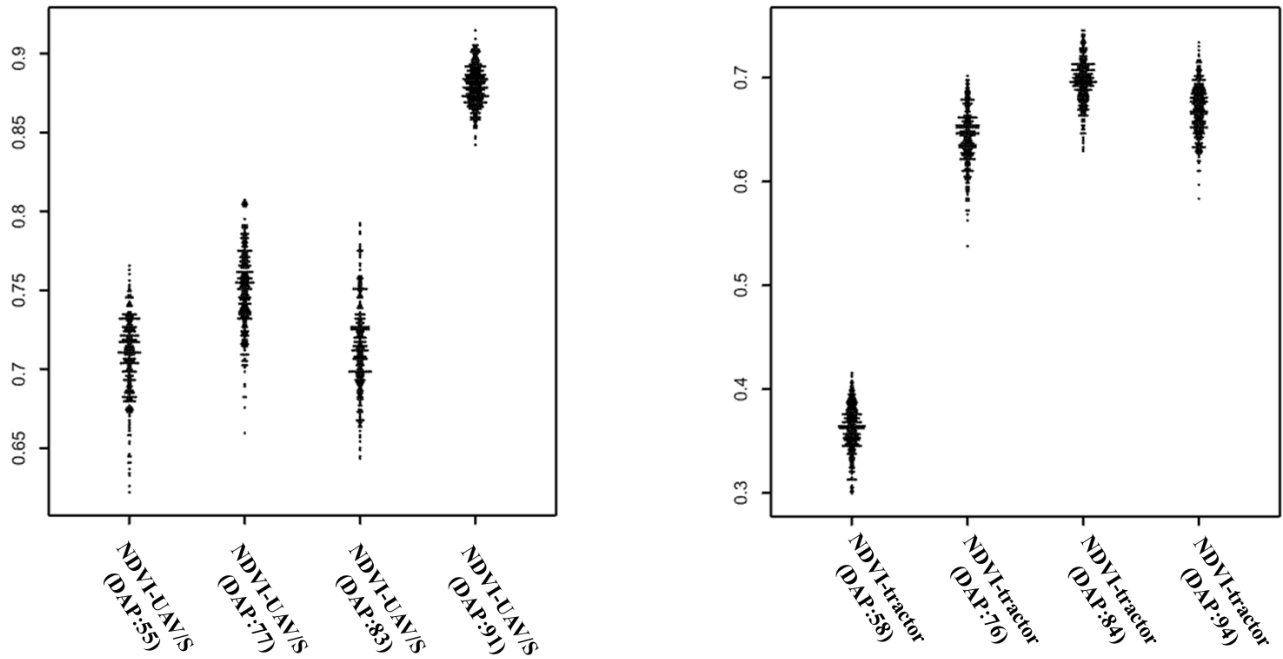


Figure 7 | The temporal trend of increased NDVI values captured on different days after planting (DAP) by UAV-Sequoia and tractor-GreenSeeker under field conditions of progressive drought severity.

Chlorophyll fluorescence (ChlF) by the manually pushed cart

In the second year, the LIFT sensor provided active chlorophyll fluorescence (ChlF) measurements (light hours) for the characterization of Fq'/Fm' as well as $Fr1'/Fm'$ and $Fr2'/Fm'$ photosynthetic traits at post-anthesis under well-watered (DAP: 103) and water-limited (DAP: 115) conditions. All traits were normally distributed; Fq'/Fm' showed a h^2 ranged from 22.5 to 44.9, $Fr1'/Fm'$ from 37.1 to 52.6 and $Fr2'/Fm'$ from 45.8 to 54.6. (Table 4). Fq'/Fm' (DAP: 115) negatively correlated with $Fr1'/Fm'$ (DAP: 115) ($r = -0.30$) but not with $Fr2'/Fm'$ (0.03), while $Fr1'/Fm'$ and $Fr2'/Fm'$ positively correlated ($r = 0.81$). In addition, Fq'/Fm' showed a weak positive correlation with OA ($r = 0.18$), ΔRWC ($r = 0.25$) and DB ($r = 0.21$) measured in 2018. $Fr1'/Fm'$ and $Fr2'/Fm'$ (DAP:

115) showed a weak negative correlation with DB ($r = -0.28$ and -0.26 respectively), but positive with NDVI by UAVs: $r = 0.26$ and 0.27 (RedEdge) and $r = 0.21$ and 0.22 (Sequoia) respectively.

Table 4 | Summary statistics for the drought adaptive traits in 2018: Fq'/Fm' , $Fr1'/Fm'$ and $Fr2'/Fm'$ captured by a manually pushed cart, infrared thermography (IRT), osmotic adjustment (OA), relative water content in well-watered (RWC-c) and water-limited (RWC-s) conditions, leaf chlorophyll content (SPAD), leaf rolling (LR), plant height (PH), wax leaf (WAXL), wax spike (WAXS) and dry biomass (DB) on different days after planting (DAP) in a panel of 248 durum wheat elite advanced lines and cultivars.

Trait (2018)	Min.	Max.	Average	St.dev.	h^2
<i>Fq'/Fm'</i> (DAP: 103)	0.39	0.58	0.50	0.03	44.9
<i>Fr1'/Fm'</i> (DAP: 103)	0.19	0.26	0.23	0.01	37.1
<i>Fr2'/Fm'</i> (DAP: 103)	0.57	0.67	0.63	0.01	45.8
<i>Fq'/Fm'</i> (DAP: 115)	0.19	0.43	0.31	0.04	22.5
<i>Fr1'/Fm'</i> (DAP: 115)	0.26	0.36	0.30	0.02	52.6
<i>Fr2'/Fm'</i> (DAP: 115)	0.59	0.74	0.68	0.02	54.6
IRT (UAV) (DAP: 112)	32.7	37.5	35.1	0.78	55.0
IRT (UAV) (DAP: 120)	38.4	41.8	40.0	0.65	52.9
OA (DAP: 119)	0.38	1.49	0.95	0.22	72.3
RWC-s (DAP: 119)	45.2	76.8	62.1	7.10	78.2
RWC-c (DAP: 104)	89.9	101.3	95.6	1.56	28.7
SPAD (DAP: 120)	31.9	48.8	42.0	3.21	75.7
LR (DAP: 120)	2.86	9.60	6.13	1.52	83.5

PH (DAP: 120)	54.5	116	75.1	9.30	65.0
WAXL (DAP: 120)	0.00	9.00	6.72	1.26	73.0
WAXS (DAP: 120)	0.00	9.00	5.77	1.75	75.1
DB (k/ha) (DAP: 125)	3,789	7,022	5,208	547.7	50.7

Stop irrigation (DAP: 103)

Physiological drought adaptive traits

$\delta^{13}\text{C-c}$ values (85 DAP, well-watered conditions) ranged from -2.00 to 1.20 with a h^2 of 86.7, while $\delta^{13}\text{C-s}$ values (93 DAP, drought) ranged from -26.6 to -24.7 with a h^2 of 70.0. Concerning the Pearson correlation coefficients (r), $\delta^{13}\text{C-s}$ more positively correlated with NDVI values by UAVs ($0.19 < r < 0.38$) than NDVI by GreenSeeker-Tractor ($0.08 < r < 0.21$) as well as with PSII data ($0.07 < r < 0.36$).

In 2017, the cessation of irrigation resulted in a progressive lowering of the leaf RWC for the four tested varieties (Gallareta, Karim, Mexicali 75 and Svevo) from 94 DAP ($68\% < \text{RWC} < 77\%$) to 101 DAP ($50\% < \text{RWC} < 62\%$). In 2018, the Durum Panel was totally investigated for OA ($h^2 = 72.3$), RWC-c ($h^2 = 28.7$) and RWC-s ($h^2 = 78.2$). OA values ranged from 0.38 to 1.49 MPa; RWC-c values ranged from 89.9 to 100% while RWC-s values from 45.2 to 76.9% by indicating severe drought conditions. In 2019, OA values ($h^2 = 74.8$) ranged from 0.0 to 0.57 MPa while ΔRWC values ($h^2 = 30.0$) from 0.0 to 8.24% by indicating a moderate drought conversely to the first two years (2017-18).

In 2018, the severe drought conditions induced a high positive correlation between OA and RWC-s ($r = 0.78$) due to the active physiological role of the osmolytes to maintain a more favorable water status and avoid the negative effects of water loss in stress (Figure 8).

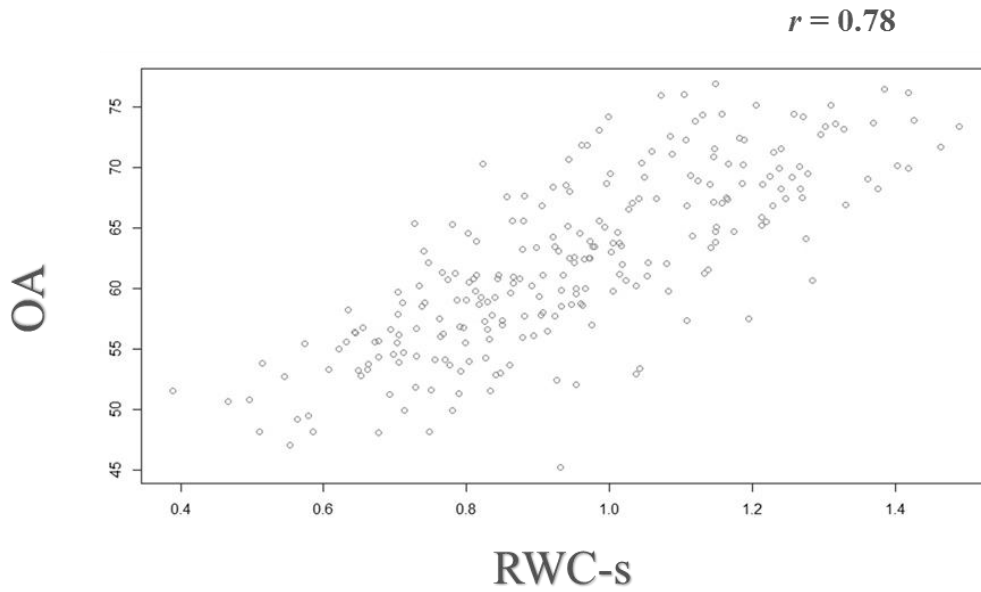


Figure 8 | The scatter plot shows the positive correlation between OA and RWC-s ($r = 0.78$) due to the physiological capacity of the osmolytes to avoid the negative effects of water loss on flag leaves under drought.

Additional drought adaptive traits

LR measured in 2017 ($h^2 = 40.4$) and 2018 ($h^2 = 83.5$) years revealed a normal distribution and a significant positive relationship ($r = 0.55$). LR ranged from 1.00 to 8.00 in the first year, while ranged from 2.86 to 9.60 in the second year. A negative correlation was observed between LR and OA ($r = -0.25$) as well as RWC-s ($r = -0.30$) measured in 2018.

Chlorophyll content (SPAD) measured in 2017 ($h^2 = 84.5$) and 2018 ($h^2 = 75.7$) years revealed a normal distribution and a significant relationship ($r = 0.58$). SPAD ranged from 35.3 to 53.6 in the first year, while ranged from 31.95 to 48.84 in the second year. Concerning the Pearson correlation coefficient (r), SPAD values positively correlated for both years ($r = 0.58$). WAXL measured in 2017 ($h^2 = 71.5$) and 2018 ($h^2 = 73.0$) revealed a more significant relationship ($r = 0.67$) than

WAXS measured in 2017 ($h^2 = 98.3$) and 2018 ($h^2 = 75.1$) with a r of 0.54. Considering both traits, WAXL and WAXS were positively associated ($r = 0.23$) in 2017 and ($r = 0.57$) in 2018.

Dry biomass

The dry biomass (DB) values showed normal distributions in 2017 ($h^2 = 63.5$) and 2018 ($h^2 = 50.7$): DB ranged from 1887 to 3697 k/ha in the first year, while from 3789 to 7022 k/ha in the second year. Considering both years, DB revealed a positive relationship ($r = 0.25$). In 2019, Δ DB ($h^2 = 15$) ranged from -45.2 to 348.5 g/m² showing a normal distribution and a low association with DB values of the two years before ($r = 0.14$).

In 2017, DB significantly correlated with NDVI ($r = 0.25$) and IRT ($r = -0.34$) by tractor on 94 DAP ($r = 0.25$). In 2018, DB significantly correlated with photosynthetic traits: Fq'/Fm' ($r = 0.21$), $Fr1'/Fm'$ ($r = -0.28$) and $Fr2'/Fm'$ ($r = 0.25$) and was influenced by flowering time (FT) with a r of -0.27. In 2019, Δ DB did not reveal significant relationships with the other investigated traits in moderate drought.

Genetic analysis

The QTL confidence interval (CI) was determined on the basis of the average genetic distance at which LD decayed below r^2 of 0.3 (Hill and Weir, 1988). The inter-marker genetic distance of the Durum Panel corresponded to 2.12 cM (CI = ± 1.06 cM) (Figure 9). The use of flowering time (FT) as covariate for the GWAS analysis reduced the genetic effects of the photoperiod/vernalization in durum wheat (Figure 10).

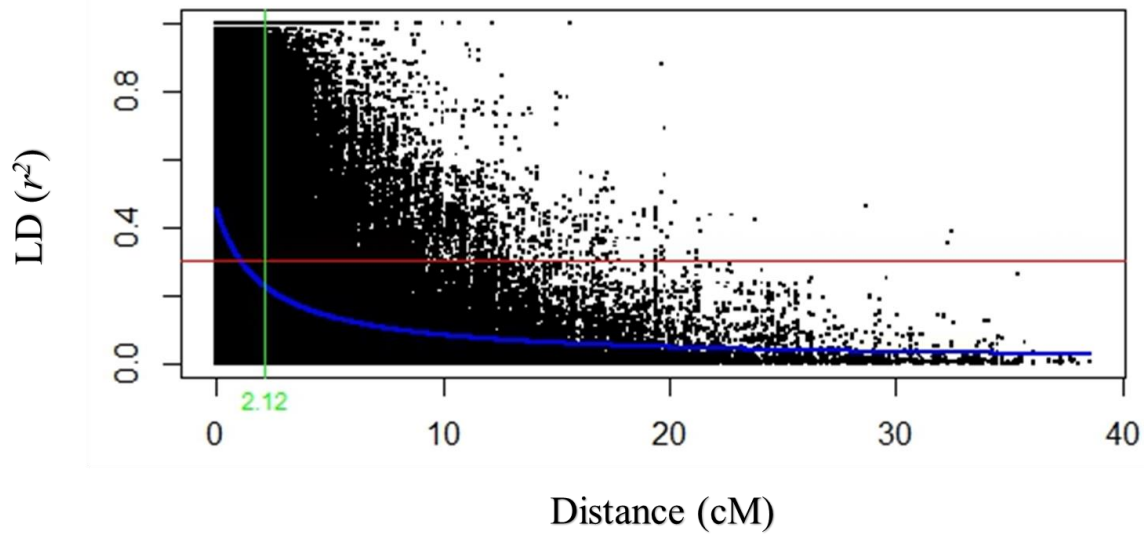


Figure 9 | The rate of linkage disequilibrium (LD) decay of the 248 durum wheat elite accessions (Durum Panel). The Hill and Weir formula (Hill and Weir, 1988) was used to describe the LD decay of r^2 . The LD among Single Nucleotide Polymorphism (SNP) markers in the panel was estimated using Haploview 4.2 (Barrett et al. 2005). The blue curve represents the model fit to LD decay (nonlinear regression of r^2 on distance). A confidence interval of 2.12 cM for the quantitative trait loci (QTL) is showed when LD (r^2) is 0.3 (red line).

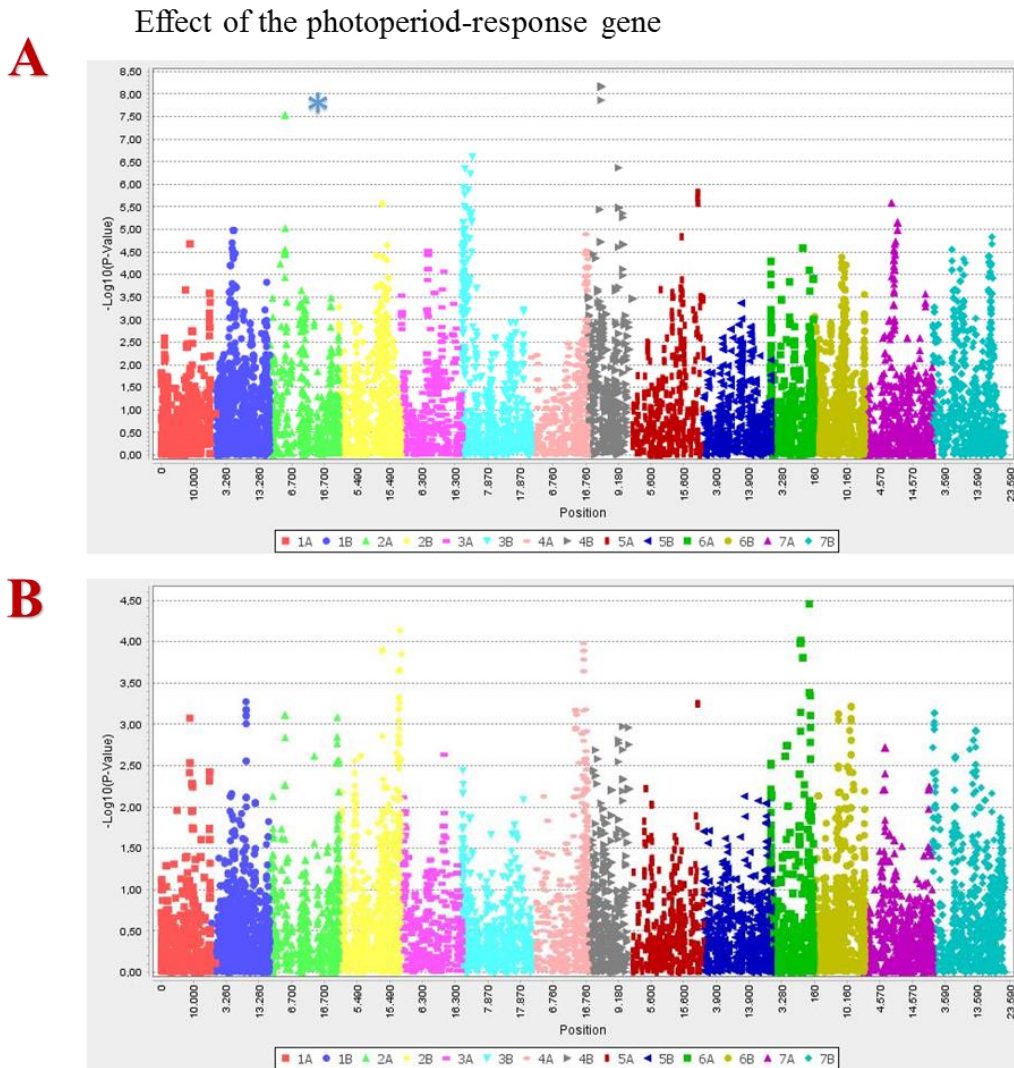


Figure 10 / Manhattan plot of the GWAS analysis for one of the investigated drought adaptive traits, osmotic adjustment (OA), using two different Mixed Linear Models (MLM) approaches: A) MLM with K (Kinship matrix), B) MLM with K (Kinship matrix) and Q (Population structure) including flowering time (FT) as covariate. MLM-Q+K using FT reduced the effect of the photoperiod-response gene on chr. 2A.

Chlorophyll fluorescence imaging (CFI) by the “Lemnatec” field scanner

The GWAS detected thirteen PSII QTL by LFS under progressive moderate drought (71, 97, 102 and 106 DAP). In detail, two loci were detected on 71 DAP on chromosome 1A ($r^2 = 5.4$ and $r^2 = 7.2$). Three QTL were detected on 97 DAP on 1AL ($r^2 = 5.7$), 3BL ($r^2 = 5.7$) and 4BS ($r^2 = 5.0$). Four QTL were detected on 102 DAP on 2AS ($r^2 = 4.3$), 2BL ($r^2 = 3.3$), 4BL ($r^2 = 4.3$) and 7AS ($r^2 = 3.2$). Four QTL were detected on 106 DAP on 1BL ($r^2 = 3.1$), 2AL ($r^2 = 3.9$), 2BS ($r^2 = 2.9$) and 5AL ($r^2 = 3.0$) (Table 5).

Table 5 | List of QTL positions only for log P value > 3.00, for PSII traits on four different days after planting (71, 97, 102 and 106 DAP) according to the tetraploid consensus map of Maccaferri et al. (2015a).

2019								
TRAIT	DAP	Marker	Chr.	Pos. (cM)	Log P value	R ²	Allele	Effect
<i>PSII 2.03.2019</i>	71	<i>IWA60</i>	1A	9.8	3.1	5.4	A/C	-0.005
		<i>IWB72161</i>	1A	120.0	4.0	7.2	A/G	-0.002
<i>PSII 28.03.2019</i>	97	<i>IWB12579</i>	1A	99.8	3.6	5.7	G/T	0.002
		<i>IWB8716</i>	3B	87.1	3.6	5.7	C/T	-0.004
		<i>IWB63894</i>	4B	12.8	3.2	5.0	C/T	-0.002
<i>PSII 02.04.2019</i>	102	<i>IWB40869</i>	2A	21.9	3.4	4.3	C/T	-0.004
		<i>IWB46532</i>	2B	119.9	3.0	3.3	C/T	0.005
		<i>wPt-6209</i>	4B	75.7	3.7	4.3	A/T	0.002
		<i>IWB319</i>	7A	82.2	3.0	3.2	A/G	-0.004
<i>PSII 06.04.2019</i>	106	<i>IWA1889</i>	1B	79.2	3.2	3.1	A/G	0.003
		<i>IWB29388</i>	2A	197.6	3.9	3.9	C/T	0.007
		<i>wPt-5513</i>	2B	45.1	3.0	2.9	A/T	-0.003
		<i>IWA6573</i>	5A	101.9	3.0	3.0	C/T	-0.006

NDVI and IRT values by UAV and ground-based platforms

In the first year, the GWAS detected thirty-five NDVI QTL; eleven loci from UAV-Sequoia (77, 83 and 91 DAP), eight loci from UAV-RedEdge (91 and 98 DAP) as well as sixteen loci from tractor-GreenSeeker (76, 84 and 94 DAP). In total, nineteen QTL were identified exclusively with the UAV platforms while sixteen QTL were uniquely detected the tractor-mounted platform. Two major NDVI QTL consistently detected in drought from UAV-Sequoia (91 DAP) and -RedEdge (94 DAP), mapped on short arm of chromosome 6A at 5.1 cM ($3.36 < r^2 < 6.81$) and 21.4 cM ($3.63 < r^2 < 3.66$) on the tetraploid consensus map of Maccaferri et al. (2015a). An additional NDVI locus overlapped using UAV-RedEdge and tractor-GreenSeeker platforms on 6BS at 31.3 cM ($2.89 < r^2 < 4.78$). In total, the GWAS detected seventy-three IRT QTL. Three major loci were obtained from UAV platforms (91 and 98 DAP) and mapped on 2AS ($4.41 < r^2 < 6.51$), 4BL ($5.16 < r^2 < 7.52$) and 6BL ($4.44 < r^2 < 5.12$). An overlapping was observed between a major locus consistently detected in drought from IRT-RedEdge (98 DAP) and IRT-GreenSeeker (94 DAP) which mapped on 4BS at 32.7 ($6.27 < r^2 < 9.64$) (Table 6). In the following year, five IRT QTL from UAV-RedEdge platform were mapped on 1BS and 7BL (112 DAP) as well as 1BL, 5BS and 6BL (120 DAP). The confidence interval of these loci did not overlap among them and among IRT QTL of the previous year.

Table 6 | List of QTL positions, only for log P value > 4.00, for IRT and NDVI by UAV- (UAVr: RedEdge) or ground-based platform (TRA) on different days after planting (DAP) according to the tetraploid consensus map of Maccaferri et al. (2015a).

2017								
TRAIT	DAP	Marker	Chr.	Pos. (cM)	Log P value	R ²	Allele	Effect
<i>IRT-TRA (24.03.2017)</i>	94	<i>IWB6937</i>	4A	64.0	4.79	7.46	A/G	-0.023
		<i>IWB7508</i>	4B	32.7	4.13	6.27	C/T	-0.347
		<i>IWB73541</i>	5A	151.2	4.64	7.20	G/T	-0.463
		<i>IWB10994</i>	5B	10.1	5.16	8.15	C/T	-0.329
		<i>IWA5784</i>	5B	48.9	4.17	6.34	A/G	-0.532
		<i>IWB2550</i>	5B	60.1	4.07	6.17	C/T	-0.552
		<i>IWA4641</i>	5B	84.7	5.02	7.88	C/T	0.371
<i>IRT-UAVr (21.03.2017)</i>	91	<i>IWB1996</i>	2A	46.6	4.25	6.51	A/G	-0.731
		<i>IWB6062</i>	3B	2.4	4.02	6.11	A/G	-0.881
		<i>IWB1757</i>	3B	32.0	4.24	6.49	A/C	0.583
<i>IRT-UAVr (28.03.2017)</i>	98	<i>IWB57483</i>	1A	50.4	4.50	6.56	A/G	0.750
		<i>IWB14601</i>	1A	70.7	5.15	7.68	A/G	-0.865
		<i>IWA5273</i>	2A	108.9	4.28	6.19	C/T	0.478
		<i>IWB32315</i>	2B	5.90	4.63	6.78	A/G	0.581
		<i>IWB27825</i>	3B	36.8	4.06	5.82	A/G	0.355
		<i>IWB8081</i>	4A	88.1	6.98	10.9	C/T	1.015
		<i>IWB53822</i>	4B	22.5	6.00	4.61	C/T	0.716
		<i>IWB7508</i>	4B	32.7	6.25	9.64	C/T	-0.530
		<i>IWB10342</i>	4B	83.1	6.99	10.9	C/T	0.992
		<i>IWB72121</i>	4B	92.9	5.06	7.52	C/T	-0.585
		<i>IWB68679</i>	5A	113.2	4.10	5.88	A/G	-0.339
		<i>IWB26265</i>	5A	147.1	4.13	5.92	C/T	0.672

		<i>IWA4238</i>	5A	178.3	7.73	12.3	A/C	-0.795
		<i>IWB73979</i>	5B	14.7	4.32	6.25	C/T	0.474
		<i>IWB44791</i>	7A	59.8	4.41	6.41	A/C	0.351
NDVI-TRA (06.03.2017)	76	<i>IWB57438</i>	2B	5.9	5.88	9.8	A/G	-0.030
NDVI-TRA (24.03.2017)	94	<i>IWB73476</i>	4A	22.2	4.08	5.28	C/T	0.013
		<i>IWB10727</i>	5A	141.0	4.24	5.52	A/C	0.013
NDVI-UAVr (21.03.2017)	91	<i>IWA7288</i>	6A	5.1	5.58	6.81	C/T	0.028
		<i>IWB66334</i>	6A	72.4	4.42	5.19	A/C	0.014
NDVI-UAVr (28.03.2017)	98	<i>IWA7288</i>	6A	5.1	4.45	3.67	C/T	0.037

Chlorophyll fluorescence (ChlF) by the manually pushed cart

Twenty-two QTL were identified for chlorophyll fluorescence (ChlF) using the LIFT sensor in the manually pushed cart. Two of these referred to Fq'/Fm' (115 DAP), nine to $Fr1'/Fm'$ (103 and 115 DAP) and eleven to $Fr2'/Fm'$ (103 and 115 DAP). In drought (115 DAP), a major Fq'/Fm' locus was detected on 3BS ($r^2 = 6.05$), two major $Fr1'/Fm'$ loci on 1BL ($r^2 = 4.85$) and 2BS ($r^2 = 4.93$) and a major $Fr2'/Fm'$ locus on 2AL ($r^2 = 4.91$). In addition, a QTL overlapping was observed between $Fr1'/Fm'$ and $Fr2'/Fm'$ on 1BL ($4.63 < r^2 < 4.85$) (Table 7).

Table 7 | List of QTL positions, only for log P value > 3.00, for *Fq'/Fm'*, *Fr1'/Fm'* and *Fr2'/Fm'* traits on two different days after planting (103 and 115 DAP) according to the tetraploid consensus map of Maccaferri et al. (2015a).

2018								
TRAIT	DAP	Marker	Chr.	Pos. (cM)	Log P value	R ²	Allele	Effect
<i>Fq'/Fm'</i> 23.03.2018	115	<i>IWB61293</i>	5A	96.6	3.1	4.99	A/G	-0.032
		<i>IWB72397</i>	7A	181.4	3.5	5.60	C/T	0.0062
<i>Fr1'/Fm'</i> 11.03.2018	103	<i>IWB9420</i>	1B	26.1	3.0	4.56	C/T	0.0091
		<i>IWB10653</i>	3B	24.6	3.8	6.05	C/T	-8.54E-03
		<i>IWA4842</i>	6A	66.9	3.1	4.74	A/G	-0.0151
		<i>IWB44978</i>	7B	108.6	3.9	6.21	A/G	-0.0120
<i>Fr1'/Fm'</i> 23.03.2018	115	<i>IWB70974</i>	1B	43.5	3.0	3.95	C/T	0.0060
		<i>IWB68093</i>	1B	158.0	3.6	4.85	A/G	-8.92E-03
		<i>IWB25893</i>	2B	63.1	3.6	4.93	A/G	0.0121
		<i>IWB71083</i>	6A	46.9	3.2	4.25	A/G	0.0066
		<i>IWB74123</i>	7A	7.2	3.1	4.10	C/T	-0.0178
<i>Fr2'/Fm'</i> 11.03.2018	103	<i>IWB59502</i>	3B	24.6	3.9	6.33	A/G	-0.0114
		<i>IWB71510</i>	3B	164.9	3.1	4.81	A/G	-0.0108
		<i>IWB60379</i>	6A	67.3	3.2	4.97	A/G	-0.0203
		<i>IWB30094</i>	3A	78.0	3.6	5.17	C/T	0.0396
		<i>IWB74726</i>	5A	52.9	3.0	4.26	A/G	-0.0129
<i>Fr2'/Fm'</i> 23.03.2018	115	<i>IWB69550</i>	1B	50.2	3.3	4.68	A/C	-0.0064
		<i>IWB68093</i>	1B	158.0	3.3	4.63	A/G	-7.13E-03
		<i>IWB62501</i>	2A	97.3	3.4	4.91	A/G	-0.0129
		<i>IWB71795</i>	3A	108.1	3.3	4.65	G/T	-9.57E-03
		<i>IWB8426</i>	3B	19.4	3.3	4.65	A/G	-8.48E-03
		<i>IWB56589</i>	5B	165.9	3.0	4.19	C/T	0.0087

Physiological drought adaptive traits

A single QTL was identified for $\delta^{13}\text{C-c}$ (85 DAP) on 1BS ($r^2 = 4.51$) while nine QTL for $\delta^{13}\text{C-s}$ (93 DAP) on 1BL (2), 2BL, 3AS, 4BL, 5AS (2), 6AS and 6BL. Two major $\delta^{13}\text{C-s}$ loci mapped on 5AS at 0.0 cM ($r^2 = 6.01$) and 6BL at 65.9 cM ($r^2 = 4.72$).

In 2018, fifteen QTL were identified for OA on 1AL, 1BL, 2AS, 2AL, 2BL (2), 4AL (2), 4BS, 5AL, 6AL (2), 6BS, 6BL and 7BS. In detail, three major loci mapped on 2BL at 185.8 cM ($r^2 = 4.37$), on 6AL at 91.2 cM ($r^2 = 4.23$) and at 117.1 cM ($r^2 = 4.78$) (Table 8). In the following year (2019), five QTL were identified for OA under moderate drought conditions (95 DAP). Specifically, two major loci mapped on 2BS at 8.3 cM ($r^2 = 6.27$) and on 2BL at 172 cM ($r^2 = 6.05$) (Table 9). The confidence interval of these OA loci did not overlap by comparing the two years.

In 2018, fifteen QTL were identified for RWC and, specifically, nine of them under drought (RWC-s, 119 DAP), while six under well-watered conditions (RWC-c, 104 DAP). In detail, two major QTL for RWC-s mapped on 4AL at 147.2 cM ($r^2 = 3.95$) and at 156.9 cM ($r^2 = 3.84$), while two major QTL for RWC-c mapped on 5BS at 7.2 ($r^2 = 5.85$) and at 48.9 ($r^2 = 8.22$) (Table 8). In the following year (2019), the GWAS detected five QTL for Δ RWC on 2AS, 4AS (2), 6BS and 7BL with a major locus on 6BS at 64.8 cM ($r^2 = 7.04$) (Table 9). Comparing both years, a significant RWC-QTL shared the confidence interval on 2AS at 9.4 cM ($2.86 < r^2 < 5.45$) in spite of the divergent drought severity conditions.

Table 8 | List of QTL positions, only for log P value > 3.00, for OA and RWC-s traits on 119 DAP (2018) according to the tetraploid consensus map of Maccaferri et al. (2015a).

2018								
TRAIT	DAP	Marker	Chr.	Pos. (cM)	Log P value	R ²	Allele	Effect
<i>OA</i>	119	<i>IWB27332</i>	1A	88.3	3.07	3.10	C/T	-1.55
		<i>IWB65251</i>	1B	93.3	3.17	3.19	C/T	-0.09
		<i>IWB34575</i>	2A	46.6	3.11	3.11	A/G	0.12
		<i>IWB39807</i>	2A	206.8	3.08	3.31	C/T	0.09
		<i>IWA2318</i>	2B	133.0	3.89	4.07	C/T	-0.11
		<i>WPT-0049</i>	2B	185.8	4.13	4.37	A/T	0.14
		<i>wPt-7289</i>	4A	136.8	3.15	3.17	A/T	0.09
		<i>IWB34029</i>	4A	161.7	3.88	4.06	C/T	1.25
		<i>IWB72203</i>	4B	28.8	3.00	2.48	A/C	0.07
		<i>IWB50381</i>	5A	198.8	3.24	3.28	A/G	0.15
		<i>WPT-2014</i>	6A	91.2	4.01	4.23	A/T	0.16
		<i>IWB70454</i>	6A	117.1	4.45	4.78	C/T	0.18
		<i>IWB33826</i>	6B	75.3	3.12	3.13	A/G	-0.10
		<i>IWB71722</i>	6B	114.3	3.21	3.24	A/G	-0.08
<i>WPT-3147</i>	7B	3.7	3.13	3.14	A/T	-0.09		
<i>RWC-s</i>	119	<i>IWB461</i>	1B	45.3	3.70	3.24	C/T	-4.29
		<i>IWB22184</i>	2A	9.4	3.33	2.86	A/G	-4.25
		<i>IWB66212</i>	4A	140.7	3.02	2.53	A/C	2.73
		<i>IWB56811</i>	4A	147.2	4.83	3.95	C/T	-5.51
		<i>IWB55093</i>	4A	156.9	4.27	3.84	A/G	5.24
		<i>IWA3449</i>	4A	161.7	3.90	3.45	C/T	4.66
		<i>IWA4603</i>	6A	117.7	3.39	2.92	A/G	3.15
		<i>IWA7962</i>	6B	78.8	3.04	2.56	A/G	-6.92
		<i>IWB71722</i>	6B	114.3	3.00	2.44	A/G	-2.46

Table 9 | List of QTL positions, only for log P value > 3.00, for OA and Δ RWC traits on 95 DAP (2019) according to the tetraploid consensus map of Maccaferri et al. (2015a).

2019								
TRAIT	DAP	Marker	Chr.	Pos. (cM)	Log P value	R ²	Allele	Effect
<i>OA</i>	95	<i>IWB26593</i>	2A	196.5	3.10	4.89	C/T	0.08
		<i>IWB51340</i>	2A	211.5	3.28	5.93	C/T	-0.06
		<i>IWB51601</i>	2B	8.3	3.43	6.27	A/C	-0.06
		<i>IWB5427</i>	2B	172	3.70	6.05	A/C	0.20
		<i>IWA196</i>	5B	170.7	3.44	5.55	C/T	2.80
<i>Δ RWC</i>	95	<i>IWB490</i>	2A	9.4	3.08	5.45	A/G	1.71
		<i>IWB72314</i>	4A	17.0	3.27	5.83	A/G	1.02
		<i>IWB24569</i>	4B	85.2	3.15	5.59	C/T	-1.47
		<i>IWA4823</i>	6B	64.8	3.82	7.04	C/T	2.79
		<i>IWB2238</i>	7B	189.3	3.66	6.67	A/G	-1.25

Additional drought adaptive traits

Three LR QTL were identified in 2017 (100 DAP). Two of these on 5BS at 63.2 cM ($r^2 = 7.44$) and at 72.9 cM ($r^2 = 4.70$) and one on 6BS at 93.4 ($r^2 = 4.38$) as well as in 2018 (120 DAP) on 1AS ($r^2 = 16.60$), 2BS ($r^2 = 13.30$) and 3BL ($r^2 = 12.83$). The confidence interval of these loci did not overlap for LR investigated in both years.

Thirty-five SPAD QTL were identified in 2017 (100 DAP) and in 2018 (120 DAP). In detail, sixteen loci in the first year and twenty-nine in the second year. In 2017, three mayor QTL mapped on 1AS at 71.6 cM ($r^2 = 7.72$), 5AL at 178.3 cM ($r^2 = 8.36$) and 7AS at 82.2 cM ($r^2 = 11.44$), while in 2018, three mayor QTL mapped on 1AS at 70.7 cM ($r^2 = 7.87$), 4BS at 32.7 cM ($r^2 = 8.69$) and 5AL at 178.3 cM ($r^2 = 8.99$). Comparing both years, two significant QTL overlaps were observed on 1AS ($7.72 < r^2 < 7.87$) and on 3BS ($3.66 < r^2 < 4.30$).

Thirty WAXL QTL were identified in 2017 (100 DAP) and 2018 (120 DAP). A larger number of loci was observed in the first year (16) than the second year (14). In detail, three mayor QTL in 2017 mapped on 1AS at 1.7 cM ($r^2 = 17.31$), on 2AS at 8.6 cM ($r^2 = 13.75$) and on 2BS at 4.1 cM ($r^2 = 12.78$), while three major QTL in 2018 mapped on 1AS at 1.7 cM ($r^2 = 16.60$), 2BS at 4.1 cM ($r^2 = 13.30$) and 3BL at 157.8 cM ($r^2 = 12.83$). Comparing both years, two significant QTL overlaps were observed on 1AS ($16.60 < r^2 < 17.31$), 2BS ($12.78 < r^2 < 13.30$) and 3BL ($12.83 < r^2 < 18.10$). In addition, nineteen WAXS QTL were identified in 2017 (100 DAP) and 2018 (120 DAP). A larger number of loci was observed in the first year (14) than the second year (5). In detail, two mayor QTL in 2017 mapped on 2AS ($r^2 = 9.61$) and on 7AS ($r^2 = 6.63$), while two major QTL in 2018 mapped on 6BL at 153.1 cM ($r^2 = 7.34$) and 7BS at 29.9 cM ($r^2 = 5.74$). Comparing both years, two significant QTL overlaps were observed on 1AS ($16.60 < r^2 < 17.31$), 2BS ($12.78 < r^2 < 13.30$) and 3BL ($12.83 < r^2 < 18.10$). Finally, two significant loci shared the confidence interval for

WAXL and WAXS (100 DAP) and mapped on 2AS ($9.61 < r^2 < 13.75$) and 7AS ($6.63 < r^2 < 10.11$), while no QTL overlaps were observed for WAXL and WAXS (120 DAP).

Ten major FT QTL were identified in 2018 on 1AL, 2AS (2), 2BS, 4AS, 4AL, 4BS, 5AL (2), 6BL with two significant loci on 4AS at 23.7 cM ($r^2 = 6.94$) and 6BL at 71.9 ($r^2 = 6.90$). In addition, twenty-six PH QTL were identified on 1AL (3), 1BL, 2AL (2), 2BS (2), 2BL (3), 3AL, 3BL, 4AS, 4BS (2), 4BL (3), 5AL, 6AL, 6BL (3), 7AS and 7BS with two major loci on 4BS at 30.8 cM ($r^2 = 10.68$) and 5AL at 178.3 ($r^2 = 9.88$). Comparing both traits (FT and PH), two significant QTL overlaps were observed on 2BS ($4.98 < r^2 < 6.75$) and 4AS ($5.95 < r^2 < 6.22$).

Dry biomass

Thirty-one DB QTL were mapped in 2017 (194 DAP) and 2018 (125 DAP) under conditions of severe drought. A larger number of these loci was observed in the second year (16) than the first year (15). In 2017, three major QTL mapped on 2BL at 160.6 cM ($r^2 = 7.59$), 4BS ($r^2 = 7.79$) and 5A ($r^2 = 7.64$) while in 2018, two major QTL mapped in 2018 on 1AS at 71.6 cM ($r^2 = 5.64$) and 7BS at 32.6 cM ($r^2 = 6.40$). Comparing both years, four significant QTL overlaps were observed on 4BS ($5.16 < r^2 < 7.79$), 4BL ($4.28 < r^2 < 6.34$), 5AL ($5.03 < r^2 < 7.64$) and 7AL ($3.88 < r^2 < 4.47$). In 2019, five Δ BM-QTL were observed under moderate drought conditions on 2AS at 50.5 cM ($r^2 = 5.86$), 2BL at 131.2 cM ($r^2 = 6.59$), 4BS at 14.4 cM ($r^2 = 7.59$) and 27.6 cM ($r^2 = 5.39$) and 7AS ($r^2 = 5.86$). The confidence interval of these DB loci did not overlap with those investigated in the two years before.

QTL clusters

Based on the results reported herein, thirty-one QTL clusters were detected influencing two or more drought adaptive traits, unrelated to phenology (FT) and plant height (PH). They mapped on 1A (*DR_QTLcluster#01*), 1B (*DR_QTLcluster#02*, *DR_QTLcluster#03*, *DR_QTLcluster#04*), 2A (*DR_QTLcluster#05*, *DR_QTLcluster#06*, *DR_QTLcluster#07*, *DR_QTLcluster#08*), 2B (*DR_QTLcluster#09*), 3A (*DR_QTLcluster#10*), 3B (*DR_QTLcluster#11*, *DR_QTLcluster#12*, *DR_QTLcluster#13*, *DR_QTLcluster#14* and *DR_QTLcluster#15*), 4A (*DR_QTLcluster#16*, *DR_QTLcluster#17*, *DR_QTLcluster#18*), 4B (*DR_QTLcluster#19*), 5A (*DR_QTLcluster#20*), 6A (*DR_QTLcluster#21*, *DR_QTLcluster#22*, *DR_QTLcluster#23*, *DR_QTLcluster#24* and *DR_QTLcluster#25*), 6B (*DR_QTLcluster#26*, *DR_QTLcluster#27*, *DR_QTLcluster#28*, *DR_QTLcluster#29*) and 7A (*DR_QTLcluster#30* and *DR_QTLcluster#31*).

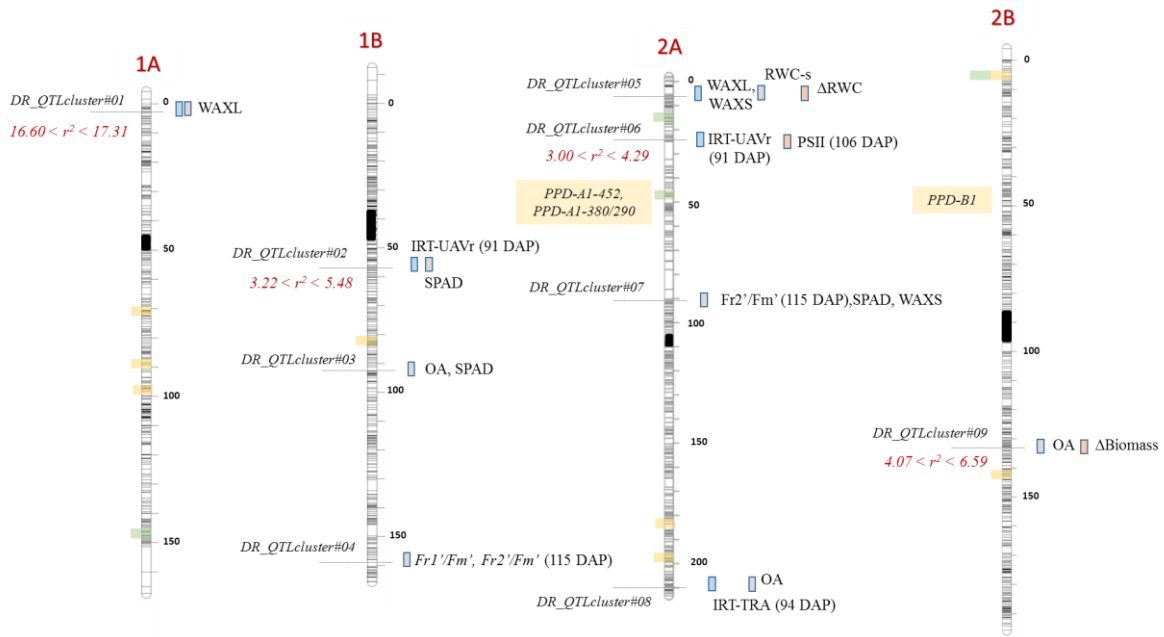
In detail, the *DR_QTLcluster#01* ($16.60 < r^2 < 17.31$) influenced the epicuticular wax content on flag leaves (WAXL) of the accessions planted in 2017 and 2018, while the *DR_QTLcluster#02* ($3.22 < r^2 < 5.48$) affected IRT by UAV-RedEdge as well as the chlorophyll content by SPAD. The *DR_QTLcluster#03* was associated with the accumulation of osmolytes (OA) as well as chlorophyll content (SPAD), while the *DR_QTLcluster#04* and *DR_QTLcluster#12* influenced the following photosynthetic traits: $Fr1'/Fm'$ and $Fr2'/Fm'$. The *DR_QTLcluster#05* affected the wax accumulation on flag leaves (WAXL) and spikes (WAXS) as well as the relative water content (RWC) in drought. The *DR_QTLcluster#06* ($3.00 < r^2 < 54.29$) was associated with the internal temperature (IRT) of the accessions as well as the photosynthetic activity (PSII). The *DR_QTLcluster#07* influenced the wax content in the spikes (WAXS), the chlorophyll content (SPAD) and the re-oxidation efficiency of QA ($Fr2'/Fm'$). The *DR_QTLcluster#08* was associated with the internal temperature (IRT) as well as the accumulation of osmolytes (OA), while the *DR_QTLcluster#09* ($4.07 < r^2 < 6.59$) with OA and the dry biomass. The *DR_QTLcluster#10* influenced the epicuticular wax content on flag leaves (WAXL) as well as the rolling on flag leaves

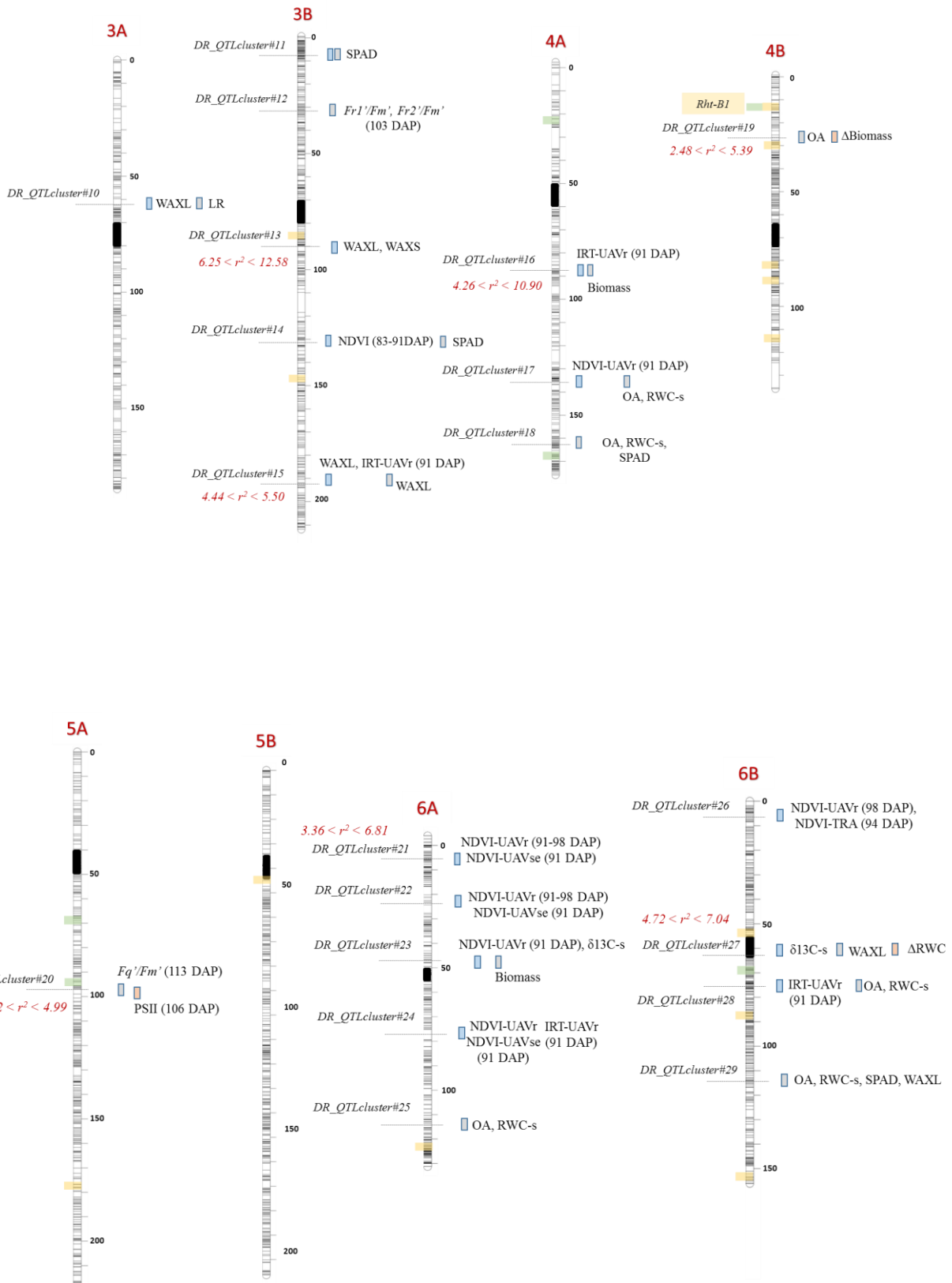
(LR) in response to drought. The *DR_QTLcluster#10* and the *DR_QTLcluster#11* were specific for the following photosynthetic traits: $Fr1'/Fm'$ and $Fr2'/Fm'$ and chlorophyll content by SPAD respectively. The *DR_QTLcluster#13* ($6.25 < r^2 < 12.58$) influenced the wax accumulation on flag leaves (WAXL) and spikes (WAXS), while *DR_QTLcluster#14*, together with *QTLcluster#21* ($3.36 < r^2 < 6.81$), *QTLcluster#22*, *DR_QTLcluster#26* and *DR_QTLcluster#31*, influenced the vegetation index (NDVI) in drought. The *DR_QTLcluster#15* ($4.44 < r^2 < 5.50$) influenced the internal temperature (IRT) and the wax accumulation on flag leaves (WAXL), while *DR_QTLcluster#16* ($4.26 < r^2 < 10.90$) influenced IRT and dry biomass. The *DR_QTLcluster#17*, together with *DR_QTLcluster#18*, *DR_QTLcluster#25*, *DR_QTLcluster#28* and *DR_QTLcluster#29*, affected the accumulation of osmolytes as well as the relative water content in flag leaves (OA and RWC). The *DR_QTLcluster#19* ($2.48 < r^2 < 5.39$) influenced OA and the dry biomass, while the *DR_QTLcluster#20* ($3.02 < r^2 < 4.99$) influenced the photosynthetic activity in light (Fq'/Fm') and in dark (PSII) hours. The *DR_QTLcluster#23* and *DR_QTLcluster#27* ($4.72 < r^2 < 7.04$) especially influenced the carbon isotope discrimination in flag leaves ($\delta^{13}C$) under drought. Finally, the *DR_QTLcluster#30* ($3.71 < r^2 < 11.44$) was specific for the chlorophyll content (SPAD) in two consecutive years (Table 10 and Figure 11).

Table 10 | Chromosome position on the durum consensus map (Maccaferri et al. 2015a) of thirty-one QTL clusters influencing two or more drought adaptive traits which unrelated to phenology (flowering time) and plant height. UAVse: UAV-Sequoia; UAVr: UAV-RedEdge; TRA: Tractor-GreenSeeker.

QTL CLUSTER	Chr.	Pos. (cM)	R^2	Trait 2017	Trait 2018	Trait 2019
<i>DR_QTLcluster#01</i>	1A	1.7	$16.60 < r^2 < 17.31$	WAXL	WAXL	-
<i>DR_QTLcluster#02</i>	1B	54.3-54.8	$3.22 < r^2 < 5.48$	IRT-UAVr	SPAD	-
<i>DR_QTLcluster#03</i>	1B	93.3	$2.60 < r^2 < 3.19$	-	OA, SPAD	-
<i>DR_QTLcluster#04</i>	1B	158	$4.63 < r^2 < 4.85$	-	<i>Fr1'/Fm', Fr2'/Fm'</i>	-
<i>DR_QTLcluster#05</i>	2A	8.6-9.4	$2.86 < r^2 < 9.61$	WAXL, WAXS	RWC	Δ RWC
<i>DR_QTLcluster#06</i>	2A	21.9	$3.00 < r^2 < 4.29$	IRT-UAVr	-	PSII
<i>DR_QTLcluster#07</i>	2A	96-97.3	$4.30 < r^2 < 4.91$	-	<i>Fr2'/Fm', SPAD, WAXL</i>	-
<i>DR_QTLcluster#08</i>	2A	206.8-208.4	$3.16 < r^2 < 3.31$	IRT-TRA	OA	-
<i>DR_QTLcluster#09</i>	2B	131.2-133	$4.07 < r^2 < 6.59$	-	OA	Δ Biomass
<i>DR_QTLcluster#10</i>	3A	59.1	$3.68 < r^2 < 4.90$	WAXL	LR	-
<i>DR_QTLcluster#11</i>	3B	6.5-7.4	$3.66 < r^2 < 4.30$	SPAD	SPAD	-
<i>DR_QTLcluster#12</i>	3B	24.6	$6.05 < r^2 < 6.33$	-	<i>Fr1'/Fm', Fr2'/Fm'</i>	-
<i>DR_QTLcluster#13</i>	3B	93.8	$6.25 < r^2 < 12.58$	WAXL, WAXS	-	-
<i>DR_QTLcluster#14</i>	3B	133.4	$4.17 < r^2 < 4.73$	NDVI-UAVse, SPAD	-	-
<i>DR_QTLcluster#15</i>	3B	209.1-209.6	$3.44 < r^2 < 5.50$	IRT-UAVr, WAXL	WAXL	-
<i>DR_QTLcluster#16</i>	4A	88.1	$4.26 < r^2 < 10.90$	IRT-UAVr	Biomass	-
<i>DR_QTLcluster#17</i>	4A	136.8-140-7	$3.02 < r^2 < 3.34$	NDVI-UAVr	OA, RWC	-
<i>DR_QTLcluster#18</i>	4A	161.7	$3.00 < r^2 < 3.90$	-	OA, RWC, SPAD	-
<i>DR_QTLcluster#19</i>	4B	27.6-28.8	$2.48 < r^2 < 5.39$	-	OA	Δ Biomass
<i>DR_QTLcluster#20</i>	5A	96.6-101.9	$3.02 < r^2 < 4.99$	-	<i>Fq'/Fm'</i>	PSII
<i>DR_QTLcluster#21</i>	6A	5.1	$3.36 < r^2 < 6.81$	NDVI-UAVr-se	-	-
<i>DR_QTLcluster#22</i>	6A	21.4	$3.00 < r^2 < 3.66$	NDVI-UAVr-se	-	-
<i>DR_QTLcluster#23</i>	6A	44.1-45.9	$3.20 < r^2 < 5.29$	NDVI-UAVr, $\delta^{13}C$ -s	<i>Fr1'/Fm', Biomass</i>	-
<i>DR_QTLcluster#24</i>	6A	71.8-72.4	$3.71 < r^2 < 5.19$	IRT-UAVr, NDVI-UAVr-se	-	-
<i>DR_QTLcluster#25</i>	6A	117.1-117.7	$2.92 < r^2 < 4.78$	-	OA, RWC	-

<i>DR_QTLcluster#26</i>	6B	31.3	$3.64 < r^2 < 3.75$	NDVI-UAVr-se	-	-
<i>DR_QTLcluster#27</i>	6B	64.8-65.9	$4.72 < r^2 < 7.04$	$\delta^{13}C$ -s	WAXL	Δ RWC
<i>DR_QTLcluster#28</i>	6B	75.3-78.8	$2.56 < r^2 < 3.13$	IRT-UAVr	OA, RWC	-
<i>DR_QTLcluster#29</i>	6B	114.3-119.3	$2.44 < r^2 < 4.02$	-	OA, RWC, SPAD, WAXL	-
<i>DR_QTLcluster#30</i>	7A	82.2	$3.71 < r^2 < 11.44$	SPAD	SPAD	-
<i>DR_QTLcluster#31</i>	7A	131.3	$3.75 < r^2 < 5.58$	NDVI-UAVse	-	-





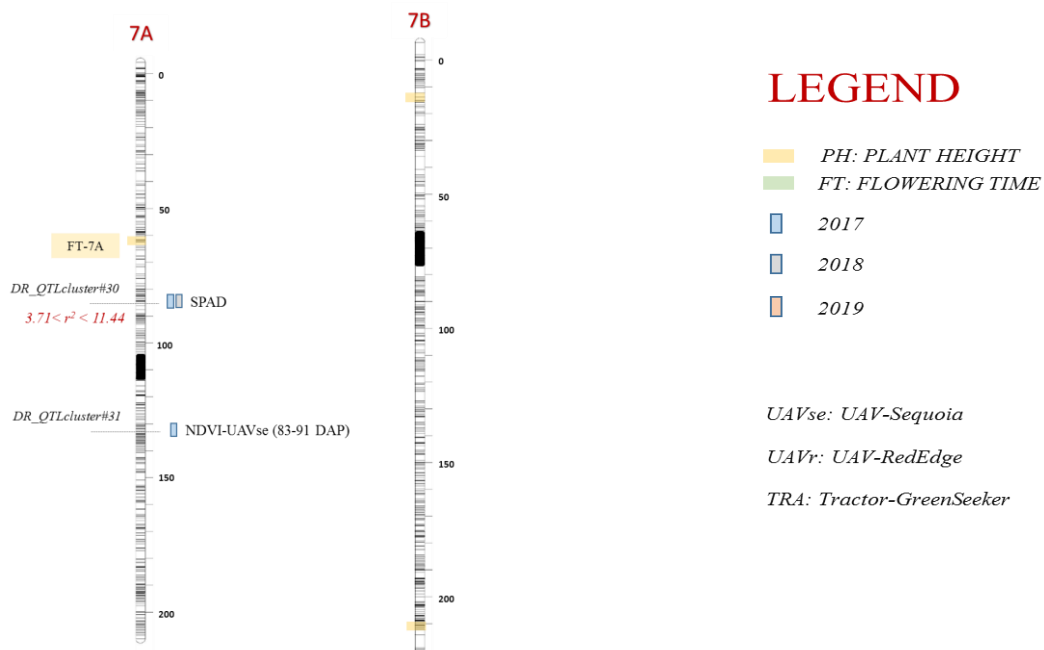


Figure 11 | Chromosome position on the durum consensus map (Maccaferri et al. 2015a) of QTL clusters identified in this study. The QTL in the first year (2017) are highlighted with a light blue bar; the QTL in the second year (2018) are highlighted with a grey bar; the QTL in the third year (2019) are highlighted with a light red bar. The QTL hotspots were independent from the effects of the flowering time (FT) and plant height (PH) as well as from the loci relevant for phenology (*PPD-A1*, *PPD-B1*, *Rht-B1b* and *FT-7A*-indel).

DISCUSSION

Chlorophyll fluorescence imaging (CFI) by the “Lemnatec” field scanner

In the last years, high-throughput digital phenotyping methods have been proposed (Busemeyer et al. 2013; White and Conley, 2013; Andrade-Sanchez et al. 2014; Deery et al. 2016; Bai et al. 2016; Underwood et al. 2017; Jimenez-Berni et al. 2018) to alleviate the current phenotyping bottleneck within modern plant breeding programs (Cobb et al. 2013; Araus and Cairns, 2014). However, current approaches are laborious or permit the use of only a few sensors at a time. In an effort to overcome this, fully or semi-automated robotic field phenotyping could ease the continual and high-throughput monitoring of crop performance (Virlet et al. 2017). This study is the first to investigate chlorophyll fluorescence imaging (CFI) data in time series using a “Lemnatec” field scanner (LFS) platform. In detail, the on-board CFI system enabled the fluorescence measurements emitted mainly by PSII during the dark hours at 71, 97, 102 and 106 DAP under progressive moderate drought conditions. PSII results showed an increased significance in heritability (h^2) under water shortage (102 and 106 DAP) as well as a progressive decreased trend of the values from 71 to 106 DAP, consequent to the heterogeneous cumulative effects of senescence and considerable damages in the photosynthetic activity under advanced drought conditions (Urban et al. 2018).

As expected, PSII data positively correlated with NDVI and negatively with IRT by UAVs, proving how these remote sensing systems could be integrated to select novel drought tolerant proxies in the future crop breeding programs (Shakoor et al. 2019).

NDVI and IRT measurements by UAV- and ground-based platforms

It is well known that HTP devices/platforms show different sensitivity features and, consequently, differ in their capacities to discriminate genotypes, specifically depending on the crop developmental stage and/or agronomic management (Marti et al. 2007; Cabrera-Bosquet et al. 2011; Christopher et al. 2016). To our best knowledge, this study is the first to report on the use of

UAV-based remote sensing for GWAS analysis in crops and to compare the results to those obtained using a ground-based platform. In detail, we compared two UAV- and one ground-based platforms to search for NDVI and IRT QTL in a field trial (2017) first conducted under well-watered conditions until flowering, then followed by 2 weeks of progressively increasing water-deficit conditions that decreased leaf relative water content (RWC) to 50%. The rapid decrease in RWC after stopping irrigation was consequent to the high evaporative demand typical of the environment where the field trial was conducted. During the time interval from 16 to 31 March when irrigation was terminated and plants experienced an increasing water-deficit stress, the average mean daily and average maximum temperatures were 20.9 and 29.7 °C, respectively while the average reference daily evapotranspiration using the standardized Penman-Monteith method was 5.41 mm.

When compared to the two UAV-based platforms, NDVI-values collected with the ground-based platform plateaued earlier from 76 to 84 DAP, indicating its lower capacity to monitor plant biomass accumulation and leaf greenness during the reproductive stage of the wheat growth cycle. Additionally, UAV-mounted platforms allowed us to measure hundreds of plots in very short time, hence minimizing the confounding effects due to time-related environmental variation, which inevitably affect the results of studies conducted with ground-based platforms (Haghighattalab et al. 2016). NDVI has been recognized for its ability to estimate crop biomass and grain yield (Lewis et al. 1998; Araus et al. 2001) and this correlation becomes stronger when estimated with UAV platforms (Kyratzis et al. 2015).

In this study, the two UAV-based platforms showed a markedly higher heritability for NDVI measurements as compared to those collected with the ground-based platform. A high h^2 is critical to effectively identify and eventually clone QTL (Tuberosa, 2012). Therefore, from a methodological perspective on the use of the aerial vs. ground-based HTPPs to detect significant loci for NDVI, our results show the increased ability of the former, particularly under terminal

drought stress, as shown by the considerably higher number of significant QTL with the UAV-based platforms. Accordingly, a recent study conducted in barley grown under 10 different nitrogen treatments has also shown an increased sensitivity of aerial vs. ground-based platforms to measure NDVI using RGB (conventional digital cameras), multispectral and thermal aerial imagery in combination with a matching suite of ground sensors (Kefauver et al. 2017).

As with NDVI, the relative benefits and comparison of UAV- and ground-based platforms were investigated for IRT, a surrogate measure of stomatal aperture and conductance as well as photosynthetic rate (Jones and Vaughan, 2010; Maes and Steppe, 2012). Our results demonstrated the more efficiency and repeatability of the UAV-based platform (RedEdge sensor) on IRT measurements than the ground-based platforms (GreenSeeker sensor). Additionally, a trend of IRT increase was observed on progressive DAP under water shortage, consequent to the cumulative effects of senescence and drought stress severity. In fact, IRT based on the fact that plant surfaces (e.g., leaves) are cooled by evaporation, so that temperatures decrease in proportion to the evaporation rate. The cooler temperature related with stomatal opening and higher transpiration rates and conversely, warmer temperature related with a reduction in transpiration rate (Deery et al. 2016).

Chlorophyll fluorescence (ChlF) by the manually pushed cart

Simultaneous Fq'/Fm' as well as $Fr1'/Fm'$ and $Fr2'/Fm'$ measurements under well-watered (WW, 103 DAP) and water-limited conditions (WL, 115 DAP) provided more detailed information about the photosynthetic rate of the accessions in ambient light. Fq'/Fm' was measured to quantify the maximum quantum efficiency of PSII (Keller et al. 2019) showing a decreased trend from 103 DAP to 115 DAP, consequent to considerable damages in the leaves and then in the photosynthetic electron transport steps sensitive to the advanced drought severity (Yordanov et al. 2000; Zandalinas et al. 2018). Contrary to Fq'/Fm' , less attention is paid to the QA re-oxidation efficiency

0.65 ms ($Fr1'/Fm'$) and 120 ms ($Fr2'/Fm'$) to monitor fluorescence relaxation (Fr). Both traits showed an increased trend from 103 DAP to 115 DAP, result of the electron transport damages under advanced drought severity. Their negative correlation with Fq'/Fm' under drought explained the reduction of the QA efficiency by PSII relative to the maintained efficiency of oxidation by PSI. Their low association with PSII data measured by LFS in the dark hours was due to the increasing light intensities and non-photochemical quenching (NPQ) processes which affect the fluorescence relaxation kinetics only in the light hours (Keller et al. 2019).

Physiological drought adaptive traits

The leaf carbon isotope discrimination ($\delta^{13}C$) was investigated under well-watered (85 DAP) and water-limited conditions (93 DAP) because represents a potentially useful trait in crop breeding for improved drought tolerance cultivars (Dixon et al. 2019), despite the selection criterion has been limited for the inconsistent relationship proved with grain yield (Araus et al. 1998; Korte and Farlow, 2013). In the present study, the differences in the photosynthetic gas exchange under well-watered ad water-limited conditions explained the decreased trend from 85 to 93 DAP.

$\delta^{13}C$ -s positively correlated with photosynthetic traits, consequent to its implication within chlorophyll activities (Wingate et al. 2015) and to its relevance as useful proxy for the selection of drought tolerant wheat genotypes to enhance wheat productivity in drought (Bachiri et al. 2018).

A number of authors have proposed OA as an important metabolic adaptation mechanism to support higher crop yield under stressful environmental conditions, as recently reviewed by Abdelrahman et al. (2017). Notably, grain yield differences have been shown to be positively correlated to OA in cereals (Morgan et al. 1984; Morgan and Condon, 1986; Blum and Pnuel, 1990 and Blum et al. 1999), hence representing a valuable proxy to evaluate not only drought effects but also to predict grain production (Blum, 2017). This notwithstanding, the genetic factors regulating OA in wheat and other crops remain unknown, the main reason being the difficulty to adequately survey and

phenotype the large number of accessions of the mapping population and/or GWAS panels required for a meaningful QTL discovery. The collection of leaves and their processing must be completed rapidly to obtain meaningful data and minimizing the bias introduced by the time of sample collection OA in an adequately large number of genotypes, an essential prerequisite for identifying and accurately mapping QTL (Tuberosa, 2012; Maccaferri et al. 2015b). Not recently, the attempt to genetically dissect OA on cereals was conducted in rice (Lilley et al. 1996; Robin et al. 2003) and in barley (Teulat et al. 1998; Teulat et al. 2001). Only in bread wheat, Morgan and Tan (1996) mapped an osmoregulation gene locus (Morgan, 1991) located in the short arm on chromosome 7A by exploring genetic linkage to restriction fragment length polymorphism (RFLP) loci. However, OA and osmoregulation terms are different. OA refers to a lowering of osmotic potential (ψ^s) due to an accumulation of osmolytes in response to water scarcities, while the osmoregulation refers to the ψ^s regulation by the addition/removal of osmolytes until the intracellular potential is approximately equal to that of the medium surrounding the cell (Turner and Jones, 1981). The gene described by Morgan is concerned with regulation of turgor pressure and water content by osmotic adjustments (Morgan 1977, 1988), hence the term osmoregulation.

In this study, OA was measured according to the “Rehydration method” (Babu et al. 1998) in two consecutive years (2018 and 2019) in drought (early grain-filling) as an assessment of adaptation to terminal drought stress. Although this method was criticized (Kikuta and Ritcher, 1992), many others considered it an optimal screening tool for large populations (Turner and Jones, 1980; Fisher et al. 2005; Mart et al. 2016). In support of this, the sizeable genetic variability and high repeatability observed for several crops (Zhang et al. 1999) and its merits in terms of labor, cost-effectiveness and plant materials as compared to the other methods (Babu et al. 1998). In our experience, the rehydration of the leaf samples greatly facilitated (i) the cell sap extraction especially in water-stressed conditions and (ii) the OA screening for all durum wheat elite accessions (Durum Panel). These evidences have led to a high OA heritability in both years of

investigation (2018 and 2019), increased values for the modern French, North American, Canadian and Australian cultivars (S8) and a negative correlation with LR. In 2018, the positive correlation between OA and RWC clearly indicates an active physiological role of osmolytes to maintain a more favorable water status of the plant playing a key role for avoiding and mitigating the negative effects of water loss under severe drought. The results validate the effectiveness of the “Rehydration method” as an ideal option for handling the large number of samples required for the genetic dissection of OA.

Additional drought adaptive traits

The LR values showed a positive correlation with IRT as well as negative with OA and RWC traits as reported by different studies, which characterized LR as related to leaf water status and canopy temperature (Turgut et al. 1998; Cal et al. 2019). Back in 1980, O'Toole and Cruz reported that the transpiration rate per unit leaf area decreased when flag leaves rolled, while in 1986 Turner et al. found significant relationships between canopy temperature and leaf rolling under water shortage conditions. LR was reported to be directly related to leaf water potential (LWP) (Dingkuhn et al. 1989) and osmotic potentials (Hsiao et al. 1984; Pandey et al. 2017) as observed in the current study.

The chlorophyll content (SPAD) was estimated in two consecutive years (2017 and 2018) as a rapid non-destructive estimation of the plant nitrogen (N) status (Yue et al. 2019) which represent a major component of the photosynthetic apparatus. SPAD correlated with $Fr1'/Fm'$ and $Fr2'/Fm'$ photosynthetic traits, despite the different methodological approaches. The epicuticular wax on the flag leaves (WAXL) and spikes (WAXS) was estimated in two consecutive years (2017 and 2018) showing no significant relationships with the other investigated traits. Except between WAXL and IRT due to the known association of epicuticular waxes with the canopy temperature in wheat as reported by Mondal et al. (2015).

Dry biomass

The DB in the first two years (2017 and 2018) showed a higher heritability than in the last year (2019). DB positively correlated with grain yield (GY) related proxies as NDVI and photosynthetic traits (Fq'/Fm' , $Fr1'/Fm'$ and $Fr2'/Fm'$) and negatively correlated with IRT. However, the influence of phenology and the harvest in advance (GS71, early milk) induced DB values to not represent a direct estimate of the final grain yield (GY) (Serrano et al. 2000; Duncan et al. 2018) in the current study.

QTL clusters

The use of the flowering time (FT) as covariate for the GWAS analysis reduced the genetic effects of the photoperiod and vernalization, which in turn allowed us to more accurately report thirty-one QTL hotspots based on the concurrent allelic effects on two or more drought adaptive traits.

All of them unrelated to the major loci for flowering time and plant height of the current study as well as the major loci known to influence photoperiod/vernalization, (Milner et al. 2016) and in part were associated with previous grain yield (GY) and related QTL studies in wheat.

DR_QTLcluster#01 shared the genetic interval with *Ws* gene on the short arm of chromosome 1AS responsible for spike glaucousness in durum wheat (Gadaleta et al. 2009). Worthy of note the overlap between the WAXL-locus on 2BS and the known *Iw1* gene, an inhibitor of the glaucousness loci (*W*) in hexaploid wheat (Wu et al. 2013). *DR_QTLcluster#04* as well as *DR_QTLcluster#05* and *DR_QTLcluster#11* overlapped with test weight (TW) and NDVI loci respectively, previously reported in a durum wheat elite population tested in contrasting thermo-pluviometric conditions by Graziani et al. (2014). *DR_QTLcluster#08* co-mapped with *QRga.ubo-2A.3* while *DR_QTLcluster#24* and *DR_QTLcluster#25* with *QRga.ubo-6A.1* and *QRga.ubo-6A.2* respectively. These important loci were identified for root growth angle (RGA) in Colosseo × Lloyd recombinant inbred lines (RILs) as well as thousand grain weight (TGW) and partially grain yield

(GY) in a panel of 183 elite durum wheat accessions under different water regimes (Maccaferri et al. 2016). *DR_QTLcluster#10* affecting WAXL and LR as well as *DR_QTLcluster#11* affecting chlorophyll content (SPAD) shared the interval with NDVI QTL on chr. 3A and 3B in hexaploid wheat (Jingdong 8/Aikang 5) under varying climate conditions across China (Li et al. 2014). *DR_QTLcluster#15* affecting IRT and WAXL as well as *DR_QTLcluster#19* affecting OA, RWC and SPAD overlapped with two major QTL for NDVI at the vegetative stage in Seri/Babax wheat mapping population. Finally, *DR_QTLcluster#18* and *DR_QTLcluster#29* affecting OA, RWC, SPAD co-mapped with two major GY QTL reported by Quarrie et al. (2005) from the hexaploid wheat cross between Chinese Spring × SQ1 evaluated across a broad combination of 24 site × treatment × year combinations.

CONCLUSIONS

This study genetically investigated drought adaptive traits in an elite durum wheat collection suitable for GWAS and representative of global durum breeding. The measurements were acquired using the traditional as well as the emerging HTP approach based on a semi-automatic platform “Lemnatec” field scanalyzer and UAV- and ground-based remote sensing. The results report herein demonstrate the great potential and effectiveness of semi-automated robots and UAV-based platforms to gather rapid, precise, and detailed measurements, which in turn considerably improved trait repeatability estimates as well as QTL identification. Additionally, they provide the detection of significant loci for OA and RWC due to the phenotypic plasticity as well as the genetic variants of our Durum Panel and support the validity of the “Rehydration method” as an optimal, fast and economical protocol for large-scale screening of OA under well-watered and drought conditions.

Twelve selected drought response-specific QTL hotspots (*DR_QTLcluster#01*, *DR_QTLcluster#04*, *DR_QTLcluster#05*, *DR_QTLcluster#08*, *DR_QTLcluster#10*, *DR_QTLcluster#11*, *DR_QTLcluster#15*, *DR_QTLcluster#18*, *DR_QTLcluster#19*, *DR_QTLcluster#24*, *DR_QTLcluster#25* and *DR_QTLcluster#29*) reveal useful markers for future breeding. Their overlap with known QTL/genes for grain yield and related traits promotes the investigated traits as prime drought stress adaptive proxies for wheat productivity in conditions of adverse water status.

Kompetitive Allele Specific Polymerase chain reaction (KASP) marker development for the genetic dissection of Fusarium Head Blight (FHB) resistance in durum wheat

INTRODUCTION

Fusarium head blight (FHB) is a fungal disease caused by pathogens belonging to the genus *Fusarium*, which infects wheat as well as several other minor cereals worldwide (Bai and Shaner, 1994; Bottalico and Perrone, 2002; Moretti et al. 2018; Castiblanco et al. 2018). In particular, *Fusarium culmorum* (WG Smith) (FC) and *Fusarium graminearum* (FG) Schwabe [telomorph: *Gibberella zae* Schw. (Petch)] species induce severe grain yield losses (Buerstmayr et al. 2012) and accumulation of mycotoxins (e.g. deoxynivalenol or DON) (Beres et al. 2018) compromising food safety and animal health (Goswami and Kistler, 2004; Petersen et al. 2017).

Two important types of FHB resistance were reported in wheat (Schroeder and Christensen, 1963). Type I operates against initial infection while type II against the spread within the head. Up to now, they are easier to evaluate and more frequently recognized than less well-known type III (DON content), type IV (kernel infection) and type V (tolerance) (Shaner, 2002).

Durum wheat (*Triticum turgidum* ssp. *durum*, tetraploid, $2n = 28$, AABB) is notorious for its high susceptibility to FHB (Miedaner et al. 2017) in comparison to bread wheat (*Triticum aestivum*, hexaploid $2n = 42$, AABBDD) for difficulties to combine the numerous small-effect resistance quantitative trait loci (QTL) in selective breeding (Steiner et al. 2019) and for its narrow genetic diversity (Rudd et al. 2001; Giancaspro et al. 2018). Szabo-Hever et al. (2018) reported a significant FHB severity reduction in synthetic hexaploid wheat (SHW) lines as compared to their tetraploid parents, mainly because of the lack of D-genome. At present, the effort to detect durum wheat resistant lines have been limited so far and none of selected durum landraces or lines show a FHB

resistance level comparable to Chinese spring wheat variety Sumai-3 (Buerstmayr et al. 2003; Miedaner and Longin, 2014; Prat et al. 2014; Zhao et al. 2018; Hadjout et al. 2017). Over 250 QTL/genes for FHB resistance have been identified in bread wheat, such as *Fhb1* and *Fhb5* in Sumai-3 and derivatives (Anderson et al. 2001; Buerstmayr et al. 2002; Jia et al. 2018). However, only a small number of FHB resistance loci have been mapped in durum wheat (Chen et al. 2007; Gladysz et al. 2007; Zhang et al. 2014; Sari et al. 2018; Zhao et al. 2018).

Although bioengineering approaches were used by manipulating *TaHRC* sequence, a key gene for *Fhb1*-mediated resistance, to improve FHB resistance in wheat (Su et al. 2019), the most widely used strategy is the *Fhb1* introgression from bread to durum wheat which has mainly led to unstable expressions in the durum genetic background (Zhu et al. 2016). However, Giancaspro et al. (2018) reported that cell wall structure as well as gene response acquired from the introgression induced to an increased FHB resistance in durum wheat, while Prat et al. (2017) successfully introgressed *Fhb1* into durum wheat advanced lines inducing high levels of FHB resistance. Additionally, Zhao et al. (2018) reported three major loci for FHB resistance on chromosomes 2A, 5A and 7B from the cross between Joppa (a durum wheat cultivar) and 10Ae564 (a durum wheat introgression line derived from the hexaploid wheat PI 277012). Recently, Sari et al. (2018) mapped a significant number of FHB resistance QTL using doubled haploid (DH) populations from *Triticum turgidum* ssp. *durum* and *T. turgidum* ssp. *carthlicum*.

Another approach is the efficient use of ‘native’ resistance sources elite durum gene pool by combining the numerous small FHB resistance effects (Steiner et al. 2017) to breeding FHB resistance. To find effective breeding tools, we identified QTL hotspots for FHB resistance in durum wheat, in part unknown in bread wheat, based on a genome-wide association study (GWAS) on durum wheat accessions as well as based on a linkage mapping study on F₆ recombinant inbred lines (RILs) from Simeto (susceptible cultivar) × Levante (moderately resistant cultivar) population. From the QTL detected, we chose specific loci in order to validate KASP (Kompetitive Allele-

Specific Polymerase chain reaction) markers suitable for haplotype-based marker-assisted selection (MAS) programs. KASP assay is shown to be suitable for the high-throughput screening of large populations as well as for the selection of cultivars pyramiding loci for DON content and other FHB traits.

MATERIALS AND METHODS

The study included four steps: (i) GWAS on Fusarium Panel, (ii) linkage mapping on RIL population Simeto × Levante, (iii) selection of QTL hotspots and haplotype analysis, and (iv) KASP validation on PSB Panel.

1. . GWAS on Fusarium Panel

1.1. Plant material and field management

A collection of 130 durum wheat accessions (Fusarium Panel) was assembled at the Department of Agriculture and Food Sciences - DISTAL, University of Bologna - UNIBO, considering the durum wheat passports as well as the phenotypic data from different countries worldwide. It included genotypes released from Mediterranean countries, breeding programs from the International Maize and Wheat Improvement Center (CIMMYT), USA breeding programs (Arizona, Minnesota, Montana and North Dakota States) as well as the International Center for Agricultural Research in the Dry Areas (ICARDA) (Supplementary Table 1). The Panel was grown and field-evaluated at the experimental fields of Società Italiana Sementi (SIS) S.p.A. in Idice (BO, Italy) in two years (2015 and 2016) and at the experimental fields of ISEA S.p.A. in Tolentino (MC, Italy) in one year (2016). In both experiments, the field trials were sown in November consisting of two 2.5 m-long

and 0.15 m-apart rows, spaced 0.55 m between rows of adjacent plots arranged in a randomized complete block (RCB) design. Selected check cultivars (Claudio, Karim, Normanno, Saragolla and Simeto) were chosen and repeated within the experimental blocks to verify the FHB disease homogeneity in the field. Seed treatment, plot size, sowing density and crop management conditions were the same as those described in Buerstmayr et al. (2002). The accessions were spray-inoculated with macroconidia of FC single-spore isolates as described by Buerstmayr et al. (2000) and of FG single-spore isolates as described by Buerstmayr et al. (2002). In both cases, a total of 50 ml of inoculum was sprayed on the heads when 50% of the plants had reached anthesis using a motor driven back-pack sprayer. A restricted number of 43 elite accessions (Fusarium Panel subset) was field-evaluated at experimental farm of University of Bologna (Cadriano, BO) in 2016. In this case, a point-inoculation procedure (Purahong et al. 2014) was carried out using FC and FG single-spore isolates.

1.2. Phenotypic analysis

The Fusarium Panel grown in Idice was field-evaluated for incidence (proportion of diseased spikelets per spike) and severity (percentage of diseased spikes) in primary spikes on the following days after planting (DAP) (168, 174, 179 and 183) in the first year while on the following DAP (172, 179 and 186) in the second year. The FHB index was measured by dividing by 100 the sum of both trait values for each accession. The Fusarium Panel grown in Tolentino was field-evaluated for incidence, severity and then FHB index in primary spikes on the following DAP (170, 178 and 187). In both environments, the area under the disease progress curve (AUDPC) was calculated taking into account all progressive dates of trait evaluation in order to provide an integrated measure of FHB disease. In addition, a considerable number of spikes for each plot was randomly harvested in order to collect 50 g of seeds from which to measure Fusarium-damaged kernels (FDK) as the percentage of shriveled, lightweight and chalky white kernels with occasional

characteristic pink coloration. The DON content was determined for the Fusarium Panel grown in Idice (2015 and 2016) and the subset of selective accessions grown in Cadriano (2017). The DON quantitative analysis (parts per billion, ppb) was measured at Genomics Research Centre (CREA-GB) in Fiorenzuola d'Arda (PC, Italy) using a Ridascreen DON (R-Biopharm AG, Darmstadt, Germany) enzyme linked immune-assay (ELISA). The AUDPC was obtained for each considered trait taking into account all progressive dates of evaluation in order to provide an integrated measure of FHB disease and DON content. Finally, the flowering time (FT) was recorded for both plant materials grown in Idice and Tolentino by integrating each year and environment.

1.3. Statistical analysis

The *lme4* package (*R-project*) was used to conduct spatial adjustment analyses of the raw plot data using a mixed procedure including row and column random effects as well as a moving mean of variable size. The resulting phenotypic data were analyzed by restricted maximum likelihood (REML) to fit a mixed model and produce best linear unbiased estimator (BLUE) values considering multiple and combined environments, years and inocula. Scripts in *R-project* were used to calculate Pearson correlation r coefficients among traits as well as the heritability value (h^2) with reference to repeatable check cultivars within the experimental blocks and analysis of variance (ANOVA) treating accession, environment, year and inoculum as well as interactions as random factors.

1.4. Genetic analysis

The Fusarium Panel genomic DNA was extracted at the Plant Genetics laboratory of DISTAL - UNIBO using NucleoSpin® 8/96 Plant II Core Kit from Macherey Nagel and sent for SNP genotyping to TraitGenetics (<http://www.traitgenetics.com/en/>). The Illumina iSelect 90K wheat SNP assay (Wang et al. 2014) was used and genotype calls were obtained as described in

Maccaferri et al. (2015b). The tetraploid-consensus-2015 (Maccaferri et al. 2015a) was considered to assign polymorphisms on chromosomes and map positions.

Haploview 4.2 software (Barrett et al. 2005) was used to exclude SNP markers with a minor allele frequency (MAF) > 0.10 and calculate the linkage disequilibrium (LD) among markers for each chromosome (A and B genomes). LD decay pattern as result of consensus genetic distances was inspected considering squared allele frequency correlation (r^2) estimates from all pairwise comparisons among intra-chromosomal SNPs in TASSEL (Trait Analysis by aSSociation, Evolution and Linkage) 5.2.37. The Hill and Weir formula (Hill and Weir, 1988) was used in *R-project* to define the QTL confidence interval (CI) in accordance with the curve fit and the distance at which LD decays below r^2 0.3.

A reduced subset of 2,656 SNP markers pruned for $r^2 = 0.5$ was used in STRUCTURE software 2.3.4 (Pritchard et al. 2000) in order to carry out the model-based quantitative assessment of subpopulation memberships of the accessions using inferences based on molecular SNP data only and including admixture and correlated allele frequencies among subpopulations. Numbers of hypothetical subpopulations ranging from $k = 2$ to 10 were assessed using 50,000 burn-in iterations followed by 100,000 recorded Markov-Chain iterations. To estimate the sampling variance (robustness) of population structure inference, five independent runs were carried out for each k . The rate of change in the logarithm of the probability of likelihood [$\ln P(D)$] value between successive k -values (Δk) (Evanno et al. 2005), the inspection of the rate of variation (decline) in number of accessions clearly attributed to subpopulations (no. of accessions with Q membership's coefficient ≥ 0.5 and ≥ 0.7) and the Fixation Index (F_{st}) among all possible population pairwise combinations were used to predict the optimal number of subpopulations. A Kinship matrix of genetic relationships among individual accessions of the Fusarium Panel was calculated with all non-redundant SNP markers using a tagger function set of $r^2 = 1.0$ in Haploview 4.2. Kinship based on Identity-by-State (IBS) among accessions was calculated in TASSEL 5.2.37. A genome-wide

association study (GWAS) was performed in TASSEL 5.2.37 using 5,004 SNP markers (MAF > 0.10) imputed with LinkImpute (LDkNNi) (Money et al. 2015). In particular, a Mixed Linear Model (MLM) was implemented for GWAS using the following formula: $y = X\beta + Zu + e$ (Zhang et al. 2010) where y is the phenotype value, β is the fixed effect due to marker and u is a vector of random effects not accounted for by the markers; X and Z are incidence matrices that related y to β and u while e is the unobserved vector of random residual.

MLM with the Kinship matrix (K) as random effect and FT as covariate was considered as the optimal model to control the P value inflation associated to population structure in all GWAS analyses. GWAS P values and R^2 effects were extracted and QTL selection criteria was carried-out based on standard conditions of significance: “highly significant” refers to $P < 0.0001$ and “significant” refers to $P < 0.001$. According to the corresponding inter-marker genetic distance (Hill and Weir, 1988), the QTL confidence interval was obtained. Finally, Minitab 18 software was performed to calculate the global percentage of phenotypic variation (R^2) explained by selected SNP markers for each trait.

2. Linkage mapping on RIL population Simeto × Levante

2.1. Plant material and field management

Syngenta - Società Produttori Sementi Bologna S.p.A. (PSB, Bologna, Italy) produced a F_6 RIL population through single-seed descent from the cross between the durum wheat cultivars Simeto (susceptible) × Levante (moderately resistant). The 165 RILs were field-evaluated in two years (2014 and 2015) and managed according to Buerstmayr et al. (2002) at the Department of Agrobiotechnology – IFA in Tulln (A) as well as spray-inoculated at anthesis with macroconidia of FG single-spore isolates. A restricted number of 34 RILs was further evaluated in greenhouse for a third year with respect to the temperature and relative humidity at the Department of Agricultural

and Food Sciences (DISTAL), University of Bologna, using a point-inoculation procedure with FG single-spore isolates.

2.2. Phenotypic analysis

The 165 RILs were field-evaluated for severity at five progressive days after anthesis (DAA) (10, 14, 18, 22 and 26) in 2014 and 2015 years, one replication per year. Then AUDPC was calculated in order to integrate the measures of the trait. Similarly, the subset of 34 F₆ RILs was evaluated for severity at five progressive DAA (10, 14, 17, 19 and 21) in 2016 from which AUDPC was calculated.

2.3. Statistical analysis

ANOVA was performed in *R-project* treating accession and year as random factors. Pearson correlation *r* coefficients were calculated among severity values using Genstat 19.

2.4. Genetic analysis

As for Fusarium Panel, the RIL population genomic DNA was extracted at the Plant Genetics laboratory of DISTAL - UNIBO using NucleoSpin® 8/96 Plant II Core Kit from Macherey Nagel and sent for SNP genotyping to TraitGenetics. The identification of QTL intervals in the genome of the RILs was carried out for 876 SNPs using a single marker analysis (SMA) in QTL Cartographer v. 2.5 (Wang et al. 2012). Then the additive effect and the percentage of total variation for each locus were calculated using the multiple interval mapping (MIM) procedure of Kao et al. (1999). The whole genome was re-scanned searching for potential new main QTL and epistatic effects between main loci using “search for new QTL” and “QTL interaction” options, respectively. Finally, each QTL with the logarithms of odds (LOD) greater than 2.0 was considered as significant for subsequent analyses.

3. Selection of QTL hotspots and haplotype analysis

3.1. Haplotype analysis

Because patterns of variation within genomes are inherited as linkage groups (Daly et al. 2001; Patil et al. 2001) and to increase the polymorphism information content (PIC), selected SNP markers from major QTL hotspots, reporting by genetic analyses, were forced to be chosen as tagger using a r^2 threshold > 0.3 of LD (Haploview 4.2. software) to obtain haplotype blocks. A “Least Significant Difference” (LSD) test ($P < 0.05$) (*Agricolae* package, *R-project*) grouped the haplotypes using letters or their combinations (a = susceptibility, ab = susceptibility/tolerance and b = tolerance) as indicative of significant differences in FHB index or DON response. Genetic relationships among haplotypes were assessed through median joining networks from *PopART* software (Leigh and Bryant, 2015) while phenotype relationships were showed through box-plots and pie charts from Genstat 19 software.

3.2. KASP assays

Single or multiple SNP markers were chosen to discriminate the “LSD” haplotype groups using a KASP genotyping assay which exhibit superior properties compared to other marker systems in terms of low cost, high-throughput analysis, accuracy, reproducibility and flexibility (Segman et al. 2014). The link <https://biosearch-cdn.azureedge.net/assetsv6/KASP-genotyping-chemistry-User-guide.pdf> describes the KASP reaction and its components. After completion of the thermal reaction, genotype clusters were acquired and results were showed in allelic discrimination plots. The plate was thermally cycled for repetitive additional three or six cycles when sufficient defined genotype clusters have not been obtained.

4. KASP validation on PSB Panel

A panel of durum wheat genotypes (PSB Panel), including a Fusarium Panel subset as well as lines provided by Syngenta - PSB (SY), was grown in Argelato (BO) and evaluated for DON content (ppb) in four different years (2009, 2010, 2017, 2018) by Syngenta - PSB. Scripts in *R-project* were used to calculate Pearson correlation r coefficients among DON values as well as analysis of variance (ANOVA) treating genotypes and years. Then, best linear unbiased estimator (BLUE) values were generated from the DON measurements by the integration of the years and adjusted for heading data (HD) using Genstat 19 for the final haplotype-tagging KASPar marker validation, main purpose of this study.

RESULTS

Phenotypic analyses

As for elite accessions (Fusarium Panel), Table 1 shows summary statistics for incidence, severity, FHB index (AUDPC values) as well as deoxynivalenol (DON) and Fusarium-damaged kernels (FDK) referring to year (2015 and 2016) and inoculum (FG and FC) evaluated in Idice and Tolentino. Considering both years (2015 and 2016) in Idice, the h^2 showed high values for incidence ($63.6 < h^2 < 94.4$), severity ($63.1 < h^2 < 98.5$), FHB index ($54.1 < h^2 < 83.5$), DON ($82.1 < h^2 < 90.4$) and FDK ($79.7 < h^2 < 90.8$). Similarly, the h^2 showed high values in Tolentino for incidence ($71.94 < h^2 < 94.8$), severity ($67.7 < h^2 < 88.6$) and FHB index ($69.4 < h^2 < 92.8$). High significant relationships were observed among accessions (A), years (Y) and inocula (I) as well as (A \times Y) and (I \times Y) interactions for DON (2015+2016 - Idice) while among A, Y and I as well as (I \times Y) interaction for FDK (2015+2016 - Idice). In addition, high significant relationships

were observed between A and Y as well as (A × Y) interaction for FHB index (2015+2016 - Idice) and between A, environment (E) and (A × E) interaction for FHB index (2015+2016 - Idice+Tolentino) (Supplementary Table 2). The phenotypic distributions approximated normality for all traits evaluated in Idice and Tolentino while Pearson correlation coefficients (r) were positively significant for incidence, severity and FHB index between environments (Supplementary Table 3): $0.30 < r < 0.46$ between FHB index-2015 and -2016 (Idice), $0.24 < r < 0.35$ between FHB index-2015 (Idice) and -2016 (Tolentino) and $0.21 < r < 0.42$ between FHB index-2016 (Idice) and -2016 (Tolentino). Pearson correlation coefficients (r) were also positively significant for DON and FDK: $0.27 < r < 0.48$ between DON-2015 and -2016 and $0.20 < r < 0.43$ between FDK-2015 and -2016. Fusarium Panel grown in Idice and obtained by the integration of 2015 and 2016 years as well as FC and FG showed a significant and positive correlation. A high correlation was observed between incidence and severity ($r = 0.76$) as well as DON and FDK ($r = 0.47$) while a slightly lower correlation between FHB index and FDK ($r = 0.41$) as well as FHB index and DON ($r = 0.41$). By comparing the different inocula, FC-specific and FG-specific DON ($r = 0.69$) as well as FC-specific and FG-specific FDK ($r = 0.36$) were positively correlated. The phenology measured as FT negatively correlated with all traits evaluated in Idice by the integration of years as well as inocula, from $r = -0.11$ with FDK to $r = -0.62$ with incidence. In reference to single or multiple comparisons among inocula (FC and FG), years and environments (2015, 2016 in Idice and 2017 in Cadriano) as well as accessions for DON content, ANOVA showed high significant relationships among accessions years (Y) and (I × Y) interactions for DON (Table 2). Pearson correlation coefficients (r) were positively significant: from $r = 0.40$ between DON-2015-16 FC (Idice) and DON-2017 FG (Cadriano) to $r = 0.78$ between DON-2015-16 FC (Idice) and DON-2015-16 FG (Idice). Based on a range of optimal k subpopulations between 2 and 10, $k = 3$ was considered using Bayesian algorithm implemented as described by Evanno et al. (2005). A total of 108 accessions (83%) were grouped into one of the main gene pools at a Q membership coefficient \geq

0.5, while the remaining 22 (17%) were considered as admixed. Three subgroups (S) were identified: S1 included Italian germplasm, S2 included Mediterranean germplasm, CIMMYT and ICARDA selections for temperate areas and S3 included accessions from Canada and USA (Arizona, Minnesota, Montana and North Dakota). The Italian (S1) and the North American groups (S3) showed a high genetic diversity as evidenced by the box-plot distribution trends of decreased incidence, severity, FHB index as well as DON and FDK from S1 to S3 (Supplementary Figures 1 and 2).

Concerning the F₆ RILs (Table 2), the severity ranged from 87.6 to 661.8 in the first year (2014) while ranged from 190.01 to 975.16 in the second year (2015). The phenotypic values approximated normality and were positively correlated ($r = 0.51$) by comparing the two years. Regarding the third year (2016), the severity of the restricted number of 34 F₆ RILs was significantly correlated only with values in 2015 ($r = 0.46$) but not with values in 2014 ($r = 0.08$). High significant relationships were observed between accessions (A) and years (Y) for 2014+2015 - Tulln and 2015+2016 - Tulln+Bologna while not significant relationships for 2014+2016 - Tulln+Bologna) (Supplementary Table 4).

Table 1 | Summary statistics for incidence, severity, FHB index (AUDPC values) as well as deoxynivalenol (DON) content and Fusarium-damaged kernels (FDK) referring to year (2015 and 2016) and inoculum (FG: *Fusarium graminearum* and FC: *Fusarium culmorum*) on durum wheat accessions (Fusarium Panel) grown in Idice and Tolentino.

IDICE						
<i>Trait</i>	<i>Year</i>	<i>Fusarium spp.</i>	<i>Range</i>	<i>Mean</i>	<i>St. dev</i>	<i>h²</i>
INCIDENCE	2015	FG	0-2,742	1,358	555.3	63.6
	2015	FC	0-2,593	1,457	583.7	85.1

SEVERITY	2015	FG	0-3,923	1,167	514.9	85.7
	2015	FC	0-2,145	890.6	450.2	84.9
FHB index	2015	FG	0-69,591	18,214	12,64	70.3
	2015	FC	0-53,354	15,059	11,13	79.4
INCIDENCE	2016	FG	0-1,707	841.3	371.7	79.9
	2016	FC	0-2,077	953	418.3	94.4
SEVERITY	2016	FG	0-1,669	568.8	333.1	63.1
	2016	FC	0-1,773	675.5	328.7	98.5
FHB index	2016	FG	0-24,237	5,408	4,65	83.5
	2016	FC	0-31,810	7,230	5,76	54.1
<i>Trait</i>	<i>Year</i>	<i>Fusarium spp.</i>	<i>Range</i>	<i>Mean</i>	<i>St. dev</i>	<i>h²</i>
DON	2015	FG	2,316-18,675 ^a	8,160	3,90	83.9
	2015	FC	3,301-18,290	8,987	4,06	83.9
FDK	2015	FG	0-40 ^b	3.77	4.46	81.4
	2015	FC	0-40	3.61	5.34	79.7
DON	2016	FG	0-20,258	6,072	3,24	90.4
	2016	FC	0-16,116	6,357	3,16	82.1
FDK	2016	FG	0-22.28	7.73	3.1	90.8
	2016	FC	0-18.7	6.01	2.74	89.5

TOLENTINO

<i>Trait</i>	<i>Year</i>	<i>Fusarium spp.</i>	<i>Range</i>	<i>Mean</i>	<i>St. dev</i>	<i>h²</i>
INCIDENCE	2016	FG	0-3,577	1,695	771.5	94.8
	2016	FC	0-3,695	1,740	820.8	71.5
SEVERITY	2016	FG	18.73-3,137	1,406	601.9	88.6
	2016	FC	160.4-2,888	1,388	609.3	67.7
FHB index	2016	FG	0-90,406	27,191	21,244	92.8
	2016	FC	0-101,297	27,229	21,514	69.4

^a Parts per billion (ppb). ^b Percentage (%).

Table 2 | Summary statistics for severity referring to 2014 and 2015 years as well as *F. graminearum* as inoculum in 165 F₆ RILs from the population Simeto × Levante grown in Tulln (AT).

TULLN (AT) – Simeto × Levante

<i>Trait</i>	<i>Year</i>	<i>Fusarium spp.</i>	<i>Range</i>	<i>Mean</i>	<i>St. dev</i>
SEVERITY	2014	FG	87.6-661.8	288.0	117.2
	2015	FG	190.0-975.2	494.8	177.1

PSB Panel for KASP validation. The panel was evaluated for DON in four different years (2009, 2010, 2017 and 2018) by Syngenta - PSB. High correlations were observed between DON-2009 and DON-2010 ($r = 0.71$), DON-2009 and DON-2017 ($r = 0.78$) as well as DON 2009 and DON-2010 ($r = 0.95$). ANOVA showed high significant relationships between accessions (A) and years (Y) (Supplementary Table 5). These results have allowed the BLUE creation by the integration of the years as well as the adjustment using heading time (HD) values considering the high impact on DON ($r = -0.60$) in order to validate the haplotype-tagging KASPar markers.

Genetic analyses

Fusarium Panel. The confidence interval (CI) for QTL was based on the Hill and Weir formula (Hill and Weir, 1988). CI was of 1.58 (± 0.79) for QTL in accordance with the curve fit and the distance at which LD decays below r^2 of 0.3 (Hill and Weir, 1988) (Figure 1).

A total of forty-five *per se* QTL were identified for flowering time (FT) on Fusarium Panel by combining the results of the two year (2015 and 2016). Three of them mapped on chr. 3A, 5A and 7B explaining 28.9, 29.5 and 27.0% of phenotypic variation. A total of forty-three *per se* QTL were detected for incidence, severity and FHB index by the integration of both years and inocula (Idice). Fifteen of them were unique for incidence with two major loci on chr. 5A ($r^2 = 8.5$ and $r^2 = 8.6$) and 6A ($r^2 = 8.4$); the global R^2 (%) was highly significant (54.50). Fifteen of them were unique for severity with four major loci on 2A ($r^2 = 10.6$), 5A ($r^2 = 10.7$ and $r^2 = 11.9$) and 7A ($r^2 = 13.5$); the global R^2 (%) for the severity was similar to the incidence (54.35). Finally, thirteen of them were unique for FHB index with three major loci on 3B ($r^2 = 13.0$), 4B ($r^2 = 12.1$) and 7A ($r^2 = 20.6$); the global R^2 (%) was highly significant (61.24). A single QTL for FG-specific FDK ($r^2 = 8.80$) and four QTL for FC-specific FDK ($9.1 < r^2 < 12.7$) by integration of the two years in Idice. In addition, a total of three QTL were detected for FDK by the integration of both years and inocula with a major locus on chr. 4B ($r^2 = 10.5$). The global R^2 (%) of multiple QTL models ranged from 4.70

(FG-specific FDK) to 16.70 (FG+FC-specific FDK). A total of eleven QTL were detected for FG-specific DON with four major loci on chr. 1A ($r^2 = 11.9$), 2A ($r^2 = 10.6$ and $r^2 = 11.6$) and 6A ($r^2 = 10.7$); the global R^2 (%) was of 38.37. A total of six QTL for FC-specific DON were detected with two major loci on chr. 1A (10.7) and 1B (9.4); the global R^2 (%) was of 25.26. In addition, eleven QTL were identified for DON by the integration of both years and inocula. Five major locus were mapped on chr. 1A ($r^2 = 13.4$), 2A ($10.1 < r^2 < 12.1$), 6A ($r^2 = 11.1$) and 7B ($r^2 = 10.1$); the global R^2 (%) was 37.77. Further investigations allowed the detection of four major overlapping QTL intervals linked to more traits. The loci on chr. 2A ($6.4 < r^2 < 10.6$) and 5A ($5.9 < r^2 < 8.9$) influenced the incidence and DON; the locus on 4A influenced the FHB index ($r^2 = 12.1$) and FDK ($r^2 = 10.5$); the locus on 7A influenced the incidence ($r^2 = 4.1$), the severity ($r^2 = 5.1$) and the FHB index ($r^2 = 20.6$) as well as FDK ($7.3 < r^2 < 9.1$). In addition, five major QTL intervals were DON-specific, very representative by considering single or both inocula (FC and/or FG) and located on chr. 1A ($10.7 < r^2 < 13.4$), 1B ($9.4 < r^2 < 9.6$), 2A ($8.6 < r^2 < 12.1$), 3A ($7.4 < r^2 < 8.2$) and 4B ($8.3 < r^2 < 9.7$). A total of thirty-nine *per se* QTL were detected for incidence, severity and FHB index by the integration of both inocula (Tolentino). Eleven of them were unique for incidence with one major locus on chr. 4A ($r^2 = 7.5$); the global R^2 (%) was of 33.75. Fourteen of them were unique for severity with two major loci on 1A ($r^2 = 8.1$) and 5B ($r^2 = 8.4$); the global R^2 (%) for the severity was slightly higher than the incidence (41.98). Finally, fifteen of them were unique for FHB index with two major loci on 3B ($r^2 = 9.5$) and 4A ($r^2 = 9.3$); the global R^2 (%) was the lowest (20.69). Further investigations allowed the detection of five major overlapping QTL intervals, which influenced the three traits on chr. 1A ($4.8 < r^2 < 8.1$), 1B ($4.5 < r^2 < 6.2$ and $5.2 < r^2 < 6.7$), 3B ($5.2 < r^2 < 9.5$) and 4A ($7.5 < r^2 < 12.0$). A total of sixteen *per se* QTL were detected for FHB index mapped by integrating Idice and Tolentino environments. Six of them were FC-specific and mapped on 2A ($r^2 = 7.3$; $r^2 = 6.9$; $r^2 = 9.5$), 4A ($r^2 = 7.0$), 4B ($r^2 = 7.3$) and 5A ($r^2 = 8.9$). Four of them were FG-specific and mapped on 2A ($r^2 = 6.7$ and $r^2 = 7.7$), 4B ($r^2 = 5.9$) and 5B ($r^2 = 6.7$). Six of them

were FC+FG-specific and mapped on 2A ($r^2 = 6.2$; $r^2 = 7.8$; $r^2 = 9.7$), 3B ($r^2 = 6.7$), 4B ($r^2 = 7.3$) and 5B ($r^2 = 5.8$). The global R^2 (%) of multiple QTL models ranged from 7.65 (FG-specific FHB index) to 8.60 (FG+FC-specific FHB index).

On the RIL population Simeto × Levante grown in Tulln in 2014 and 2015, a total of twelve *per se* QTL were detected for severity. In the first year, a major locus was identified on chr. 3A (LOD = 4.15 and $r^2 = 4.31$) while, in the second year, two major loci were identified on 2A (LOD = 4.88 and $r^2 = 8.82$) and 4A (LOD = 12.19 and $r^2 = 23.02$). A total of four loci influenced the severity in both years and located on 2A, 2B, 3A and 4A.

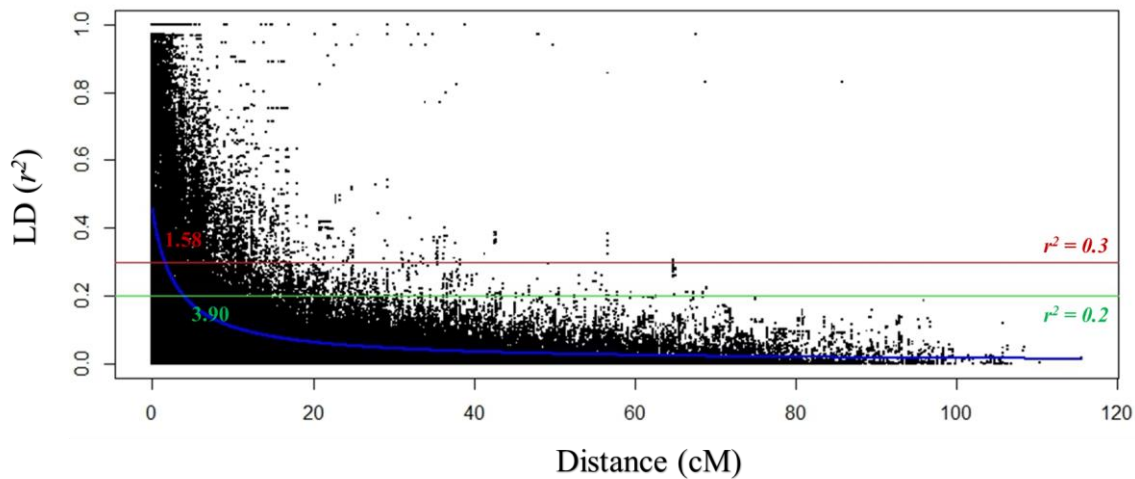


Figure 1 | The rate of linkage disequilibrium (LD) decay of the 130 durum wheat elite accessions (Panel Fusarium). The Hill and Weir formula was used to describe the LD decay of r^2 . The LD among Single Nucleotide Polymorphism (SNP) markers in the Panel Fusarium was estimated using Haploview 4.2 (Barrett et al. 2005). The blue curve represents the model fit to LD decay (nonlinear regression of r^2 on distance). A confidence interval of 1.58 cM for the quantitative trait loci (QTL) is showed when LD (r^2) is 0.3 (red line) while 3.90 cM when LD (r^2) is 0.2 (green line).

Selection of QTL hotspots and haplotype analysis. Based on the results reported herein, sixteen QTL hotspots were detected on chromosome arms 1AS, 1BL (2), 2AL (2), 3AL, 3BL, 4AL, 4BL, 5AL (2), 5BL, 6AL (2), 6BL and 7BL unrelated to phenology for the majority (Table 3). *QFHB.ubo-1A.1* ($10.7 < r^2 < 13.4$), *QFHB.ubo-1B.1* ($8.5 < r^2 < 9.6$), *QFHB.ubo-3A.1* ($7.4 < r^2 < 8.6$), *QFHB.ubo-6A.1* ($10.7 < r^2 < 11.1$), *QFHB.ubo-6A.3* ($9.2 < r^2 < 9.4$), *QFHB.ubo-7B.1* ($9.9 < r^2 < 10.1$) were DON-specific. *QFHB.ubo-4B.1* ($7.3 < r^2 < 12.7$) influenced DON and FDK as well as FHB index from both environments (Idice and Tolentino). *QFHB.ubo-2A.2* ($7.7 < r^2 < 12.1$) influenced DON as well as FHB index (Idice and Tolentino). *QFHB.ubo-5A.2* ($7.1 < r^2 < 13.8$) influenced incidence, severity (Idice) and FHB index (Idice and Tolentino). *QFHB.ubo-1B.2* ($6.6 < r^2 < 11.2$) was incidence-specific (Idice). *QFHB.ubo-2A.1* ($6.0 < r^2 < 10.6$) influenced severity and FHB index (Idice) while *QFHB.ubo-6A.2* ($6.5 < r^2 < 10.3$) influenced incidence and severity (Idice). *QFHB.ubo-3B.1* ($7.8 < r^2 < 13.7$) and *QFHB.ubo-5A.1* ($8.5 < r^2 < 9.7$) influenced incidence, severity and FHB index. *QFHB.ubo-4A.1* ($2.3 < r^2 < 5.8$) influenced incidence (Idice) and severity (Tulln) while *QFHB.ubo-5B.1* ($5.2 < r^2 < 7.8$) influenced incidence (Tolentino) and severity (Idice). *QFHB.ubo-2A.1*, *QFHB.ubo-4B.1*, *QFHB.ubo-5B.1* and *QFHB.ubo-6A.2* could be influenced by plant height and/or phenology due to the overlapping with flowering time (FT) loci.

Table 3 | List of sixteen GWAS-QTL hotspots significantly associated with incidence (INC), severity (SEV), FHB index (FHB), Fusarium-damaged kernels (FDK) and deoxynivalenol (DON) content.

QTL hotspot	Trait	Position (cM)	Log (P value)	R ² %
<i>QFHB.ubo-1A.1</i>	DON	10.16	3.51 - 4.22	10.7 - 13.4
<i>QFHB.ubo-1B.1</i>	DON	78.6 - 79.2	3.00 - 3.14	8.5 - 9.6
<i>QFHB.ubo-1B.2</i>	INC (I)	136.6 - 136.8	3.17 - 3.49	6.6 - 11.2
<i>QFHB.ubo-2A.1</i>	SEV, FHB (I)	107 - 109.5	3.00 - 4.17	6.0 - 10.6
<i>QFHB.ubo-2A.2</i>	DON, FHB (I), FHB (I+T)	208.7	3.00 - 4.73	7.7 - 12.1
<i>QFHB.ubo-3A.1</i>	DON	109.5	3.00 - 3.08	7.4 - 8.6
<i>QFHB.ubo-3B.1</i>	INC, SEV, FHB (I)	209.6	3.64 - 4.79	7.8 - 13.7
<i>QFHB.ubo-4A.1</i>	INC (I), SEV (TU)	144.6 - 150.9	3.13	2.3 - 5.8
<i>QFHB.ubo-4B.1</i>	DON, FDK, FHB (I), FHB (T), FHB (I+T)	81.5 - 83.1	3.22 - 4.57	7.3 - 12.7
<i>QFHB.ubo-5A.1</i>	INC, SEV, FHB (I)	91.6	3.35 - 4.23	8.5 - 9.7
<i>QFHB.ubo-5A.2</i>	INC, SEV, FHB (I), FHB (T), FHB (I+T)	114 - 119.4	3.27 - 4.80	7.1 - 13.8
<i>QFHB.ubo-5B.1</i>	SEV (I), INC (T)	145.2 - 148.6	3.04 - 3.20	5.2 - 7.8
<i>QFHB.ubo-6A.1</i>	DON	29.10	3.45 - 3.56	10.7 - 11.1
<i>QFHB.ubo-6A.2</i>	INC, SEV (I)	85.7	3.00 - 4.63	6.5 - 10.3
<i>QFHB.ubo-6A.3</i>	DON	123.0 - 126.8	3.09 - 3.17	9.2 - 9.4
<i>QFHB.ubo-7B.1</i>	DON	150.8	3.19 - 3.26	9.9 - 10.1

I: IDICE; T: TOLENTINO; TU: TULLN

For the haplotype analysis a total of eight QTL hotspots were selected in order to obtain haplotype blocks for DON and FHB index traits and increase the polymorphism information content (PIC) for future wheat breeding strategies. Six of them were specific for DON (*QFHB.ubo-1A.1*, *QFHB.ubo-1B.1*, *QFHB.ubo-2A.2*, *QFHB.ubo-3A.1*, *QFHB.ubo-6A.1* and *QFHB.ubo-7B.1*) while two for FHB index (*QFHB.ubo-2A.1* and *QFHB.ubo-5A.2*). To follow, the list and description of the eight linkage blocks:

HAP-QFHB.ubo-1A.1: three haplotypes containing ten markers were obtained from the peak SNP *IWB42976* ($r^2 = 0.8$). The “LSD” letters (*a*, *b*) and combination (*ab*) grouped them in response to DON. *IWB46412* discriminated the “*b* haplotype group” characterized by a low accumulation of the mycotoxin.

HAP-QFHB.ubo-1B.1: four haplotypes containing four markers were obtained from the peak SNP *IWB47303* ($r^2 = 0.8$). The “LSD” letters (*a*, *b*) grouped them in response to DON. Three haplotypes belonged to the “*b* haplotype group” characterized by a low accumulation of the mycotoxin and were discriminated using the same peak SNP.

HAP-QFHB.ubo-2A.1: three haplotypes containing nine markers were obtained from the peak SNP *IWB39681* ($r^2 = 0.3$). The “LSD” letters (*a*, *b*) and combination (*ab*) grouped them in response to FHB index. *IWB39681* and *IWB52471* discriminated the “*b* haplotype group” linked to FHB index tolerance.

HAP-QFHB.ubo-2A.2: seven haplotypes containing fourteen markers were obtained from the peak SNP *IWA6963* ($r^2 = 0.3$). The “LSD” letters (*a*, *b*) and combination (*ab*) grouped them in response to DON. Two haplotypes belonged to the “*b* haplotype group” characterized by a low accumulation of the mycotoxin and were discriminated using the following SNP markers: *IWA6963* and *IWB44619*.

HAP-QFHB.ubo-3A.1: four haplotypes containing thirteen markers were obtained from the peak SNP *IWB53914* ($r^2 = 0.8$). The “LSD” letters (*a*, *b*) grouped them in response to DON. Two

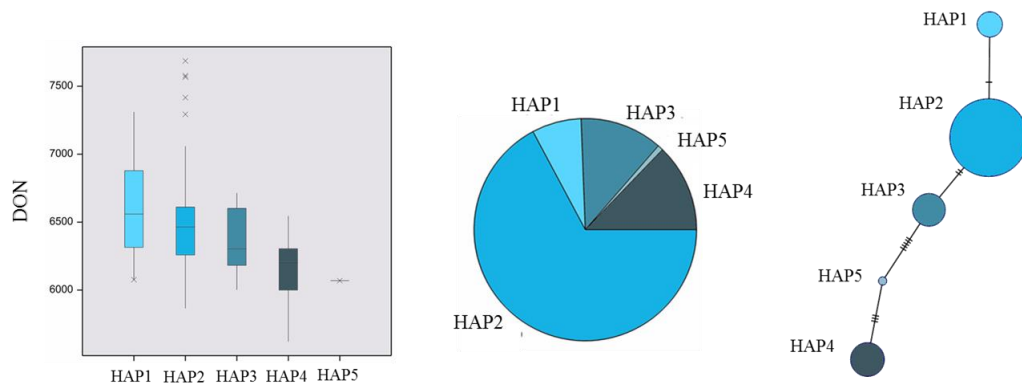
haplotypes belonged to the “*b* haplotype group” characterized by a low accumulation of the mycotoxin and were discriminated using the same peak marker.

HAP-QFHB.ubo-5A.2: seven haplotypes containing five markers were obtained from the peak SNP *IWB26027* ($r^2 = 0.8$). The “LSD” letter (*a*) and combination (*ab*) grouped them in response to FHB index. One haplotype belonged to the “*a* haplotype group” linked to FHB index tolerance susceptibility and was discriminated using the following SNP markers: *IWB75269* and *IWB70054*.

HAP-QFHB.ubo-6A.1: five haplotypes containing nine markers were obtained from the peak SNP *IWB56969* ($r^2 = 0.3$). The “LSD” letters (*a*, *b*) and combination (*ab*) grouped them in response to DON. Two haplotypes belonged to “*b* haplotype group” characterized by a low accumulation of the mycotoxin and were discriminated using *IWB56969* together with *IWB35328* (Figure 2).

HAP-QFHB.ubo-7B.1: three haplotypes containing three markers were obtained from the peak SNP *IWB60960* ($r^2 = 0.3$). The “LSD” letters (*a*, *b*) grouped them in response to DON. Two haplotypes belonged to “*b* haplotype group” characterized by a low accumulation of the mycotoxin and were discriminated using the same peak SNP marker.

HAP-QFHB.ubo-1A.1, *HAP-QFHB.ubo-1B.1*, *HAP-QFHB.ubo-3A.1* and *HAP-QFHB.ubo-6A.1* showed a high compatibility genetic relationship between intraspecific haplotype sequences and response to deoxynivalenol (DON) content as reported by the use of haplotype median joining networks (Leigh and Bryant, 2015). The box-plot showed the difference in DON accumulation between the different haplotype groups per linkage block. The pie charts illustrated the numerical proportion of the haplotype group frequency within the Fusarium Panel as well as the relative three subgroups (S1, S2 and S3) with a decreasing trend of DON content from the old Italian cultivars (S1) to the modern North American cultivars (S3) (Supplementary Figure 3).



Markers	Chr.	Pos.	r^2	Alleles	Haplotypes	Code	Frequency (%)	Group (LSD test)	DON
<i>IWB11722</i>	6A	29.10	0.96	T/C	TGTTACCCCTG	HAP1	7.2	a	6624.126
<i>IWB35328</i>	6A	29.10	0.48	G/A	TGTTACCCCTT	HAP2	67.2	a	6500.755
<i>IWB35338</i>	6A	29.10	1	T/C	TATTACCCT	HAP3	12.0	ab	6363.969
<i>IWB35923</i>	6A	29.10	0.53	T/C	CACCGTTTCG	HAP4	12.8	b	6141.082
<i>IWB56969</i>	6A	29.10	1	A/G	TACTGTCCG	HAP5	0.08	b	6069.488
<i>IWB64837</i>	6A	29.10	1	G/A					
<i>IWB66392</i>	6A	29.10	1	A/G					
<i>IWB71341</i>	6A	29.10	0.58	C/T					
<i>IWB36506</i>	6A	34.90	0.36	T/G					

Subgroup 1: Italy
 Subgroup 2: CIMMYT-Mediterranean
 Subgroup 3: North-America

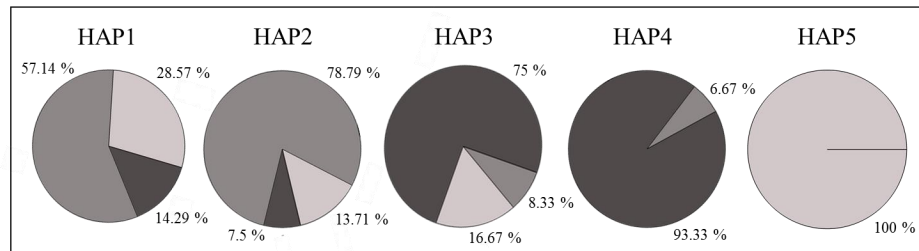
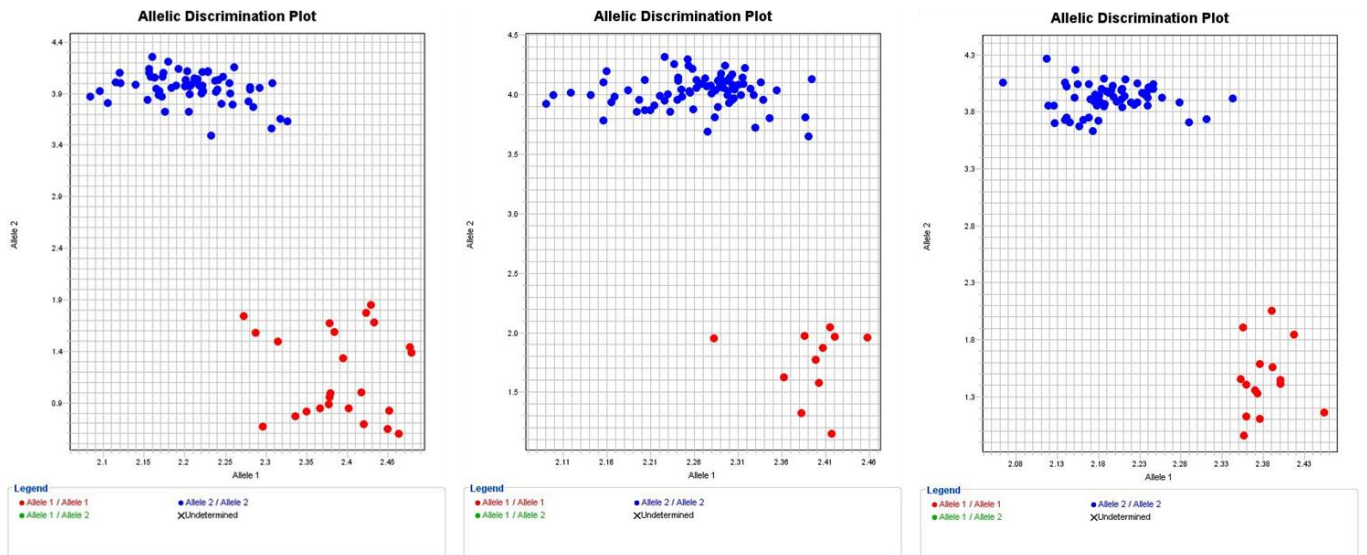


Figure 2 | Box-plot, pie chart and median joining network of the linkage block *HAP-QFHB.ubo-6A.1*. Five haplotype groups (HAP1-5) from designated TAG-SNP markers (yellow) of the QTL hotspot *QFHB.ubo-6A.1* showed a different response to deoxynivalenol (DON) content as well as distribution in the three subgroups (S1-S3).

KASP validation on PSB Panel. KASP assays on *K-IWB46412* for *HAP-QFHB.ubo-1A.1*, *K-IWB47303* for *HAP-QFHB.ubo-1B.1*, *K-IWB53914* for *HAP-QFHB.ubo-3A.1*, *K-IWB70054* for *HAP-QFHB.ubo-5A.2*, *K-IWB35328* and *K-IWB56969* for *HAP-QFHB.ubo-6A.1* (Table 4) showed the effectiveness in differentiating resistant and susceptible genotypes (Supplementary Figure 4). The alleles identified per genotype in KASP results had a complete correspondence with the respective haplotypes. Considering *HAP-QFHB.ubo-1A.1*, the KASP assay identified the favorable allele (T) for *IWB46412* (T/C) in 75.4% of elite/SY genotypes. Considering *HAP-QFHB.ubo-1B.1* (Figure 3), the KASP assay identified the favorable allele (C) for *IWB47303* (C/A) in 17.1% of elite/SY genotypes. Considering *HAP-QFHB.ubo-3B.1*, the KASP assay identified the favorable allele (C) in *IWB53914* (T/C) in 84.3% of elite/SY genotypes. Considering *HAP-QFHB.ubo-6A.1*, the KASP assay identified the favorable allele combination (AG) for *IWB56969* (A/G) and *IWB35328* (A/G) in 7.3% of elite/SY genotypes. The KASP assays validated the haplotype-tagging markers against response to DON content for *HAP-QFHB.ubo-1A.1*, *HAP-QFHB.ubo-1B.1* and *HAP-QFHB.ubo-6A.1* as revealed by ANOVA results (Supplementary Table 6) which demonstrated their potential application in durum wheat breeding programs.

Table 4 | List of KASPar markers used to discriminate the haplotype groups with susceptibility/tolerance to deoxynivalenol (DON) content or FHB index (*K-IWB46412*, *K-IWB47303*, *K-IWB53914*, *K-IWB70054*, *K-IWB35328* and *K-IWB56969*).

KASPar marker	
<i>K-IWB46412</i>	FAM GAAGGTGACCAAGTTCATGCTGCAGCAACATCCCGAAGCTA
	HEX GAAGGTCTGGAGTCAACGGATTGCAGCAACATCCCGAAGCTG
	Common CGCCATGCGGGGAACTATC
<i>K-IW47303</i>	FAM GAAGGTGACCAAGTTCATGCTGAAACTGACCTGCCTCAAGTAA
	HEX GAAGGTCTGGAGTCAACGGATTGAAACTGACCTGCCTCAAGTAC
	Common CTCGATCTGGTCTGGAAATG
<i>K-IWB53914</i>	FAM GAAGGTGACCAAGTTCATGCTTCTTGACATGGTCAGTGTAATGCTT
	HEX GAAGGTCTGGAGTCAACGGATTTCTTGACATGGTCAGTGTAATGCTC
	Common TATTTGTGCTGTGCGGTAAACAGATGACAT
<i>K-IWB70054</i>	FAM GAAGGTGACCAAGTTCATGCTAGTGCCAAGGGAGCTCTTAGTT
	HEX GAAGGTCTGGAGTCAACGGATTAGTGCCAAGGGAGCTCTTAGTC
	Common GCATCGATGTTTTCTTACCGAAGAAATA
<i>K-IWB35328</i>	FAM GAAGGTGACCAAGTTCATGCTCACAGGGAAAAACAAAGCTCATCG
	HEX GAAGGTCTGGAGTCAACGGATTACAGGGAAAAACAAAGCTCATCA
	Common GGCCTCTGTTGCTGGTCC
<i>K-IWB56969</i>	FAM GAAGGTGACCAAGTTCATGCTAAGGACTTGCGGACCTACCA
	HEX GAAGGTCTGGAGTCAACGGATTAAGGACTTGCGGACCTACCG
	Common CGAGCCCCTGCCTCATG



IWB47303

FAM **GAAGGTGACCAAGTTCATGCTGAAACTGACCTGCCTCAAGTAA**
 HEX **GAAGGTCGGAGTCAACGGATTGAAACTGACCTGCCTCAAGTAC**
 Common **CTCGATCTGGTCTGGAAATG**

Figure 3 | Allelic discrimination plots using the KASP assay for the alleles (C/A) of the SNP *IWB47303* on chromosome 1B. The red and blue dots refer to the two homozygous genotypes with opposite DON accumulation response.

DISCUSSION

Phenotypic analyses

The greater efforts in North American durum wheat breeding programs (Clarke et al. 2010; Steiner et al. 2019) led the S3 accessions to a higher FHB resistance/tolerance as well as a lower DON content than S1 accessions, consequent to their high genetic diversity revealed in the current study. In this respect, five cultivars belonging to S3 (Edmore, Levante, Neodur, Provenzal and Shabha) exhibited low DON values in their kernels, in contrast to three cultivars belonging to S1 (Colosseo, Normanno and Simeto).

The high heritability per trait referred to repeatable check cultivars within the experimental blocks showed how the variation in genetic factors highly affected the phenotypic values, while the positive Pearson correlations (r) among traits reflected their same direction in the FHB response. The ANOVA results indicated significant relationships mainly for DON, FDK and FHB index within the single environments by considering accessions and years as well as interactions.

The inoculum, consisting of FC or FG single-spore isolates, produced more differences in FDK than DON and other FHB responses. Additionally, FC showed a higher aggressiveness than FG isolates (Mesterhazy et al. 2002; Tóth et al. 2008) leading to a higher DON-producing capacity (ppb) and damaged kernels, although the ecological requirements for growth and mycotoxin production could differ considerably in basis of water activity, temperature and time effects (Hope et al. 2005). In the current study, we discriminated cultivars (Cappelli, Karim, Kofa, Latino, Maier and Sfinge) which accumulated DON especially from FC and cultivars (Ardente, Don Pedro, Guerou-1, Kronos, Lloyd and Monastir) from FG isolates .

A restricted number of elite accessions was evaluated for DON in the third year (2017) using a point-inoculation method (Purahong et al. 2014), contrary to the spray-inoculation method in the years before. The investigated accessions reacted differently to the DON response comparing both

procedures. As reported by Miedaner et al. (2003), type I resistance is the most appropriate for large-scale routine screening of breeding materials but is not fully appropriate to reduce infection efficiency, while type II seems to be more useful to reduce FHB progress in terms of limit yield losses and DON content.

A restricted number of RILs was investigated for severity in greenhouse conditions using a FG point-inoculation method. As reported by Imathiu et al. (2014), the spray-procedure has the advantage to detect both resistance types I and II, in contrast to the point-procedure which is type II-specific. Comparing the point- (2016) and the spray-inoculation (2014-15), high significant relationships were observed for severity between 2015 and 2016 years but not between 2014 and 2016 years by evidencing a scarce repeatability.

Genetic analyses

The study illustrated the utility of haplotypes to identify potential novel sources of FHB resistance/tolerance in durum wheat based on their known superior performance over single markers (Terwilliger, 1995; Meuwissen and Goddard, 2001) to increment the polymorphic information content (PIC) for future breeding programs (N'Diaye et al. 2017). GWAS model (MLM+K) with FT as covariate revealed sixteen genetic QTL hotspots for INC, SEV, FHB index, FDK and/or DON into BLUE considering multiple and combined environments, years and inocula. *QFHB.ubo-2A.1*, *QFHB.ubo-4B.1*, *QFHB.ubo-5B.1* and *QFHB.ubo-6A.2* could be influenced by phenology for the overlapping with flowering time (FT) loci. According with the chromosome position on the durum consensus map (Maccaferri et al. 2015a) they overlapped with FHB QTL/genes mapped on *Triticum aestivum* and/or *Triticum turgidum ssp. durum* genomes by previous studies in literature even if *QFHB.ubo-1B.2* and *QFHB.ubo-6A.2* represented a novelty in wheat. According to a phenotypic variance (r^2) > 10, three QTL hotspots (*QFHB.ubo1A.1*, *QFHB.ubo-6A.1* and *QFHB.ubo-7B.1*) were DON-specific, while *QFHB.ubo-5A.2* influenced FHB

index in multiple environments (Idice and Tolentino). *QFHB.ubo-2A.1*, explaining from 6.0 to 10.6% of the FHB variation, was identified by Zhang et al. (2014) in emmer and durum wheat using a SNP based linkage map and by Zhao et al. (2018) from the cross between Joppa (a durum wheat cultivar) and 10Ae564 (a durum wheat introgression line). *Qfhb.ndwp-2A* reported by Zhao explained 14% and 15% of severity in two greenhouse experiments as well as 9 % of DON. Additionally, Sari et al. (2018) mapped two loci overlapping *QFHB.ubo-1A.1* as well as *QFHB.ubo-2A.1* explaining 12.2 % of severity from a doubled haploid (DH) population developed from cross between *T. turgidum ssp. durum* cultivar Strongfield and *T. turgidum ssp. carthlicum* cultivar Blackbird. Most of the QTL hotspots are DON-specific (*QFHB.ubo-1A.1*, *QFHB.ubo-1B.1* and *QFHB.ubo-3A.1*, *QFHB.ubo-6A.1*, *QFHB.ubo-6A.3* and *QFHB.ubo-7B.1*). Until now, DON content was genetically investigated in *Triticum aestivum*. In this regards, Wu et al. (2019) performed a GWAS in a Chinese elite wheat germplasm and mapped *QFHB-2BL.1* and *QFHB-3A* linked to DON content and fungal spread. He et al. (2018) investigated RILs from the cross between a FHB-susceptible cultivar “NASMA” and FHB-resistant CIMMYT breeding line “IAS20*5/H567.71” detecting two significant DON QTL on chromosome 3B and 3D in response to FG inoculum. Draeger et al. (2007) studied the genetics of DON in a DH population from a cross between cultivars Arina (FHB resistant) and Riband (FHB susceptible) inoculated with macroconidia of FG and mapped a DON-locus on the chromosome arm 6BL. In all these cases, we did not observe QTL overlaps towards our DON-specific loci in durum wheat.

Haplotype analysis and KASP assays

Although SNP markers represent the genotyping system of choice for crop genetic studies as well as MAS (Liu et al. 2014; Randhawa et al. 2013; Dreisigacker et al. 2015; Rasheed et al. 2016) due to their genomic abundance and detection easiness, the bi-allelic form is a limiting factor according to the resolution at which SNP-trait relationships can be delineated. An efficient way to overcome

this limitation is to construct linkage blocks based on LD (Qian et al. 2017). In this respect, eight of sixteen QTL hotspots were chosen in order to generate linkage blocks, based on three parameters: i) high r^2 value, ii) haplotype diversity in response to DON or FHB index and iii) absence of phenological influence. Six linkage blocks discriminated haplotype groups for DON (*HAP-QFHB.ubo-1A.1*, *HAP-QFHB.ubo-1B.1*, *HAP-QFHB.ubo-2A.2*, *HAP-QFHB.ubo-3A.1*, *HAP-QFHB.ubo-6A.1* and *HAP-QFHB.ubo-7B.1*) and two for FHB index (*HAP-QFHB.ubo-2A.1* and *HAP-QFHB.ubo-5A.2*) according to a linkage disequilibrium threshold of $r^2 > 0.3$. The linkage blocks identified potential novel sources of FHB resistance/tolerance based on their known superior performance over single markers (Terwilliger, 1995; Meuwissen and Goddard, 2001) and PIC increase (N'Diaye et al. 2017) by providing a higher average genetic diversity among cultivars in order to optimize the breeding strategies (Chao et al. 2009). The haplotype median joining networks (Leigh and Bryant, 2015) reflected a high compatibility among intraspecific sequences and DON or FHB index response.

Singh et al. (2019) developed a KASPar marker for *Fhb1* in bread wheat to enhance the breeding efficiency for FHB resistance. In a similar way, the study supported the design of diagnostic KASPar markers to discriminate the haplotype groups mentioned above and select for novel FHB resistant durum wheat cultivars. The KASP assays demonstrated the effectiveness of “LSD” haplotype group discriminations within three DON-specific linkage blocks (*HAP-QFHB.ubo-1A.1*, *HAP-QFHB.ubo-1B.1* and *HAP-QFHB.ubo-6A.1*) by providing useful ways to facilitate MAS in durum wheat breeding programs in a timely and cost-effective manner and ensure future sustainable food production.

CONCLUSIONS

This study applied two genetic approaches to detect sixteen genetic QTL hotspots for FHB tolerance in durum wheat and illustrated the utility of haplotypes to identify potential genetic sources of FHB tolerance based on their known superior performance over single SNPs in MAS programs. Our results are the first to validate suitable KASPar markers against the DON accumulation (*K-IWB46412*, *K-IWB47303*, *K-IWB35328* and *K-IWB56969*) by testing them in over 100 lines and proving to be effective in differentiating resistant and susceptible genotypes.

The KASP assay is shown to be suitable for the high-throughput screening of large populations and for the selection of cultivars pyramiding loci for resistance/tolerance to DON content and other FHB traits.

APPENDIX

Supplementary Table 1 | List of the 130 durum wheat accessions (cultivars, landrace selections and breeding lines) with registration details.

Fusarium Panel	Short name	Origin	Donation	Year
DP004	Lesina	ITALY	CRA-CER	1998
DP005	MERIDIANO	ITALY	UNIBO	1999
DP008	PIETRAFITTA	ITALY	UNIBO	n.a.
DP010	TORREBIANCA	ITALY	UNIBO	n.a.
DP012	CIMMYT-36	CIMMYT	UNIBO	n.a.
DP028	ALDEANO	IRTA	UNIBO	n.a.
DP029	ARIESOL	IRTA	UNIBO	1993
DP034	BOLIDO	IRTA	UNIBO	n.a.
DP039	DURCAL	IRTA	UNIBO	n.a.
DP040	DUROI	IRTA	UNIBO	n.a.
DP055	MARZAK	INRA	UNIBO	1984
DP064	KARIM	ICARDA	UNIBO	1985
DP066	KRS/HAUCAN	ICARDA	UNIBO	n.a.
DP068	MOULSABIL-2	ICARDA	UNIBO	n.a.
DP077	APPIO	ITALY	UNIBO	1982
DP081	BRAVADUR	USA: Arizona	UNIBO	1993
DP082	BRONTE	ITALY	UNIBO	1996
DP083	CAPEITL_8	ITALY	UNIBO	1955
DP084	CAPPELLI	ITALY	UNIBO	1930
DP086	COLORADO	USA/ITALY	UNIBO	1995
DP087	COLOSSEO	ITALY	UNIBO	1995
DP088	CORTEZ	USA: Montana	UNIBO	1995
DP089	CRESO	ITALY	SIS	1974
DP090	DON PEDRO	CIMMYT	UNIBO	n.a.
DP091	DUILIO	ITALY	SIS	1984
DP096	GRAZIA	ITALY	ISEA	1985
DP097	IRIDE	ITALY	SIS	1996
DP100	KRONOS	USA: Arizona	UNIBO	1992
DP104	MOHAWK	USA	UNIBO	1998
DP105	OFANTO	ITALY	CRA-CER	1990
DP108	PRODURA	ITALY	UNIBO	1975
DP111	SVEVO	ITALY	UNIBO	1996

DP112	TRINAKRIA	ITALY	UNIBO	1970
DP116	WESTBRED_881	USA	UNIBO	1985
DP117	WESTBRED_TURBO	USA	UNIBO	n.a.
DP122	AMMAR-1	ICARDA	UNIBO	2010
DP126	AWALI-1	ICARDA	UNIBO	n.a.
DP142	GUEROU-1	ICARDA	UNIBO	n.a.
DP145	HEIDER	ICARDA	UNIBO	1997
DP148	ICARDA 125	ICARDA	UNIBO	n.a.
DP167	OMLAHN-3	ICARDA	UNIBO	n.a.
DP168	OMRUF-2	ICARDA	UNIBO	n.a.
DP172	OUASERL-1	ICARDA	UNIBO	n.a.
DP181	SHABHA	ICARDA	UNIBO	n.a.
DP189	KOFA	USA: Montana	UNIBO	1995
DP194	ARDEnte	FRANCE	UNIBO	1984
DP206	NEODUR	FRANCE	UNIBO	1987
DP217	MORSE	CANADA	UNIBO	1996
DP227	BELZER	USA: North-Dakota	UNIBO	1997
DP229	LLOYD	USA: North-Dakota	CREA-GPG	1983
DP238	EDMORE	USA: North-Dakota	UNIBO	1978
DP240	MINDUM	USA: Minnesota	UNIBO	1917
DP248	SIMETO	PSB ITALY	UNIBO	1988
DP249	LEVANTE	ITALY	UNIBO	2002
DP255	CHEN_1	CIMMYT	UNIBO	1983
DP256	MALMUK_1	CIMMYT	UNIBO	1992
DP258	HESSIAN-F	CIMMYT	UNIBO	n.a.
DP259	AJAIA_12	CIMMYT	UNIBO	1987
DP261	CNDO/PRIMADUR	CIMMYT	UNIBO	2008
DP263	VANRRIKSE_6.2	CIMMYT	UNIBO	1993
DP264	RANCO	CIMMYT	UNIBO	n.a.
DP265	PLATA_10	CIMMYT	UNIBO	1992
FP101	D-ISEASOF-7	ITALY	ISEA	n.a.
FP102	D-ISEASOF-8	ITALY	ISEA	n.a.
FP103	D-ISEASOF-9	ITALY	ISEA	n.a.
FP104	DURANGO	ITALY	ISEA	n.a.
FP105	ETTORE	ITALY	ISEA	n.a.
FP107	PROVENZAL	ITALY	ISEA	1998
FP108	SAN CARLO	ITALY	ISEA	n.a.
FP109	SPARTACO	ITALY	ISEA	n.a.
FP135	508GD07/10T	ITALY	SIS	n.a.
FP136	909GD08/77	ITALY	SIS	n.a.
FP137	ALEMANN0	ITALY	SIS	2006
FP138	ASTERIX	ITALY	SIS	n.a.

FP139	ATHORIS	n.a.	SIS	n.a.
FP140	AUREO	ITALY	SIS	2009
FP141	BABYLONE	ITALY	SIS	n.a.
FP142	BACARDI	ITALY	SIS	n.a.
FP143	BIENSUR	ITALY	SIS	n.a.
FP144	CESARE	ITALY	SIS	n.a.
FP147	DAKTER	ITALY	SIS	n.a.
FP148	DGE-1	USA: North-Dakota	SIS	2006
FP150	FURIO CAMILLO	ITALY	SIS	n.a.
FP151	GIBRALTAR	ITALY	SIS	n.a.
FP153	ISILDUR	ITALY	SIS	2007
FP154	JOYAU	ITALY	SIS	n.a.
FP155	KANAKIS	ITALY	SIS	n.a.
FP156	KARUR	ITALY	SIS	n.a.
FP157	LIBERDUR	ITALY	SIS	2007
FP158	MAGELLANO	ITALY	SIS	n.a.
FP159	MIRADOUX	FRANCE	SIS	2007
FP160	MURANO	n.a.	SIS	n.a.
FP161	OBELIX	n.a.	SIS	n.a.
FP162	OVIDIO	ITALY	SIS	2012
FP163	PESCADOU	n.a.	SIS	n.a.
FP164	RAMIREZ	n.a.	SIS	n.a.
FP165	SARAGOLLA	ITALY	SIS	n.a.
FP166	SCULPTUR	n.a.	SIS	n.a.
FP167	SERAFO NICK	n.a.	SIS	n.a.
FP168	SEVERO	n.a.	SIS	n.a.
FP169	SY CISCO	n.a.	SIS	n.a.
FP170	SY LIDO	n.a.	SIS	n.a.
FP171	TIREX	n.a.	SIS	n.a.
FP172	ACHILLE	n.a.	UNIBO	n.a.
FP189	CLAUDIO	ITALY	UNIBO	1998
FP195	Dupri	ITALY	UNIBO	n.a.
FP198	Dylan	ITALY	UNIBO	2002
FP206	JORDAN	ICARDA	UNIBO	n.a.
FP214	MAIER	AUSTRALIA	UNIBO	n.a.
FP221	MONASTIR	n.a.	UNIBO	n.a.
FP225	NORMANNO	ITALY	UNIBO	2002
FP226	ODISSEO	ITALY	UNIBO	2012
FP239	TIZIANA	ITALY	UNIBO	2001
FP26	L2300	n.a.	CRA-CER	n.a.
FP27	L2443	n.a.	CRA-CER	n.a.
FP34	Sfinge	n.a.	CRA-CER	n.a.

FP52	LATINO	ITALY	CREA-GPG	1982
FP54	SACHEM	FRANCE	CREA-GPG	1999
FP55	ZARDAK	n.a.	CREA-GPG	n.a.
FP86	CUSPIDE	ITALY	ISEA	n.a.
FP87	D-ISEASOF-1	ITALY	ISEA	n.a.
FP89	D-ISEASOF-10	ITALY	ISEA	n.a.
FP91	D-ISEASOF-12	ITALY	ISEA	n.a.
FP92	D-ISEASOF-13	ITALY	ISEA	n.a.
FP93	D-ISEASOF-14	ITALY	ISEA	n.a.
FP94	D-ISEASOF-15	ITALY	ISEA	n.a.
FP95	D-ISEASOF-16	ITALY	ISEA	n.a.
FP96	D-ISEASOF-17	ITALY	ISEA	n.a.
FP98	D-ISEASOF-4	ITALY	ISEA	n.a.
FP99	D-ISEASOF-5	ITALY	ISEA	n.a.

Supplementary Table 2 | Analysis of Variance (ANOVA), table of degrees of freedom (Df) and P values referring to single or multiple comparisons among *Fusarium culmorum* (FC) and *Fusarium graminearum* (FG) inocula, years (2015-2016 in IDICE and 2016 in TOLENTINO) and durum wheat accessions (Fusarium Panel) for deoxynivalenol (DON) content, Fusarium-damaged kernels (FDK), incidence, severity and FHB index.

<i>TRAIT</i>	<i>YEAR-ENVIRONMENT</i>	<i>VARIABLE</i>	<i>Df</i>	<i>Pr(>F)</i>
DON	2015-IDICE	A ¹	129	2.414e-07 ***
		I ²	1	0.1063
DON	2016-IDICE	A	129	2.230e-08 ***
		I	1	1.462e-07 ***
DON	2015+2016-IDICE	A	129	2.456e-10 ***
		I	1	9.288e-06 ***
		Y ³	1	1.175e-14 ***
		A × I	129	0.650353
		A × Y	129	0.001477 **
		I × Y	1	0.002585 **
FDK	2015-IDICE	A	129	1.2e-03 **
		I	1	7.6e-01
FDK	2016-IDICE	A	129	1.3e-03**
		I	1	< 2.2e-16 ***
FDK	2015+2016-IDICE	A	129	9.296e-05 ***
		I	1	1.057e-05 ***

		Y	1	9.471e-11 ***
		A × I	129	0.9122
		A × Y	129	0.5916
		I × Y	1	8.948e-05 ***
INCIDENCE	2015-IDICE	A	129	1.0000
		I	1	0.2706
		A × I	129	1.0000
INCIDENCE	2016-IDICE	A	129	0.07044
		I	1	0.14090
		A × I	129	1.00000
INCIDENCE	2016-TOLENTINO	A	129	2.318e-09 ***
		I	1	0.7511
		A × I	129	0.9086
INCIDENCE	2015+2016-IDICE	A	129	1.0000
		I	1	0.03083 *
		Y	1	1.623e-10 ***
		A × I	129	1.00000
		A × Y	129	0.9972
		I × Y	129	0.001756 **
INCIDENCE	2016-IDICE+TOLENTINO	A	129	6.470e-11 ***
		E ⁴	1	< 2.2e-16 ***
		I	1	0.2093
		A × E	129	1.155e-07 ***
		A × I	129	1.0000
		E × I	1	0.5522
		A × E × I	129	1.0000
INCIDENCE	2015+2016-IDICE+TOLENTINO	A	129	1.00000
		E	1	0.16264
		I	1	0.12195
		A × E	129	1.00000
		A × I	129	1.00000
		E × I	1	00.07504
		A × E × I		1.00000
SEVERITY	2015-IDICE	A	129	1.000
		I	1	0.455
		A × I	129	1.000
SEVERITY	2016-IDICE	A	129	0.3024
		I	1	0.6995
		A × I	129	1.0000
SEVERITY	2016-TOLENTINO	A	129	2.51e-08 ***
		I	1	0.8203
		A × I	129	0.9189
SEVERITY	2015+2016-IDICE	A	129	0.9996
		I	1	0.1152
		Y	1	5.378e-13 ***
		A × I	129	1.0000
		A × Y	129	0.9977
		I × Y	129	0.05267
SEVERITY	2016-IDICE+TOLENTINO	A	129	6.026e-07 ***
		E	1	< 2.2e-16 ***
		I	1	0.6588

		A × E	129	9.621e-06 ***
		A × I	129	1.0000
		E × I	1	0.7094
		A × E × I	129	1.0000
SEVERITY	2015+2016-IDICE+TOLENTINO	A	129	1.0000
		E	1	0.8301
		I	1	0.2847
		A × E	129	1.0000
		A × I	129	1.0000
		E × I	1	0.1635
		A × E × I	129	1.0000
FHB INDEX	2015-IDICE	A	129	0.9067
		I	1	0.6136
		A × I	129	1.0000
FHB INDEX	2016-IDICE	A	129	0.006208 **
		I	1	< 2.2e-16 ***
		A × I	129	0.056995
FHB INDEX	2016-TOLENTINO	A	129	5.032e-10 ***
		I	1	0.8988
		A × I	129	0.7337
FHB INDEX	2015+2016-IDICE	A	129	6.179e-13 ***
		Y	1	< 2.2e-16 ***
		I	1	0.4211
		A × I	129	1.0000
		A × Y	129	2.237e-14 ***
		I × Y	129	0.4265
FHB INDEX	2016-IDICE+TOLENTINO	A	129	<2e-16 ***
		E	1	<2e-16 ***
		I	1	0.9200
		A × E	129	<2e-16 ***
		A × I	129	0.7363
		E × I	1	0.9280
		A × E × I	129	0.8019
FHB INDEX	2015+2016-IDICE+TOLENTINO	A	129	5.111e-08 ***
		E	1	1.544e-11 ***
		I	1	0.714587
		A × E	129	0.002137 **
		A × I	129	0.999930
		E × I	1	0.703661
		A × E × I	129	0.999213

¹ Accession, ² Inoculum, ³ Year, ⁴ Environment;
0 < P value < 0.001 ***; 0.001 < P value < 0.01 **; 0.01 < P value < 0.05*.

Supplementary Table 3 | Pearson correlation coefficients (*r*) for incidence, severity and FHB index traits evaluated on durum wheat accessions referring to Idice (2015, 2016) and Tolentino (TOL, 2016) environments.

Pearson Correlation Coefficient (<i>r</i>)	INCIDENCE 15 FC IDICE	INCIDENCE 15 FG IDICE	SEVERITY 15 FC IDICE	SEVERITY 15 FG IDICE	FHB index 15 FC IDICE	FHB index 15 FG IDICE	INCIDENCE 16 FC IDICE	INCIDENCE 16 FG IDICE	SEVERITY 16 FC IDICE	SEVERITY 16 FG IDICE	FHB index 16 FC IDICE	FHB index 16 FG IDICE	INCIDENCE 16 FC TOL	INCIDENCE 16 FG TOL	SEVERITY 16 FC TOL	SEVERITY 16 FG TOL	FHB index 16 FC TOL	FHB index 16 FG TOL
INCIDENCE 15 FC IDICE	1	0.72	0.72	0.55	0.83	0.61	0.42	0.47	0.40	0.32	0.49	0.44	0.45	0.40	0.44	0.29	0.39	0.35
INCIDENCE 15 FG IDICE	-	1	0.66	0.71	0.70	0.83	0.36	0.37	0.33	0.32	0.40	0.37	0.39	0.38	0.35	0.29	0.32	0.31
SEVERITY 15 FC IDICE	-	-	1	0.54	0.95	0.60	0.37	0.38	0.43	0.33	0.45	0.38	0.41	0.36	0.39	0.29	0.35	0.32
SEVERITY 15 FG IDICE	-	-	-	1	0.55	0.95	0.29	0.29	0.28	0.24	0.33	0.27	0.32	0.27	0.34	0.23	0.30	0.24
FHB index 15 FC IDICE	-	-	-	-	1	0.64	0.36	0.41	0.44	0.33	0.46	0.41	0.41	0.36	0.40	0.31	0.35	0.33
FHB index 15 FG IDICE	-	-	-	-	-	1	0.29	0.30	0.29	0.25	0.36	0.30	0.32	0.28	0.3	0.25	0.30	0.24
INCIDENCE 16 FC IDICE	-	-	-	-	-	-	1	0.64	0.43	0.39	0.88	0.57	0.47	0.43	0.41	0.25	0.44	0.34
INCIDENCE 16 FG IDICE	-	-	-	-	-	-	-	1	0.39	0.52	0.59	0.87	0.44	0.40	0.36	0.18	0.38	0.29
SEVERITY 16 FC IDICE	-	-	-	-	-	-	-	-	1	0.31	0.69	0.39	0.29	0.29	0.30	0.16	0.26	0.24
SEVERITY 16 FG IDICE	-	-	-	-	-	-	-	-	-	1	0.42	0.82	0.37	0.17	0.23	0.01	0.26	0.06
FHB index 16 FC IDICE	-	-	-	-	-	-	-	-	-	-	1	0.58	0.45	0.42	0.40	0.28	0.42	0.36
FHB index 16 FG IDICE	-	-	-	-	-	-	-	-	-	-	-	1	0.45	0.33	0.34	0.13	0.37	0.21
INCIDENCE 16 FC TOL	-	-	-	-	-	-	-	-	-	-	-	-	1	0.75	0.86	0.64	0.93	0.68
INCIDENCE 16 FG TOL	-	-	-	-	-	-	-	-	-	-	-	-	-	1	0.70	0.82	0.71	0.93
SEVERITY 16 FC TOL	-	-	-	-	-	-	-	-	-	-	-	-	-	-	1	0.71	0.94	0.72
SEVERITY 16 FG TOL	-	-	-	-	-	-	-	-	-	-	-	-	-	-	-	1	0.68	0.93
FHB index 16 FC TOL	-	-	-	-	-	-	-	-	-	-	-	-	-	-	-	-	1	0.71
FHB index 16 FG TOL	-	-	-	-	-	-	-	-	-	-	-	-	-	-	-	-	-	1

Supplementary Table 4 | Analysis of Variance (ANOVA), table of degrees of freedom (Df) and P values referring to single comparisons among years (2014, 2015 and 2016) and F₆ recombinant inbred lines (RILs) from the cross Simeto × Levante for severity.

<i>TRAIT</i>	<i>YEAR-ENVIRONMENT</i>	<i>VARIABLE</i>	<i>Df</i>	<i>Pr(>F)</i>
SEVERITY	2014+2015-TULLN	A ¹	164	1.809e-08 ***
		Y ²	1	< 2.2e-16 ***
SEVERITY	2014+2016-TULLN+BOLOGNA	A	33	0.35145
		Y	1	0.07468
SEVERITY	2015+2016-TULLN+BOLOGNA	A	33	0.0052889 **
		Y	1	0.0005842 ***

¹RILs, ²Year;
 $0 < P \text{ value} < 0.001$ ***; $0.001 < P \text{ value} < 0.01$ **.

Supplementary Table 5 | Analysis of Variance (ANOVA), table of degrees of freedom (Df) and P-values referring to single comparisons among years (2009, 2010, 2017 and 2018) and durum wheat lines provided by Syngenta - PSB for deoxynivalenol (DON) content.

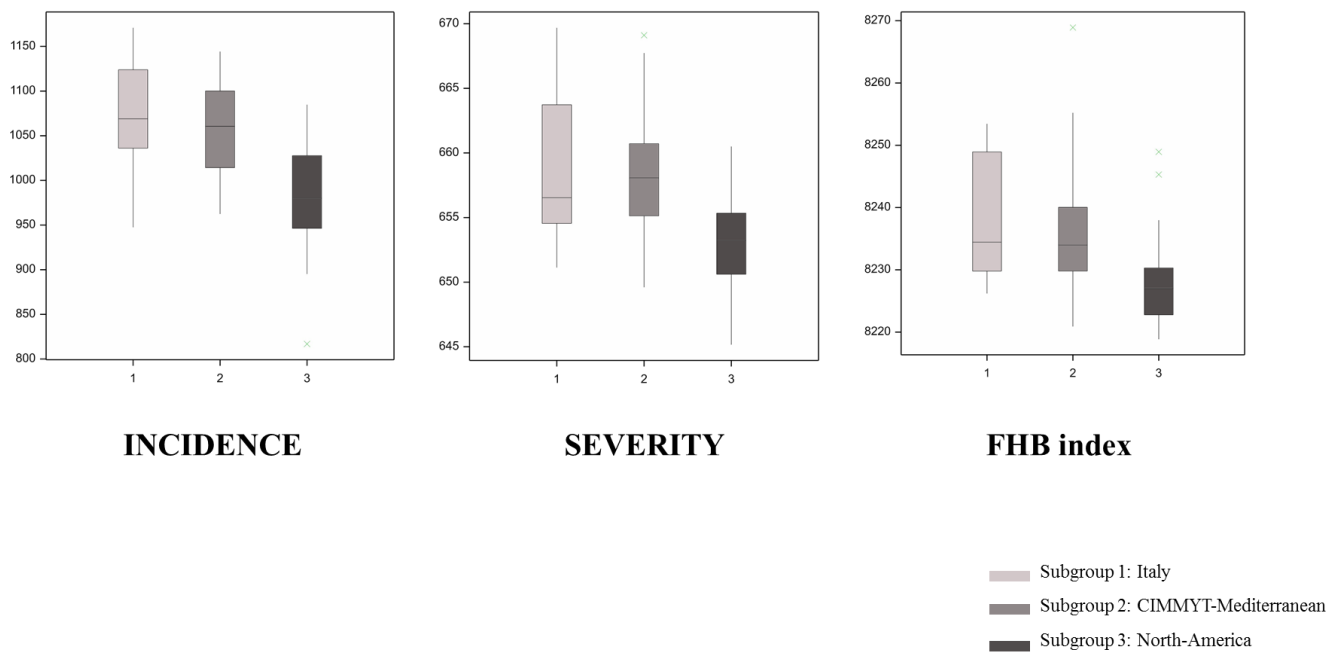
<i>TRAIT</i>	<i>YEAR-ENVIRONMENT</i>	<i>VARIABLE</i>	<i>Df</i>	<i>Pr(>F)</i>
DON	2009+2010+2017+2018-ARGELATO	A ¹	226	0.0003582 ***
		Y ²	3	< 2.2e-16 ***

¹ Genotypes provided by Syngenta - PSB, ² Year;
 $0 < P \text{ value} < 0.001$ ***; $0.001 < P \text{ value} < 0.01$ **; $0.01 < P \text{ value} < 0.05$ *.

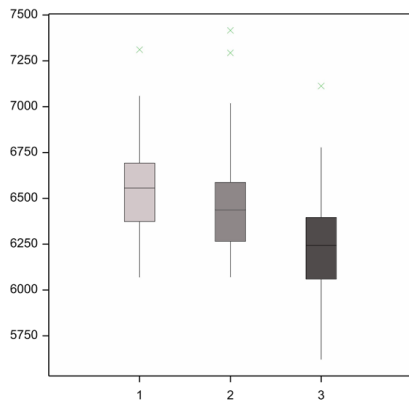
Supplementary Table 6 | PSB Panel including a subset of Fusarium Panel elite accessions as well as SY-lines provided by Syngenta - PSB was genotyped with four KASP assays in order to discriminate the “LSD” haplotype groups of interest within four DON-specific linkage blocks (*HAP-QFHB.ubo-1A.1*, *HAP-QFHB.ubo-1B.1*, *HAP-QFHB.ubo-3A.1* and *HAP-QFHB.ubo-6A.1*). The results reported a significant association ($P < 0.05$) between KASP genotyping data and DON analysis in elite/SY genotypes for *HAP-QFHB.ubo-1A.1*, *HAP-QFHB.ubo-1B.1* and *HAP-QFHB.ubo-6A.1* revealing their potential application in durum wheat breeding programs.

Analysis of variance (ANOVA)					
DON-specific linkage block	Trait	KASPar marker	VARIABLE	Df	Pr(>F)
<i>HAP-QFHB.ubo-1A.1</i>	DON	<i>K-IWB46412</i>	A ¹	165	0.017*
<i>HAP-QFHB.ubo-1B.1</i>	DON	<i>K-IWB47303</i>	A	190	0.042*
<i>HAP-QFHB.ubo-3A.1</i>	DON	<i>K-IWB53914</i>	A	151	0.249
<i>HAP-QFHB.ubo-6A.1</i>	DON	<i>K-IWB35328</i>	A	187	0.011*
		<i>K-IWB56969</i>			

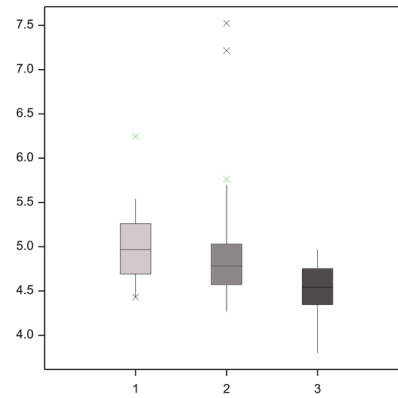
¹Genotypes provided by Syngenta - PSB;
0.01 < P value < 0.05*.



Supplementary Figure 1 | Box-plot distributions for the three durum wheat subpopulations (S1, S2 and S3) related to incidence, severity and FHB index of durum wheat accessions grown in Idice and obtained by the integration of 2015 and 2016 years as well as *Fusarium culmorum* (FC) and *Fusarium graminearum* (FG) inocula.



DON

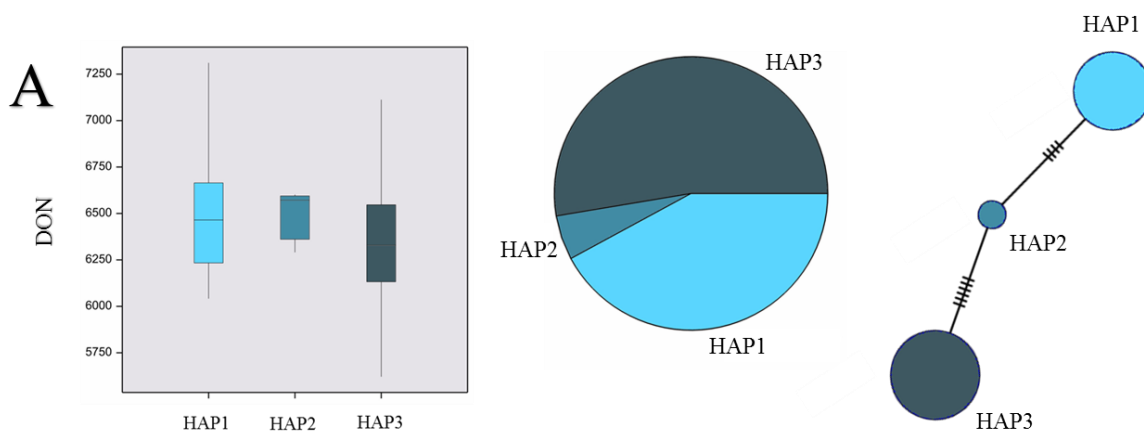


FDK



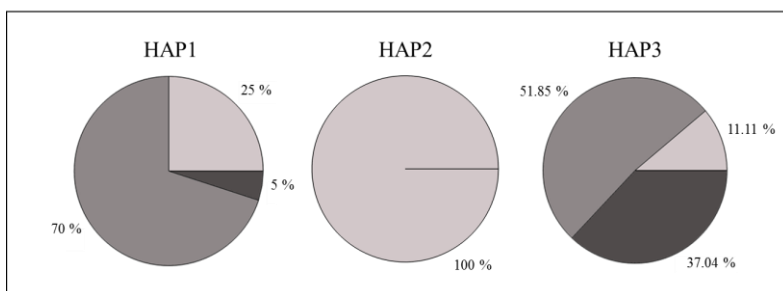
Supplementary Figure 2 | Box-plot distributions for the three durum wheat subpopulations (S1, S2 and S3) related to deoxynivalenol (DON) content and Fusarium-damaged kernels (FDK) of durum wheat accessions grown in IDICE and obtained by the integration of 2015 and 2016 years as well as *Fusarium culmorum* (FC) and *Fusarium graminearum* (FG) inocula.

Supplementary Figure 3 | Box-plot, pie charts and median joining networks of haplotype groups on Fusarium Panel from a designated TAG-SNP marker (bold) of four selected QTL hotspots (A: *QFHB.ubo-1A.1*, B: *QFHB.ubo-1B.1*, C: *QFHB.ubo-3A.1* and D: *QFHB.ubo-6A.1*) in response to deoxynivalenol (DON) content. I selected specific SNP markers (yellow) whose alleles were used to discriminate specific haplotype groups within block. The QTL hotspots showed a different response to deoxynivalenol (DON) content as well as distribution in the three subgroups (S1-S3).

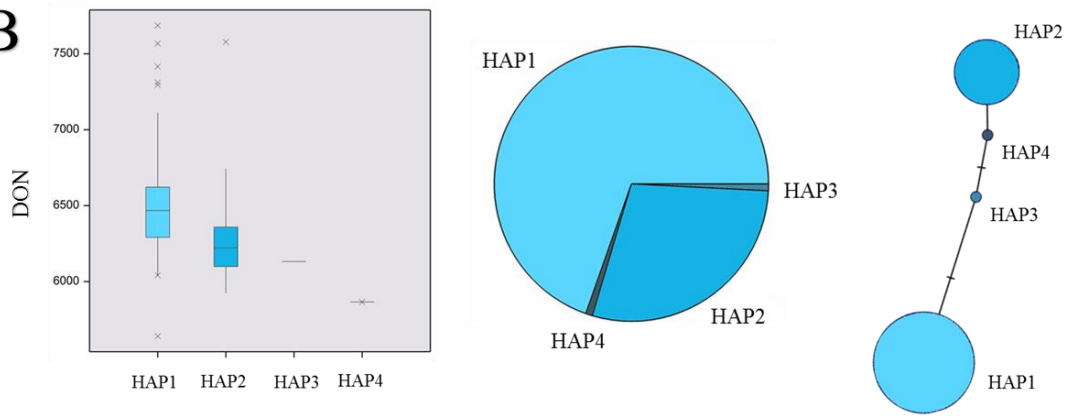


Markers	Chr.	Pos.	r ²	Alleles	Haplotypes	Code	Frequency	Group (LSD test)	DON
<i>IWB54411</i>	1A	8.4	1	A/G	GTTG C TCGCG	HAP1	41.2	a	6506.074
<i>IWB44057</i>	1A	8.6	0.93	T/C	GTTG C CTATG	HAP2	5.3	ab	6488.098
<i>wPt-4177</i>	1A	9.5	1	A/T	ACAA T CTATA	HAP3	53.5	b	6326.062
<i>IWB4497</i>	1A	9.8	0.93	A/G					
<i>IWB46412</i>	1A	9.8	0.86	T/C					
<i>IWB13068</i>	1A	9.9	0.81	T/C					
<i>IWB45715</i>	1A	9.9	0.81	T/C					
<i>IWB73129</i>	1A	9.9	0.81	A/G					
<i>IWB7333</i>	1A	9.9	0.81	T/C					
<i>IWB42976</i>	1A	10.6	1	A/G					

Subgroup 1: Italy
 Subgroup 2: CIMMYT-Mediterranean
 Subgroup 3: North-America

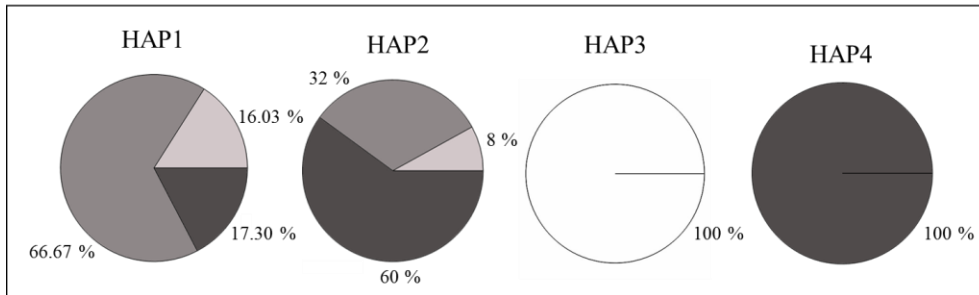


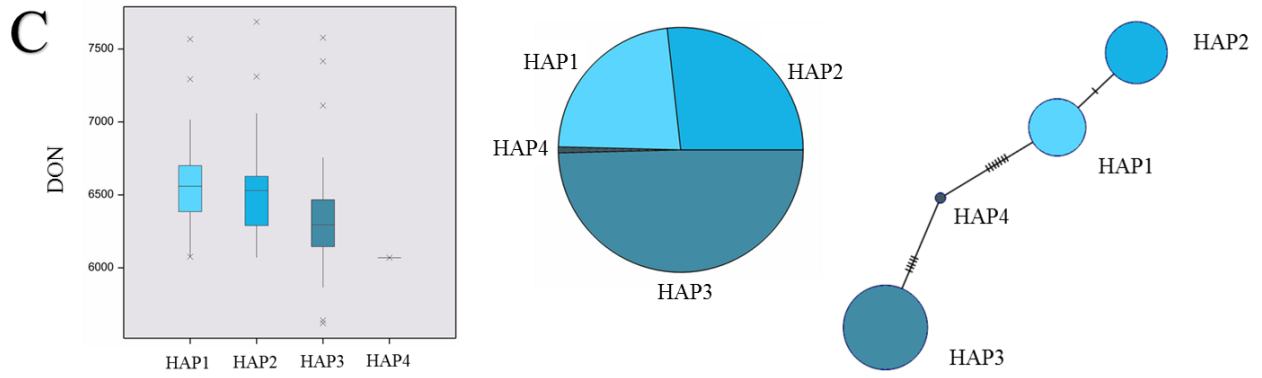
B



Markers	Chr.	Pos.	r^2	Alleles	Haplotypes	Code	Frequency	Group (LSD test)	DON
<i>IWB47303</i>	1B	78.6	1	A/C	A TAA	HAP1	69.6	a	6514.026
<i>IWB61864</i>	1B	78.6	0.88	T/C	CCGG	HAP2	28.8	b	6287.967
<i>IWB71347</i>	1B	78.6	0.84	A/G	CTAA	HAP3	0.8	b	6132.109
<i>IWB71353</i>	1B	78.6	0.82	T/C	CCAA	HAP4	0.8	b	5865.434

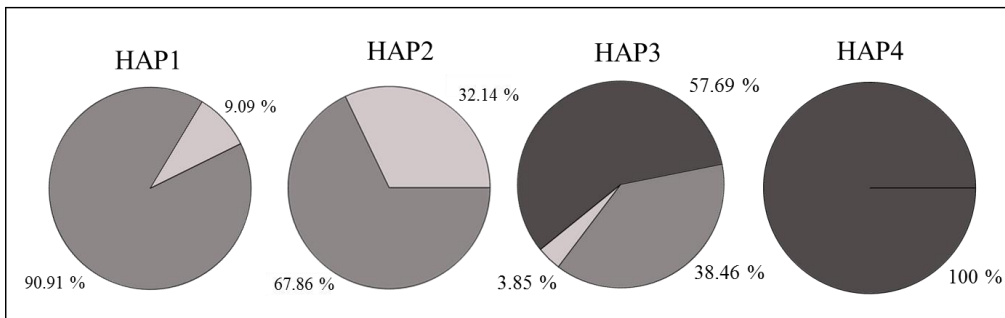
■ Subgroup 1: Italy
 ■ Subgroup 2: CIMMYT-Mediterranean
 ■ Subgroup 3: North-America



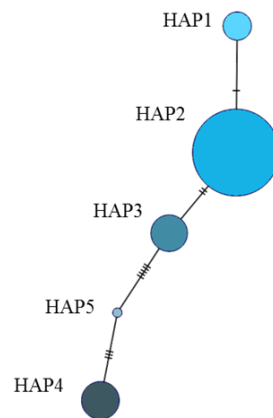
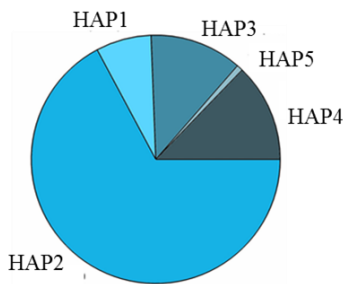
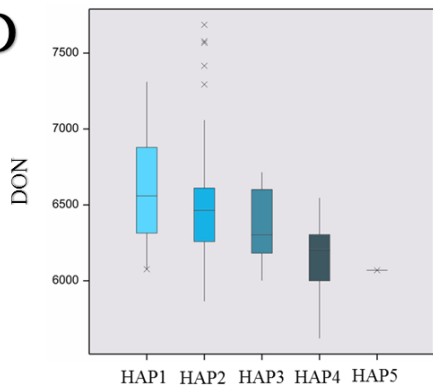


Markers	Chr.	Pos.	r^2	Alleles	Haplotypes	Code	Frequency	Group (LSD test)	DON
<i>IWB10137</i>	3A	108.10	0.86	A/G	AACACGTGCCGCT	HAP1	22.8	a	6559.667
<i>IWB32569</i>	3A	108.10	0.90	A/G	AACACGTGCCGCG	HAP2	26.8	a	6547.501
<i>IWB47928</i>	3A	108.10	0.90	C/T	AGCGCGTTCA TT	HAP3	49.6	b	6069.488
<i>IWB27980</i>	3A	108.40	0.88	C/T	GGTGTCTTTATT	HAP4	0.8	b	6333.524
<i>IWB65142</i>	3A	108.90	0.91	G/T					
<i>IWB7220</i>	3A	109.10	0.93	T/C					
<i>IWB72506</i>	3A	109.10	0.93	G/T					
<i>IWB72528</i>	3A	109.10	0.95	C/T					
<i>IWB7357</i>	3A	109.10	0.93	C/T					
<i>IWA5114</i>	3A	109.50	0.98	G/A					
<i>IWB53914</i>	3A	109.50	1	C/T					
<i>IWB71328</i>	3A	110.20	0.40	T/G					

■ Subgroup 1: Italy
 ■ Subgroup 2: CIMMYT-Mediterranean
 ■ Subgroup 3: North-America

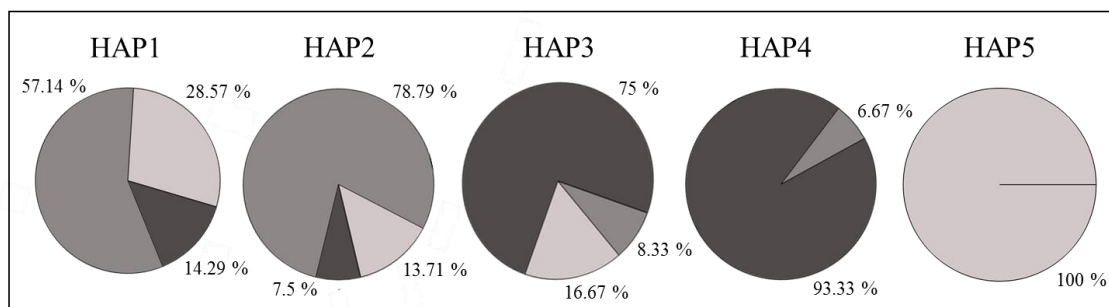


D

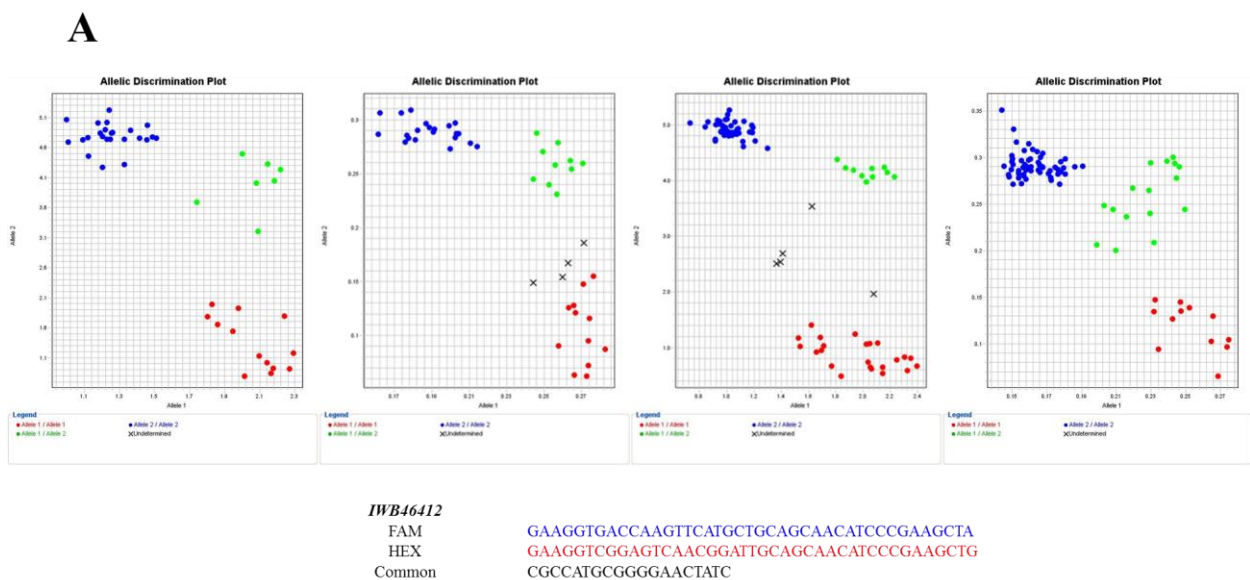


Markers	Chr.	Pos.	r ²	Alleles	Haplotypes	Code	Frequency (%)	Group (LSD test)	DON
<i>IWB11722</i>	6A	29.10	0.96	T/C	TGTTACCTG	HAP1	7.2	a	6624.126
<i>IWB35328</i>	6A	29.10	0.48	G/A	TGTTACCTT	HAP2	67.2	a	6500.755
<i>IWB35338</i>	6A	29.10	1	T/C	TATTCCCT	HAP3	12.0	ab	6363.969
<i>IWB35923</i>	6A	29.10	0.53	T/C	CACCGTTTCG	HAP4	12.8	b	6141.082
<i>IWB56969</i>	6A	29.10	1	A/G	TACTGTTCCG	HAP5	0.08	b	6069.488
<i>IWB64837</i>	6A	29.10	1	G/A					
<i>IWB66392</i>	6A	29.10	1	A/G					
<i>IWB71341</i>	6A	29.10	0.58	C/T					
<i>IWB36506</i>	6A	34.90	0.36	T/G					

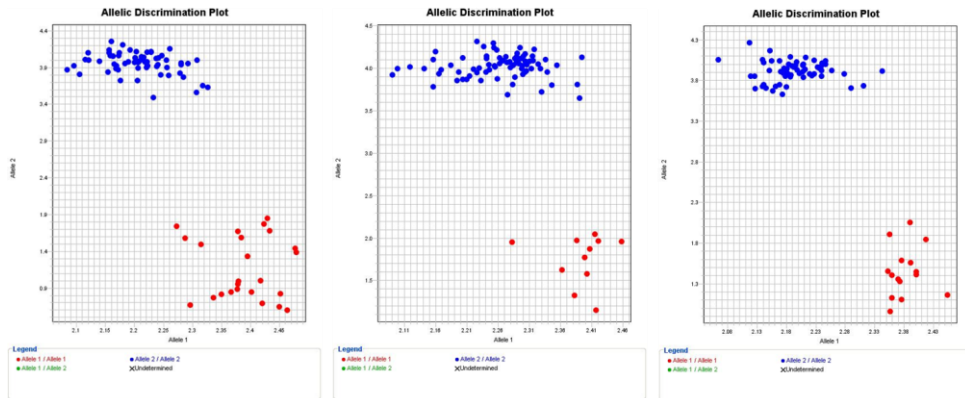
- Subgroup 1: Italy
- Subgroup 2: CIMMYT-Mediterranean
- Subgroup 3: North-America



Supplementary Figure 4 | Allelic discrimination plots using the KASP assay for the following single nucleotide polymorphisms (SNPs): A) *IWB46412* on chr. 1A, B) *IWB47303* on chr. 1B, C) *IWB53914* on chromosome 3A, D) *IWB70054* on chr. 5A, E) *IWB35328* and F) *IWB56969* on chr. 6A. *IWB46412*, *IWB47303*, *IWB53914*, *IWB35328* and *IWB56969* discriminated for haplotype groups with different response to deoxynivalenol (DON) content while *IWB70054* to FHB index. The red and blue dots refer to the homozygous genotypes, the green dots refer to heterozygous genotypes and the black crosses refer to not discriminatory genotypes.



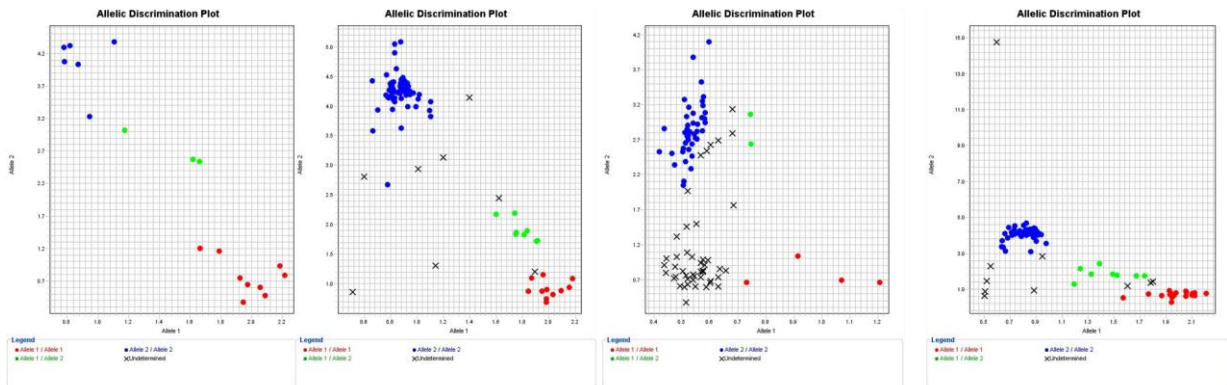
B



IWB47303

FAM **GAAGGTGACCAAGTTCATGCTGAAACTGACCTGCCTCAAGTAA**
 HEX **GAAGGTCGGAGTCAACGGATTGAAACTGACCTGCCTCAAGTAC**
 Common **CTCGATCTGGTCTGGAATG**

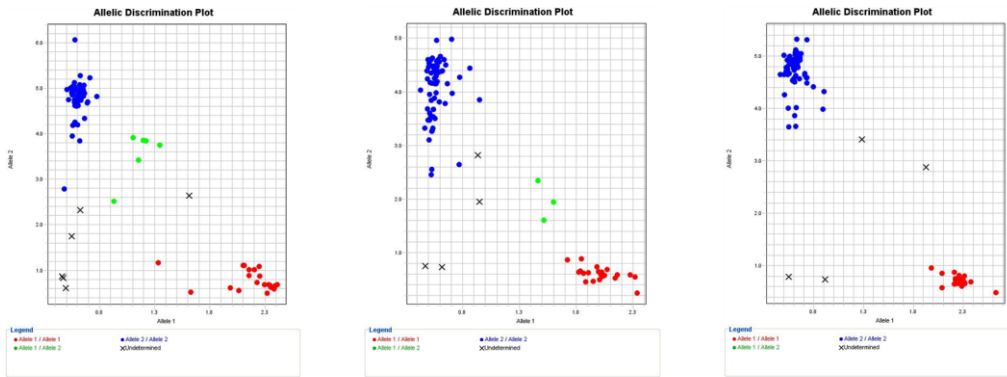
C



IWB53914

FAM **GAAGGTGACCAAGTTCATGCTTCTTGACATGGTCAGTGTAAAGCTT**
 HEX **GAAGGTCGGAGTCAACGGATTCTTGACATGGTCAGTGTAAAGCTC**
 Common **TATTGTGCTGTGCGTAAACAGATGACAT**

D

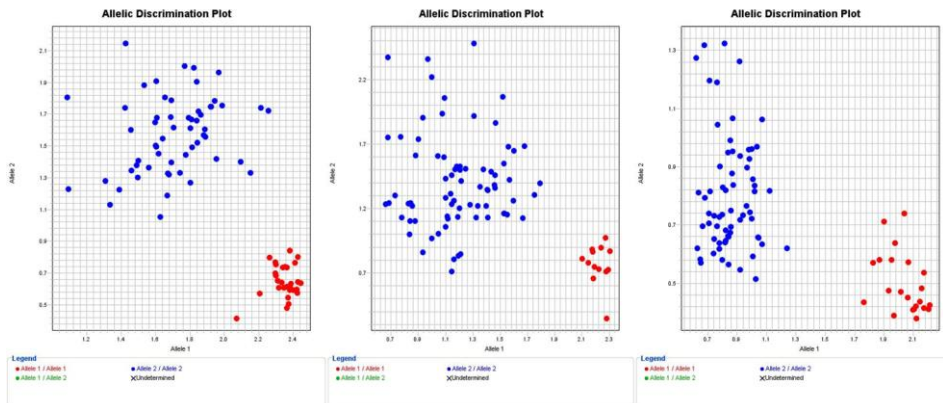


IWB70054

FAM
HEX
Common

GAAGGTGACCAAGTTCATGCTAGTGCCAAGGGAGCTCTTAGTT
GAAGGTCGGAGTCAACGGATTAGTGCCAAGGGAGCTCTTAGTC
GCATCGATGTTTCTTACCGAAGAAATA

E

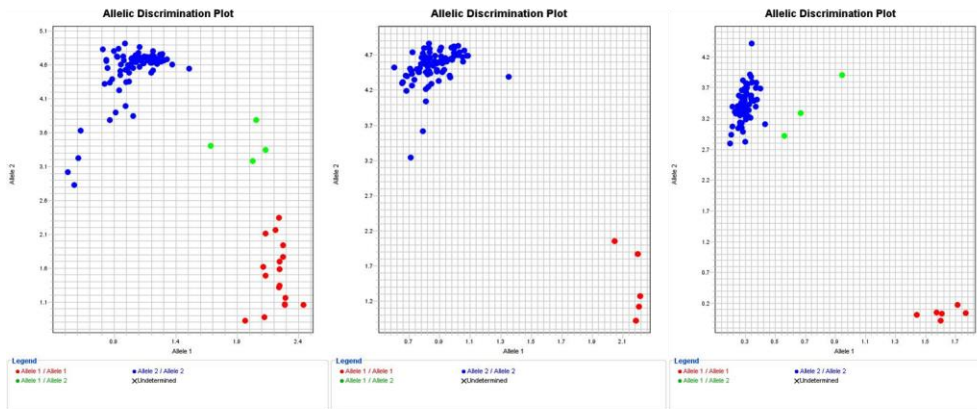


IWB35328

FAM
HEX
Common

GAAGGTGACCAAGTTCATGCTCACAGGGAAAAACAAAGCTCATCG
GAAGGTCGGAGTCAACGGATTCACAGGGAAAAACAAAGCTCATCA
GGCCTCTGTTGCTGGTCC

F



IWB56969

FAM GAAGGTGACCAAGTTCATGCTAAGGACTTGGGACCTACCA
 HEX GAAGTCTGGAGTCAACGGATTAAAGGACTTGGGACCTACCG
 Common CGAGCCCCTGCCTCATG

GENERAL CONCLUSIONS

Both studies presented in the current thesis aimed to dissect the genetic bases of durum wheat responses to drought and FHB disease using a common GWAS approach. Based on the literature, GWAS is optimal for mapping in natural populations or in panels of diverse cultivars with the purpose of capitalizing abundant recombination events allowing a higher resolution in finding genetic regions (QTL intervals) associated to the traits of interest. However, the main limitation in those panels is the occurrence of false positive associations as artifact arising from population structure, which in turn could lead to waste resources, time, and money. In the present thesis, GWAS-MLM methods have proven useful in controlling for population structure and relatedness. In addition, the use of flowering time as covariate led to a consistent reduction of the genetic bias due to the photoperiod/vernalization.

In *Chapter 1*, improving of drought adaptive trait repeatability as well as of the GWAS-QTL identification was obtained by taking advantage of the great potential and effectiveness of semi-automated robots and of UAV-based platforms to gather rapid, precise, and detailed high-throughput phenotypic measurements. Additionally, the validity of the “Rehydration method” for large-scale screening of osmotic adjustment trait under drought conditions was demonstrated. The results indicate that HTP-based approaches allow collection of phenotypic data with precision high enough to discern genetic differences and to facilitate QTL for drought-adaptive traits detection. The “Rehydration method” was useful to support osmotic adjustment for promoting wheat productivity and maintaining a more favorable water status of the crops.

In *Chapter 2*, I illustrate the utility of haplotypes to identify potential sources of FHB tolerance based on their known superior performance over single SNPs previously selected by GWAS. Suitable KASPar markers were validated for haplotype-based MAS programs against the deoxynivalenol (DON) accumulation, and tested in over 100 lines thus proving to be effective in discriminating resistant and susceptible genotypes. The study reveals (i) the efficiency of LD-based

haplotype construction to overcome the bi-allelic form-limiting factor at which SNP-trait relationships can be delineated and (ii) the importance of resulting KASPar makers to provide useful ways to accelerate the next durum wheat breeding schemes.

In conclusion, the whole research described here represents an endeavor to get a deeper insight into the principles governing the genetic response to biotic and abiotic stresses in durum wheat. The novel high-throughput phenotyping (HTP) approaches described in *Chapter 1* as well as the validation of suitable KASPar markers against the deoxynivalenol (DON) accumulation described in *Chapter 2* share a joint determination to a better understanding of genotype-phenotype relationship and will accelerate the selection of resistance loci in future wheat breeding programs.

REFERENCES

- Abdelrahman, H., ElHady, M., Alcivar-Warren, A., Allen, S., Al-Tobasei, R., Bao, L., ... & Chappell, J. (2017). Aquaculture genomics, genetics and breeding in the United States: current status, challenges, and priorities for future research. *BMC genomics*, *18*(1), 191.
- Anderson, J. A., Stack, R. W., Liu, S., Waldron, B. L., Fjeld, A. D., Coyne, C., ... & Frohberg, R. C. (2001). DNA markers for Fusarium head blight resistance QTL in two wheat populations. *Theoretical and Applied Genetics*, *102*(8), 1164-1168.
- Andrade-Sanchez, P., & Heun, J. T. (2013). Yield monitoring technology for irrigated cotton and grains in Arizona: hardware and software selection.
- Andrade-Sanchez, P., Gore, M. A., Heun, J. T., Thorp, K. R., Carmo-Silva, A. E., French, A. N., ... & White, J. W. (2014). Development and evaluation of a field-based high-throughput phenotyping platform. *Functional Plant Biology*, *41*(1), 68-79.
- Araus, J. L., Amaro, T., Casadesus, J., Asbati, A., & Nachit, M. M. (1998). Relationships between ash content, carbon isotope discrimination and yield in durum wheat. *Functional Plant Biology*, *25*(7), 835-842.
- Araus, J. L., Casadesus, J., & Bort, J. (2001). *Recent tools for the screening of physiological traits determining yield. Application of Physiology in Wheat Breeding* (No. 631.53 REY. CIMMYT.).
- Araus, J. L., Cabrera-Bosquet, L., Serret, M. D., Bort, J., & Nieto-Taladriz, M. T. (2013). Comparative performance of $\delta^{13}\text{C}$, $\delta^{18}\text{O}$ and $\delta^{15}\text{N}$ for phenotyping durum wheat adaptation to a dryland environment. *Functional Plant Biology*, *40*(6), 595-608.
- Araus, J. L., & Cairns, J. E. (2014). Field high-throughput phenotyping: the new crop breeding frontier. *Trends in plant science*, *19*(1), 52-61.
- Araus, J. L., Kefauver, S. C., Zaman-Allah, M., Olsen, M. S., & Cairns, J. E. (2018). Translating high-throughput phenotyping into genetic gain. *Trends in plant science*, *23*(5), 451-466.

- Atwell, S., Huang, Y. S., Vilhjálmsson, B. J., Willems, G., Horton, M., Li, Y., ... & Jiang, R. (2010). Genome-wide association study of 107 phenotypes in *Arabidopsis thaliana* inbred lines. *Nature*, *465*(7298), 627.
- Babu, R. C., Pathan, M. S., Blum, A., & Nguyen, H. T. (1998). Comparison of measurement methods of osmotic adjustment in rice cultivars. *Crop Science*, *39*(1), 150-158.
- Bachiri, H., Djebbar, R., Mekliche, A., Djenadi, C., & Ghanim, A. M. A. (2018). Carbon Isotope Discrimination as Physiological Marker to Select Tolerant Wheat Genotypes (*Triticum aestivum* L.) Under Water-limited Conditions. *American Journal of Plant Physiology*, *13*, 1-7.
- Bai, G., & Shaner, G. (1994). Scab of wheat: prospects for control. *Plant disease*, *78*(8), 760-766.
- Bai, G., Ge, Y., Hussain, W., Baenziger, P. S., & Graef, G. (2016). A multi-sensor system for high throughput field phenotyping in soybean and wheat breeding. *Computers and Electronics in Agriculture*, *128*, 181-192.
- Bajji, M., Lutts, S., & Kinet, J. M. (2001). Water deficit effects on solute contribution to osmotic adjustment as a function of leaf ageing in three durum wheat (*Triticum durum* Desf.) cultivars performing differently in arid conditions. *Plant Science*, *160*(4), 669-681.
- Barrett, J. C., Fry, B., Maller, J. D. M. J., & Daly, M. J. (2005). Haploview: analysis and visualization of LD and haplotype maps. *Bioinformatics*, *21*(2), 263-265.
- Barrs, H. D. (1968). Determination of water deficits in plant tissues. *Water deficit and plant growth*, 235-368.
- Begg, J. E. (1980). Morphological adaptations of leaves to water stress. In 'Adaptation of Plants to Water and High Temperature Stress'. (Eds NC Turner and PJ Kramer.) pp. 33-42.
- Beres, B. L., Brule-Babel, A. L., Ye, Z., Graf, R. J., Turkington, T. K., Harding, M. W., ... & Hooker, D. C. (2018). Exploring Genotype× Environment× Management synergies to manage fusarium head blight in wheat. *Canadian journal of plant pathology*, *40*(2), 179-188.

- Blum, A., & Pnuel, Y. (1990). Physiological attributes associated with drought resistance of wheat cultivars in a Mediterranean environment. *Australian Journal of Agricultural Research*, *41*(5), 799-810.
- Blum, A., Zhang, J., & Nguyen, H. T. (1999). Consistent differences among wheat cultivars in osmotic adjustment and their relationship to plant production. *Field Crops Research*, *64*(3), 287-291.
- Blum, A. (2017). Osmotic adjustment is a prime drought stress adaptive engine in support of plant production. *Plant, Cell & Environment*, *40*(1), 4-10.
- Bottalico, A., & Perrone, G. (2002). Toxigenic *Fusarium* species and mycotoxins associated with head blight in small-grain cereals in Europe. In *Mycotoxins in plant disease* (pp. 611-624). Springer, Dordrecht.
- Bradbury, P. J., Zhang, Z., Kroon, D. E., Casstevens, T. M., Ramdoss, Y., & Buckler, E. S. (2007). TASSEL: software for association mapping of complex traits in diverse samples. *Bioinformatics*, *23*(19), 2633-2635.
- Buerstmayr, H., Steiner, B., Lemmens, M., & Ruckenbauer, P. (2000). Resistance to *Fusarium* head blight in winter wheat: heritability and trait associations. *Crop Science*, *40*(4), 1012-1018.
- Buerstmayr, H., Lemmens, M., Hartl, L., Doldi, L., Steiner, B., Stierschneider, M., & Ruckenbauer, P. (2002). Molecular mapping of QTL for *Fusarium* head blight resistance in spring wheat. I. Resistance to fungal spread (Type II resistance). *Theoretical and Applied Genetics*, *104*(1), 84-91.
- Buerstmayr, H., Steiner, B., Hartl, L., Griesser, M., Angerer, N., Lengauer, D., ... & Lemmens, M. (2003). Molecular mapping of QTL for *Fusarium* head blight resistance in spring wheat. II. Resistance to fungal penetration and spread. *Theoretical and Applied Genetics*, *107*(3), 503-508.
- Buerstmayr, H., Adam, G., & Lemmens, M. (2012). 12 Resistance to Head Blight Caused by *Fusarium* spp. in Wheat. *Disease resistance in wheat*, *1*, 236.

Busemeyer, L., Ruckelshausen, A., Möller, K., Melchinger, A. E., Alheit, K. V., Maurer, H. P., ... & Würschum, T. (2013). Precision phenotyping of biomass accumulation in triticale reveals temporal genetic patterns of regulation. *Scientific reports*, 3, 2442.

Cabrera-Bosquet, L., Sanchez, C., Rosales, A., Palacios-Rojas, N., & Araus, J. L. (2011). Near-Infrared Reflectance Spectroscopy (NIRS) Assessment of $\delta^{18}\text{O}$ and nitrogen and ash contents for improved yield potential and drought adaptation in maize. *Journal of agricultural and food chemistry*, 59(2), 467-474.

Caemmerer, S. V., Ghannoum, O., Pengelly, J. J., & Cousins, A. B. (2014). Carbon isotope discrimination as a tool to explore C4 photosynthesis. *Journal of experimental botany*, 65(13), 3459-3470.

Cal, A. J., Sanciangco, M., Rebolledo, M. C., Luquet, D., Torres, R. O., McNally, K. L., & Henry, A. (2019). Leaf morphology, rather than plant water status, underlies genetic variation of rice leaf rolling under drought. *Plant, cell & environment*, 42(5), 1532-1544.

Castiblanco, V., Castillo, H., & Miedaner, T. (2018). Candidate genes for aggressiveness in a natural *Fusarium culmorum* population greatly differ between wheat and rye head blight. *Journal of Fungi*, 4(1), 14.

Chao, S., Zhang, W., Akhunov, E., Sherman, J., Ma, Y., Luo, M. C., & Dubcovsky, J. (2009). Analysis of gene-derived SNP marker polymorphism in US wheat (*Triticum aestivum* L.) cultivars. *Molecular Breeding*, 23(1), 23-33.

Chen, X., Faris, J. D., Hu, J., Stack, R. W., Adhikari, T., Elias, E. M., ... & Cai, X. (2007). Saturation and comparative mapping of a major Fusarium head blight resistance QTL in tetraploid wheat. *Molecular Breeding*, 19(2), 113-124.

Christopher, J. T., Christopher, M. J., Borrell, A. K., Fletcher, S., & Chenu, K. (2016). Stay-green traits to improve wheat adaptation in well-watered and water-limited environments. *Journal of Experimental Botany*, 67(17), 5159-5172.

- Clarke, J. M., Clarke, F. R., & Pozniak, C. J. (2010). Forty-six years of genetic improvement in Canadian durum wheat cultivars. *Canadian Journal of Plant Science*, 90(6), 791-801.
- Cobb, J. N., DeClerck, G., Greenberg, A., Clark, R., & McCouch, S. (2013). Next-generation phenotyping: requirements and strategies for enhancing our understanding of genotype–phenotype relationships and its relevance to crop improvement. *Theoretical and Applied Genetics*, 126(4), 867-887.
- Condorelli, G. E., Maccaferri, M., Newcomb, M., Andrade-Sanchez, P., White, J. W., French, A. N., ... & Tuberosa, R. (2018). Comparative aerial and ground based high throughput phenotyping for the genetic dissection of NDVI as a proxy for drought adaptive traits in durum wheat. *Frontiers in plant science*, 9, 893.
- Coplen, T. B., Brand, W. A., Gehre, M., Gröning, M., Meijer, H. A., Toman, B., & Verkouteren, R. M. (2006). New guidelines for δ 13C measurements. *Analytical Chemistry*, 78(7), 2439-2441.
- Daly, M. J., Rioux, J. D., Schaffner, S. F., Hudson, T. J., & Lander, E. S. (2001). High-resolution haplotype structure in the human genome. *Nature genetics*, 29(2), 229.
- Daryanto, S., Wang, L., & Jacinthe, P. A. (2016). Global synthesis of drought effects on maize and wheat production. *PloS one*, 11(5), e0156362.
- De Vita, P., & Taranto, F. (2019). Durum Wheat (*Triticum turgidum* ssp. *durum*) Breeding to Meet the Challenge of Climate Change. In *Advances in Plant Breeding Strategies: Cereals* (pp. 471-524). Springer, Cham.
- Deery, D. M., Rebetzke, G. J., Jimenez-Berni, J. A., James, R. A., Condon, A. G., Bovill, W. D., ... & Furbank, R. T. (2016). Methodology for high-throughput field phenotyping of canopy temperature using airborne thermography. *Frontiers in plant science*, 7, 1808.
- Dingkuhn, M., Cruz, R. T., & O'Toole, J. C. (1989). Net photosynthesis, water use efficiency, leaf water potential and leaf rolling as affected by water deficit in tropical upland rice. *Australian Journal of Agricultural Research*, 40(6), 1171-1181.

- Dixon, L. S., Godoy, J. V., & Carter, A. H. (2019). Evaluating the Utility of Carbon Isotope Discrimination for Wheat Breeding in the Pacific Northwest. *Plant Phenomics*, 2019, 4528719.
- Draeger, R., Gosman, N., Steed, A., Chandler, E., Thomsett, M., Schondelmaier, J., ... & Nicholson, P. (2007). Identification of QTL for resistance to Fusarium head blight, DON accumulation and associated traits in the winter wheat variety Arina. *Theoretical and Applied Genetics*, 115(5), 617-625.
- Dreisigacker, S., Sukumaran, S., Guzmán, C., He, X., Bonnett, D., & Crossa, J. (2015). Molecular marker-based selection tools in spring bread wheat improvement: CIMMYT experience and prospects. In *Molecular breeding for sustainable crop improvement* (pp. 421-474). Springer, Cham.
- Duan, T., Chapman, S. C., Guo, Y., & Zheng, B. (2017). Dynamic monitoring of NDVI in wheat agronomy and breeding trials using an unmanned aerial vehicle. *Field Crops Research*, 210, 71-80.
- Duncan, E. G., O'Sullivan, C. A., Roper, M. M., Palta, J., Whisson, K., & Peoples, M. B. (2018). Yield and nitrogen use efficiency of wheat increased with root length and biomass due to nitrogen, phosphorus, and potassium interactions. *Journal of Plant Nutrition and Soil Science*, 181(3), 364-373.
- Ehleringer, J., & Forseth, I. (1980). Solar tracking by plants. *Science*, 210(4474), 1094-1098.
- Evanno, G., Regnaut, S., & Goudet, J. (2005). Detecting the number of clusters of individuals using the software STRUCTURE: a simulation study. *Molecular ecology*, 14(8), 2611-2620.
- Fahlgren, N., Gehan, M. A., & Baxter, I. (2015). Lights, camera, action: high-throughput plant phenotyping is ready for a close-up. *Current opinion in plant biology*, 24, 93-99.
- Farquhar, G. D., & Richards, R. A. (1984). Isotopic composition of plant carbon correlates with water-use efficiency of wheat genotypes. *Functional Plant Biology*, 11(6), 539-552.
- Farquhar, G. D., Ehleringer, J. R., & Hubick, K. T. (1989). Carbon isotope discrimination and photosynthesis. *Annual review of plant biology*, 40(1), 503-537.

Fischer, R. A., Sayre, K. D., & Reynolds, M. P. (2005). Osmotic adjustment in wheat in relation to grain yield under water deficit environments. *Agronomy Journal*, 97(4), 1062-1071.

Gadaleta, A., Giancaspro, A., Giove, S. L., Zacheo, S., Mangini, G., Simeone, R., ... & Blanco, A. (2009). Genetic and physical mapping of new EST-derived SSRs on the A and B genome chromosomes of wheat. *Theoretical and Applied Genetics*, 118(5), 1015.

Giancaspro, A., Lionetti, V., Giove, S. L., Zito, D., Fabri, E., Reem, N., ... & Gadaleta, A. (2018). Cell wall features transferred from common into durum wheat to improve Fusarium Head Blight resistance. *Plant science*, 274, 121-128.

Gladysz, C., Lemmens, M., Steiner, B., & Buerstmayr, H. (2007). Evaluation and genetic mapping of resistance to Fusarium head blight in *Triticum dicoccoides*. *Israel journal of plant sciences*, 55(3-4), 263-266.

Goswami, R. S., & Kistler, H. C. (2004). Heading for disaster: *Fusarium graminearum* on cereal crops. *Molecular plant pathology*, 5(6), 515-525.

Graziani, M., Maccaferri, M., Royo, C., Salvatorelli, F., & Tuberosa, R. (2014). QTL dissection of yield components and morpho-physiological traits in a durum wheat elite population tested in contrasting thermo-pluviometric conditions. *Crop and Pasture Science*, 65(1), 80-95.

Guo, J., Xu, W., Yu, X., Shen, H., Li, H., Cheng, D., ... & Song, J. (2016). Cuticular wax accumulation is associated with drought tolerance in wheat near-isogenic lines. *Frontiers in plant science*, 7, 1809.

Hadjout, S., Chéreau, S., Atanasova-Pénichon, V., Marchegay, G., Mekliche, L., Bouregghda, H., ... & Richard-Forget, F. (2017). Phenotypic and biochemical characterization of new advanced durum wheat breeding lines from Algeria that show resistance to fusarium head blight and to mycotoxin accumulation. *Journal of plant pathology*, 99(3), 671-680.

- Haghighattalab, A., Pérez, L. G., Mondal, S., Singh, D., Schinstock, D., Rutkoski, J., ... & Poland, J. (2016). Application of unmanned aerial systems for high throughput phenotyping of large wheat breeding nurseries. *Plant Methods*, 12(1), 35.
- Hall, D., Tegström, C., & Ingvarsson, P. K. (2010). Using association mapping to dissect the genetic basis of complex traits in plants. *Briefings in Functional Genomics*, 9(2), 157-165.
- He, Y., Ahmad, D., Zhang, X., Zhang, Y., Wu, L., Jiang, P., & Ma, H. (2018). Genome-wide analysis of family-1 UDP glycosyltransferases (UGT) and identification of UGT genes for FHB resistance in wheat (*Triticum aestivum* L.). *BMC plant biology*, 18(1), 67.
- Hill, W. G., & Weir, B. S. (1988). Variances and covariances of squared linkage disequilibria in finite populations. *Theoretical population biology*, 33(1), 54-78.
- Imathiu, S., Edwards, S., Ray, R., & Back, M. (2014). Artificial inoculum and inoculation techniques commonly used in the investigation of Fusarium head blight in cereals. *Acta Phytopathologica et Entomologica Hungarica*, 49(2), 129-139.
- Ji, L., & Peters, A. J. (2003). Assessing vegetation response to drought in the northern Great Plains using vegetation and drought indices. *Remote Sensing of Environment*, 87(1), 85-98.
- Jia, H., Zhou, J., Xue, S., Li, G., Yan, H., Ran, C., ... & Luo, J. (2018). A journey to understand wheat Fusarium head blight resistance in the Chinese wheat landrace Wangshuibai. *The Crop Journal*, 6(1), 48-59.
- Jimenez-Berni, J. A., Deery, D. M., Rozas-Larraondo, P., Condon, A. T. G., Rebetzke, G. J., James, R. A., ... & Sirault, X. R. (2018). High throughput determination of plant height, ground cover, and above-ground biomass in wheat with LiDAR. *Frontiers in plant science*, 9, 237.
- Johnson, R. C., Nguyen, H. T., & Croy, L. I. (1984). Osmotic Adjustment and Solute Accumulation in Two Wheat Genotypes Differing in Drought Resistance 1. *Crop Science*, 24(5), 957-962.

- Jones, H. G., & Vaughan, R. A. (2010). *Remote sensing of vegetation: principles, techniques, and applications*. Oxford university press.
- Kao, C. H., Zeng, Z. B., & Teasdale, R. D. (1999). Multiple interval mapping for quantitative trait loci. *Genetics*, *152*(3), 1203-1216.
- Kefauver, S. C., Vicente, R., Vergara-Díaz, O., Fernandez-Gallego, J. A., Kerfal, S., Lopez, A., ... & Araus, J. L. (2017). Comparative UAV and field phenotyping to assess yield and nitrogen use efficiency in hybrid and conventional barley. *Frontiers in plant science*, *8*, 1733.
- Keller, B., Vass, I., Matsubara, S., Paul, K., Jedmowski, C., Pieruschka, R., ... & Muller, O. (2019). Maximum fluorescence and electron transport kinetics determined by light-induced fluorescence transients (LIFT) for photosynthesis phenotyping. *Photosynthesis research*, *140*(2), 221-233.
- Kikuta, S. B., & Richter, H. (1992). Leaf discs or press saps? A comparison of techniques for the determination of osmotic potentials in freeze-thawed leaf material. *Journal of Experimental Botany*, *43*(8), 1039-1044.
- Knoch, D., Abbadi, A., Grandke, F., Meyer, R. C., Samans, B., Werner, C. R., ... & Altmann, T. (2019). Strong temporal dynamics of QTL action on plant growth progression revealed through high-throughput phenotyping in canola. *Plant biotechnology journal*.
- Kollers, S., Rodemann, B., Ling, J., Korzun, V., Ebmeyer, E., Argillier, O., ... & Röder, M. S. (2013). Whole genome association mapping of Fusarium head blight resistance in European winter wheat (*Triticum aestivum* L.). *PLoS One*, *8*(2), e57500.
- Korte, A., & Farlow, A. (2013). The advantages and limitations of trait analysis with GWAS: a review. *Plant methods*, *9*(1), 29.
- Kyrtziz, A., Skarlatos, D., Fotopoulos, V., Vamvakousis, V., & Katsiotis, A. (2015). Investigating correlation among NDVI index derived by unmanned aerial vehicle photography and grain yield under late drought stress conditions. *Procedia Environmental Sciences*, *29*, 225-226.

- Leigh, J. W., & Bryant, D. (2015). popart: full-feature software for haplotype network construction. *Methods in Ecology and Evolution*, 6(9), 1110-1116.
- Letta, T., Maccaferri, M., Badebo, A., Ammar, K., Ricci, A., Crossa, J., & Tuberosa, R. (2013). Searching for novel sources of field resistance to Ug99 and Ethiopian stem rust races in durum wheat via association mapping. *Theoretical and Applied Genetics*, 126(5), 1237-1256.
- Lewis, J. E., Rowland, J., & Nadeau, A. (1998). Estimating maize production in Kenya using NDVI: some statistical considerations. *International Journal of Remote Sensing*, 19(13), 2609-2617.
- Li, X. M., Chen, X. M., Xiao, Y. G., Xia, X. C., Wang, D. S., He, Z. H., & Wang, H. J. (2014). Identification of QTL for seedling vigor in winter wheat. *Euphytica*, 198(2), 199-209.
- Liang, X., Zhang, L., Natarajan, S. K., & Becker, D. F. (2013). Proline mechanisms of stress survival. *Antioxidants & redox signaling*, 19(9), 998-1011.
- Lilley, J. M., Ludlow, M. M., McCouch, S. R., & O'Toole, J. C. (1996). Locating QTL for osmotic adjustment and dehydration tolerance in rice. *Journal of Experimental Botany*, 47(9), 1427-1436.
- Lin, F., Xue, S. L., Zhang, Z. Z., Zhang, C. Q., Kong, Z. X., Yao, G. Q., ... & Wei, J. B. (2006). Mapping QTL associated with resistance to Fusarium head blight in the Nanda2419× Wangshuibai population. II: Type I resistance. *Theoretical and Applied Genetics*, 112(3), 528-535.
- Liu, S., Rudd, J. C., Bai, G., Haley, S. D., Ibrahim, A. M., Xue, Q., ... & St Amand, P. (2014). Molecular markers linked to important genes in hard winter wheat. *Crop Science*, 54(4), 1304-1321.
- Liu, W., Maccaferri, M., Bulli, P., Rynearson, S., Tuberosa, R., Chen, X., & Pumphrey, M. (2017). Genome-wide association mapping for seedling and field resistance to *Puccinia striiformis* f. sp. *tritici* in elite durum wheat. *Theoretical and applied genetics*, 130(4), 649-667.

- Loriaux, S. D., Avenson, T. J., Welles, J. M., McDermitt, D. K., Eckles, R. D., Riensche, B., & Genty, B. (2013). Closing in on maximum yield of chlorophyll fluorescence using a single multiphase flash of sub-saturating intensity. *Plant, cell & environment*, *36*(10), 1755-1770.
- Lu, Q., Szabo-Hever, A., Bjørnstad, Å., Lillemo, M., Semagn, K., Mesterhazy, A., ... & Skinnes, H. (2011). Two major resistance quantitative trait loci are required to counteract the increased susceptibility to Fusarium head blight of the Rht-D1b dwarfing gene in wheat. *Crop science*, *51*(6), 2430-2438.
- Luo, L., Xia, H., & Lu, B. (2019). Crop breeding for drought resistance. *Frontiers in Plant Science*, *10*, 314.
- Maccaferri, M., Sanguineti, M. C., Demontis, A., El-Ahmed, A., Garcia del Moral, L., Maalouf, F., ... & Royo, C. (2011). Association mapping in durum wheat grown across a broad range of water regimes. *Journal of experimental botany*, *62*(2), 409-438.
- Maccaferri, M., Ricci, A., Salvi, S., Milner, S. G., Noli, E., Martelli, P. L., ... & Ammar, K. (2015a). A high-density, SNP-based consensus map of tetraploid wheat as a bridge to integrate durum and bread wheat genomics and breeding. *Plant biotechnology journal*, *13*(5), 648-663.
- Maccaferri, M., Zhang, J., Bulli, P., Abate, Z., Chao, S., Cantu, D., ... & Dubcovsky, J. (2015b). A genome-wide association study of resistance to stripe rust (*Puccinia striiformis* f. sp. *tritici*) in a worldwide collection of hexaploid spring wheat (*Triticum aestivum* L.). *G3: Genes, Genomes, Genetics*, *5*(3), 449-465.
- Maccaferri, M., El-Feki, W., Nazemi, G., Salvi, S., Canè, M. A., Colalongo, M. C., ... & Tuberosa, R. (2016). Prioritizing quantitative trait loci for root system architecture in tetraploid wheat. *Journal of experimental botany*, *67*(4), 1161-1178.
- Maccaferri, M., Harris, N. S., Twardziok, S. O., Pasam, R. K., Gundlach, H., Spannagl, M., ... & Himmelbach, A. (2019). Durum wheat genome highlights past domestication signatures and future improvement targets. *Nature genetics*, *51*(5), 885.

- Maes, W. H., & Steppe, K. (2012). Estimating evapotranspiration and drought stress with ground-based thermal remote sensing in agriculture: a review. *Journal of Experimental Botany*, *63*(13), 4671-4712.
- Mart, K. B., Veneklaas, E. J., & Bramley, H. (2016). Osmotic potential at full turgor: an easily measurable trait to help breeders select for drought tolerance in wheat. *Plant Breeding*, *135*(3), 279-285.
- Marti, J., Bort, J., Slafer, G. A., & Araus, J. L. (2007). Can wheat yield be assessed by early measurements of Normalized Difference Vegetation Index?. *Annals of Applied biology*, *150*(2), 253-257.
- Mattioni, C., Lacerenza, N. G., Troccoli, A., De Leonardis, A. M., & Di Fonzo, N. (1997). Water and salt stress-induced alterations in proline metabolism of *Triticum durum* seedlings. *Physiologia Plantarum*, *101*(4), 787-792.
- Meuwissen, T. H., & Goddard, M. E. (2001). Prediction of identity by descent probabilities from marker-haplotypes. *Genetics Selection Evolution*, *33*(6), 605.
- Miedaner, T., Moldovan, M., & Ittu, M. (2003). Comparison of spray and point inoculation to assess resistance to Fusarium head blight in a multienvironment wheat trial. *Phytopathology*, *93*(9), 1068-1072.
- Miedaner, T., & Longin, C. F. H. (2014). Genetic variation for resistance to Fusarium head blight in winter durum material. *Crop and Pasture Science*, *65*(1), 46-51.
- Miedaner, T., Gwiazdowska, D., & Waśkiewicz, A. (2017). Management of Fusarium Species and their Mycotoxins in Cereal Food and Feed. *Frontiers in microbiology*, *8*, 1543.
- Milner, S. G., Maccaferri, M., Huang, B. E., Mantovani, P., Massi, A., Frascaroli, E., ... & Salvi, S. (2016). A multiparental cross population for mapping QTL for agronomic traits in durum wheat (*Triticum turgidum* ssp. *durum*). *Plant biotechnology journal*, *14*(2), 735-748.

- Mir, R. R., Reynolds, M., Pinto, F., Khan, M. A., & Bhat, M. A. (2019). High-throughput phenotyping for crop improvement in the genomics era. *Plant science*.
- Mohammadi, R., Sadeghzadeh, B., Ahmadi, H., Bahrami, N., & Amri, A. (2015). Field evaluation of durum wheat landraces for prevailing abiotic and biotic stresses in highland rainfed regions of Iran. *The Crop Journal*, 3(5), 423-433.
- Mondal, S., Mason, R. E., Huggins, T., & Hays, D. B. (2015). QTL on wheat (*Triticum aestivum* L.) chromosomes 1B, 3D and 5A are associated with constitutive production of leaf cuticular wax and may contribute to lower leaf temperatures under heat stress. *Euphytica*, 201(1), 123-130.
- Money, D., Gardner, K., Migicovsky, Z., Schwaninger, H., Zhong, G. Y., & Myles, S. (2015). LinkImpute: fast and accurate genotype imputation for nonmodel organisms. *G3: Genes, Genomes, Genetics*, 5(11), 2383-2390.
- Moretti, A., Pascale, M., & Logrieco, A. F. (2018). Mycotoxin risks under a climate change scenario in Europe. *Trends in Food Science & Technology*, 84, 38-40.
- Morgan, J. L. (1977). Two types of convention in indirect speech acts. *Center for the Study of Reading Technical Report; no. 052*.
- Morgan, J. M. (1984). Osmoregulation and water stress in higher plants. *Annual review of plant physiology*, 35(1), 299-319.
- Morgan, J. M., & Condon, A. G. (1986). Water use, grain yield, and osmoregulation in wheat. *Functional Plant Biology*, 13(4), 523-532.
- Morgan, J. M. (1988). The use of coleoptile responses to water stress to differentiate wheat genotypes for osmoregulation, growth and yield. *Annals of Botany*, 62(2), 193-198.
- Morgan, J. M. (1991). A gene controlling differences in osmoregulation in wheat. *Functional Plant Biology*, 18(3), 249-257.

- Morgan, J. M., & Tan, M. K. (1996). Chromosomal location of a wheat osmoregulation gene using RFLP analysis. *Functional Plant Biology*, 23(6), 803-806.
- Munns, R., & Weir, R. (1981). Contribution of sugars to osmotic adjustment in elongating and expanded zones of wheat leaves during moderate water deficits at two light levels. *Functional Plant Biology*, 8(1), 93-105.
- Mwadzingeni, L., Shimelis, H., Dube, E., Laing, M. D., & Tsilo, T. J. (2016). Breeding wheat for drought tolerance: Progress and technologies. *Journal of Integrative Agriculture*, 15(5), 935-943.
- N'Diaye, A., Haile, J. K., Cory, A. T., Clarke, F. R., Clarke, J. M., Knox, R. E., & Pozniak, C. J. (2017). Single marker and haplotype-based association analysis of semolina and pasta colour in elite durum wheat breeding lines using a high-density consensus map. *PloS one*, 12(1), e0170941.
- O'Toole, J. C., & Cruz, R. T. (1980). Response of leaf water potential, stomatal resistance, and leaf rolling to water stress. *Plant physiology*, 65(3), 428-432.
- Patil, N., Berno, A. J., Hinds, D. A., Barrett, W. A., Doshi, J. M., Hacker, C. R., ... & Nguyen, B. T. (2001). Blocks of limited haplotype diversity revealed by high-resolution scanning of human chromosome 21. *Science*, 294(5547), 1719-1723.
- Pauli, D., Andrade-Sanchez, P., Carmo-Silva, A. E., Gazave, E., French, A. N., Heun, J., ... & Thorp, K. R. (2016). Field-based high-throughput plant phenotyping reveals the temporal patterns of quantitative trait loci associated with stress-responsive traits in cotton. *G3: Genes, Genomes, Genetics*, 6(4), 865-879.
- Payne, R. W. (2009). GenStat. *Wiley Interdisciplinary Reviews: Computational Statistics*, 1(2), 255-258.
- Pei, X. B. (2019). Genetic mapping of leaf rust (*Puccinia triticina* Eriks.) resistance in durum wheat (*Triticum turgidum* var. *durum* L.).

- Petersen, S., Lyerly, J. H., McKendry, A. L., Islam, M. S., Brown-Guedira, G., Cowger, C., ... & Murphy, J. P. (2017). Validation of Fusarium head blight resistance QTL in US winter wheat. *Crop Science*, 57(1), 1-12.
- Prashar, A., & Jones, H. G. (2016). Assessing drought responses using thermal infrared imaging. In *Environmental Responses in Plants* (pp. 209-219). Humana Press, New York, NY.
- Prat, N., Buerstmayr, M., Steiner, B., Robert, O., & Buerstmayr, H. (2014). Current knowledge on resistance to Fusarium head blight in tetraploid wheat. *Molecular breeding*, 34(4), 1689-1699.
- Prat, N., Guilbert, C., Prah, U., Wachter, E., Steiner, B., Langin, T., ... & Buerstmayr, H. (2017). QTL mapping of Fusarium head blight resistance in three related durum wheat populations. *Theoretical and applied genetics*, 130(1), 13-27.
- Pritchard, J. K., Stephens, M., & Donnelly, P. (2000). Inference of population structure using multilocus genotype data. *Genetics*, 155(2), 945-959.
- Purahong, W., Nipoti, P., Pisi, A., Lemmens, M., & Prodi, A. (2014). Aggressiveness of different *Fusarium graminearum* chemotypes within a population from Northern-Central Italy. *Mycoscience*, 55(1), 63-69.
- Qian, L., Hickey, L. T., Stahl, A., Werner, C. R., Hayes, B., Snowdon, R. J., & Voss-Fels, K. P. (2017). Exploring and harnessing haplotype diversity to improve yield stability in crops. *Frontiers in plant science*, 8, 1534.
- Quarrie, S. A., Steed, A., Calestani, C., Semikhodskii, A., Lebreton, C., Chinoy, C., ... & Schondelmaier, J. (2005). A high-density genetic map of hexaploid wheat (*Triticum aestivum* L.) from the cross Chinese Spring× SQ1 and its use to compare QTL for grain yield across a range of environments. *Theoretical and Applied Genetics*, 110(5), 865-880.
- Randhawa, H. S., Asif, M., Pozniak, C., Clarke, J. M., Graf, R. J., Fox, S. L., ... & Cuthbert, R. D. (2013). Application of molecular markers to wheat breeding in Canada. *Plant Breeding*, 132(5), 458-471.

- Rasheed, A., Xia, X., Mahmood, T., Quraishi, U. M., Aziz, A., Bux, H., ... & He, Z. (2016). Comparison of economically important loci in landraces and improved wheat cultivars from Pakistan. *Crop Science*, *56*(1), 287-301.
- Robin, S., Pathan, M. S., Courtois, B., Lafitte, R., Carandang, S., Lanceras, S., ... & Li, Z. (2003). Mapping osmotic adjustment in an advanced back-cross inbred population of rice. *Theoretical and applied genetics*, *107*(7), 1288-1296.
- Rudd, J. C., Horsley, R. D., McKendry, A. L., & Elias, E. M. (2001). Host plant resistance genes for Fusarium head blight. *Crop Science*, *41*(3), 620-627.
- Sadeghi-Tehran, P., Sabermanesh, K., Virlet, N., & Hawkesford, M. J. (2017). Automated method to determine two critical growth stages of wheat: heading and flowering. *Frontiers in plant science*, *8*, 252.
- Sadras, V. O., & Lawson, C. (2011). Genetic gain in yield and associated changes in phenotype, trait plasticity and competitive ability of South Australian wheat varieties released between 1958 and 2007. *Crop and Pasture Science*, *62*(7), 533-549.
- Saitou, N., & Nei, M. (1987). The neighbor-joining method: a new method for reconstructing phylogenetic trees. *Molecular biology and evolution*, *4*(4), 406-425.
- Sari, E., Berraies, S., Knox, R. E., Singh, A. K., Ruan, Y., Cuthbert, R. D., ... & N'Diaye, A. (2018). High density genetic mapping of Fusarium head blight resistance QTL in tetraploid wheat. *PLoS one*, *13*(10), e0204362.
- Schroeder, H. W., & Christensen, J. J. (1963). Factors affecting resistance of wheat to scab caused by *Gibberella zeae*. *Phytopathology*, *53*(7, 1), 831-838.
- Serrano, L., Filella, I., & Penuelas, J. (2000). Remote sensing of biomass and yield of winter wheat under different nitrogen supplies. *Crop science*, *40*(3), 723-731.

Shakoor, N., Lee, S., & Mockler, T. C. (2017). High throughput phenotyping to accelerate crop breeding and monitoring of diseases in the field. *Current opinion in plant biology*, 38, 184-192.

Shakoor, N., Northrup, D., Murray, S., & Mockler, T. C. (2019). Big Data Driven Agriculture: Big Data Analytics in Plant Breeding, Genomics, and the Use of Remote Sensing Technologies to Advance Crop Productivity. *The Plant Phenome Journal*, 2(1).

Shaner, G. (2002). Resistance in hexaploid wheat to Fusarium head blight. In *2002 National Fusarium Head Blight Forum Proceedings* (p. 208).

Shi, S., Azam, F. I., Li, H., Chang, X., Li, B., & Jing, R. (2017). Mapping QTL for stay-green and agronomic traits in wheat under diverse water regimes. *Euphytica*, 213(11), 246.

Singh, L., Anderson, J. A., Chen, J., Gill, B. S., Tiwari, V. K., & Rawat, N. (2019). Development and Validation of a Perfect KASP Marker for Fusarium Head Blight Resistance Gene Fhb1 in Wheat. *The Plant Pathology Journal*, 35(3), 200.

Steiner, B., Buerstmayr, M., Michel, S., Schweiger, W., Lemmens, M., & Buerstmayr, H. (2017). Breeding strategies and advances in line selection for Fusarium head blight resistance in wheat. *Tropical Plant Pathology*, 42(3), 165-174.

Steiner, B., Michel, S., Maccaferri, M., Lemmens, M., Tuberosa, R., & Buerstmayr, H. (2019). Exploring and exploiting the genetic variation of Fusarium head blight resistance for genomic-assisted breeding in the elite durum wheat gene pool. *Theoretical and Applied Genetics*, 132(4), 969-988.

Su, Z., Bernardo, A., Tian, B., Chen, H., Wang, S., Ma, H., ... & Trick, H. (2019). A deletion mutation in TaHRC confers Fhb1 resistance to Fusarium head blight in wheat. *Nature genetics*, 1.

Sun, S., Li, C., Paterson, A. H., Jiang, Y., Xu, R., Robertson, J. S., ... & Chee, P. W. (2018). In-field high throughput phenotyping and cotton plant growth analysis using LiDAR. *Frontiers in Plant Science*, 9, 16.

Szabo-Hever, A., Zhang, Q., Friesen, T. L., Zhong, S., Elias, E. M., Cai, X., ... & Xu, S. S. (2018). Genetic diversity and resistance to Fusarium head blight in synthetic hexaploid wheat derived from *Aegilops tauschii* and diverse *Triticum turgidum* subspecies. *Frontiers in plant science*, 9, 1829.

Tattaris, M., Reynolds, M. P., & Chapman, S. C. (2016). A direct comparison of remote sensing approaches for high-throughput phenotyping in plant breeding. *Frontiers in Plant Science*, 7, 1131.

Terwilliger, J. D. (1995). A powerful likelihood method for the analysis of linkage disequilibrium between trait loci and one or more polymorphic marker loci. *American journal of human genetics*, 56(3), 777.

Teulat, B., This, D., Khairallah, M., Borries, C., Ragot, C., Sourdille, P., ... & Charrier, A. (1998). Several QTL involved in osmotic-adjustment trait variation in barley (*Hordeum vulgare* L.). *Theoretical and Applied Genetics*, 96(5), 688-698.

Teulat, B., Borries, C., & This, D. (2001). New QTL identified for plant water status, water-soluble carbohydrate and osmotic adjustment in a barley population grown in a growth-chamber under two water regimes. *Theoretical and Applied Genetics*, 103(1), 161-170.

Thompson, A. L., Thorp, K. R., Conley, M., Andrade-Sanchez, P., Heun, J. T., Dyer, J. M., & White, J. W. (2018). Deploying a proximal sensing cart to identify drought adaptive traits in upland cotton for high-throughput phenotyping. *Frontiers in plant science*, 9, 507.

Tilman, D., Balzer, C., Hill, J., & Befort, B. L. (2011). Global food demand and the sustainable intensification of agriculture. *Proceedings of the National Academy of Sciences*, 108(50), 20260-20264.

Tóth, B., Kaszonyi, G., Bartok, T., Varga, J., & Mesterhazy, A. (2008). Common resistance of wheat to members of the *Fusarium graminearum* species complex and *F. culmorum*. *Plant Breeding*, 127(1), 1-8.

Trapp, J. J., Urrea, C. A., Zhou, J., Khot, L. R., Sankaran, S., & Miklas, P. N. (2016). Selective phenotyping traits related to multiple stress and drought response in dry bean. *Crop Science*, 56(4), 1460-1472.

Tuberosa, R. (2012). Phenotyping for drought tolerance of crops in the genomics era. *Frontiers in physiology*, 3, 347.

Tucker, C. J. (1979). Red and photographic infrared linear combinations for monitoring vegetation. *Remote sensing of Environment*, 8(2), 127-150.

Turgut, R., & Kadioglu, A. (1998). The effect of drought, temperature and irradiation on leaf rolling in *Ctenanthe setosa*. *Biologia Plantarum*, 41(4), 629-633.

Turner, N. C., & Jones, M. M. (1980). Turgor maintenance by osmotic adjustment: a review and evaluation. *Turgor maintenance by osmotic adjustment: a review and evaluation.*, 87-103.

Turner, N. C., O'Toole, J. C., Cruz, R. T., Namuco, O. S., & Ahmad, S. (1986). Responses of seven diverse rice cultivars to water deficits I. Stress development, canopy temperature, leaf rolling and growth. *Field Crops Research*, 13, 257-271.

Underwood, J., Wendel, A., Schofield, B., McMurray, L., & Kimber, R. (2017). Efficient in-field plant phenomics for row-crops with an autonomous ground vehicle. *Journal of field robotics*, 34(6), 1061-1083.

Urban, O., Hlaváčová, M., Klem, K., Novotná, K., Rapantová, B., Smutná, P., ... & Trnka, M. (2018). Combined effects of drought and high temperature on photosynthetic characteristics in four winter wheat genotypes. *Field Crops Research*, 223, 137-149.

Virlet, N., Sabermanesh, K., Sadeghi-Tehran, P., & Hawkesford, M. J. (2017). Field Scanalyzer: An automated robotic field phenotyping platform for detailed crop monitoring. *Functional Plant Biology*, 44(1), 143-153.

Wang, S., Basten, C.J. and Zeng, Z.B. (2012). Windows QTL Cartographer 2.5. Raleigh, NC: Department of Statistics, North Carolina State University.

- Wang, S., Wong, D., Forrest, K., Allen, A., Chao, S., Huang, B. E., ... & Mastrangelo, A. M. (2014). Characterization of polyploid wheat genomic diversity using a high-density 90 000 single nucleotide polymorphism array. *Plant biotechnology journal*, *12*(6), 787-796.
- Wang, S., Mo, X., Hu, S., Liu, S., & Liu, Z. (2018). Assessment of droughts and wheat yield loss on the North China Plain with an aggregate drought index (ADI) approach. *Ecological indicators*, *87*, 107-116.
- Wang, S., Xu, S. S., Chao, S., Sun, Q., Liu, S., & Xia, G. (2019). A genome-wide association study of highly heritable agronomic traits in durum wheat. *Frontiers in plant science*, *10*, 919.
- White, J. W., & Conley, M. M. (2013). A flexible, low-cost cart for proximal sensing. *Crop Science*, *53*(4), 1646-1649.
- Wingate, L., Ogée, J., Cremonese, E., Filippa, G., Mizunuma, T., Migliavacca, M., ... & Hörtnagl, L. (2015). Interpreting canopy development and physiology using the EUROPhen camera network at flux sites. *Biogeosciences Discussions*.
- Wu, H., Qin, J., Han, J., Zhao, X., Ouyang, S., Liang, Y., ... & Cui, Y. (2013). Comparative high-resolution mapping of the wax inhibitors Iw1 and Iw2 in hexaploid wheat. *PLoS One*, *8*(12), e84691.
- Wu, L., Zhang, Y., He, Y., Jiang, P., Zhang, X., & Ma, H. (2019). Genome-Wide Association Mapping of Resistance to Fusarium Head Blight Spread and Deoxynivalenol Accumulation in Chinese Elite Wheat Germplasm. *Phytopathology*, *109*(7), 1208-1216.
- Yi, X., Cheng, J., Jiang, Z., Hu, W., Bie, T., Gao, D., ... & Cheng, X. (2018). Genetic analysis of Fusarium head blight resistance in CIMMYT bread wheat line C615 using traditional and conditional QTL mapping. *Frontiers in plant science*, *9*, 573.
- Yordanov, I., Velikova, V., & Tsonev, T. (2000). Plant responses to drought, acclimation, and stress tolerance. *Photosynthetica*, *38*(2), 171-186.

- Yousfi, S., Kellas, N., Saidi, L., Benlakehal, Z., Chaou, L., Siad, D., ... & Araus, J. L. (2016). Comparative performance of remote sensing methods in assessing wheat performance under Mediterranean conditions. *Agricultural Water Management*, *164*, 137-147.
- Yu, J., Pressoir, G., Briggs, W. H., Bi, I. V., Yamasaki, M., Doebley, J. F., ... & Kresovich, S. (2006). A unified mixed-model method for association mapping that accounts for multiple levels of relatedness. *Nature genetics*, *38*(2), 203.
- Yue, X., Hu, Y., Zhang, H., & Schmidhalter, U. (2019). Evaluation of Both SPAD Reading and SPAD Index on Estimating the Plant Nitrogen Status of Winter Wheat. *International Journal of Plant Production*, 1-9.
- Zadoks, J. C., Chang, T. T., & Konzak, C. F. (1974). A decimal code for the growth stages of cereals. *Weed research*, *14*(6), 415-421.
- Zandalinas, S. I., Mittler, R., Balfagón, D., Arbona, V., & Gómez-Cadenas, A. (2018). Plant adaptations to the combination of drought and high temperatures. *Physiologia plantarum*, *162*(1), 2-12.
- Zhang, J., Nguyen, H. T., & Blum, A. (1999). Genetic analysis of osmotic adjustment in crop plants. *Journal of Experimental Botany*, *50*(332), 291-302.
- Zhang, Q., Axtman, J. E., Faris, J. D., Chao, S., Zhang, Z., Friesen, T. L., ... & Xu, S. S. (2014). Identification and molecular mapping of quantitative trait loci for Fusarium head blight resistance in emmer and durum wheat using a single nucleotide polymorphism-based linkage map. *Molecular breeding*, *34*(4), 1677-1687.
- Zhao, M., Leng, Y., Chao, S., Xu, S. S., & Zhong, S. (2018). Molecular mapping of QTL for Fusarium head blight resistance introgressed into durum wheat. *Theoretical and applied genetics*, *131*(9), 1939-1951.
- Zhu, C., Gore, M., Buckler, E. S., & Yu, J. (2008). Status and prospects of association mapping in plants. *The plant genome*, *1*(1), 5-20.

Zhu, Z., Bonnett, D., Ellis, M., He, X., Heslot, N., Dreisigacker, S., ... & Singh, P. (2016). Characterization of Fusarium head blight resistance in a CIMMYT synthetic-derived bread wheat line. *Euphytica*, 208(2), 367-375.

